



**OFFSHORE TECHNOLOGY  
RESEARCH CENTER**

**Submarine Slope Stability Forecasting  
and  
Back Analyses in Deep Water**

by

Eric Arthur Liedtke B.S.

AE

A NATIONAL SCIENCE FOUNDATION ENGINEERING RESEARCH CENTER

24.5

**Submarine Slope Stability Forecasting  
and  
Back Analyses in Deep Water**

by

Eric Arthur Liedtke B.S.

Supervised by  
Dr. Stephen G. Wright

1997

NSF# CDR-8721512



OFFSHORE  
TECHNOLOGY  
RESEARCH  
CENTER

*A National Science Foundation Engineering Research Center*

12/97B9375

*For more information contact:*

**Offshore Technology Research Center**  
Texas A&M University  
1200 Mariner Drive  
College Station, TX 77845  
(409) 845-6000

*or,*

**Center for Offshore Technology**  
The University of Texas at Austin  
2901 North IH 35, Suite 101  
Austin, Texas 78722  
(512) 471-3753

## Acknowledgments

I would like to express my sincere appreciation to my supervisor Stephen G. Wright for his guidance and inspiration in the course of this work. I also appreciate the effort and recommendations provided by Robert. B. Gilbert in reviewing this thesis. I would like to acknowledge the faculty of the Geotechnical Engineering Program at the University of Texas at Austin for their efforts put forth in teaching the courses that ultimately provided the backbone for this thesis. In addition, my earnest appreciation goes to the staff of the Geotechnical Engineering Program for their relentless efforts both directly and indirectly that allowed this work to be completed.

I wish to acknowledge the Offshore Technology Research Center, funded through the National Science Foundation, grant No. CDR-8721512, for their financial support which made this course of work possible. Additionally, I wish thank the members of the Offshore Technology Research Center for the opportunity to learn about the many engineering aspects involved in the production of petroleum in deep water.

Submarine Slope Stability Forecasting  
and  
Back Analyses in Deep Water

by

Eric Arthur Liedtke

Deep water presents special problems in determining shear strengths, stratigraphy and bathymetry. Slope stability analyses can be used to back-calculate shear strengths, however, there is greater uncertainty than on dry land because there is greater uncertainty in the bathymetry. The purpose of this thesis is to determine uncertainty in submarine slope stability and back-calculated shear strengths in deep water. In addition, a methodology for dealing with nonlinear envelopes when back calculating shear strengths is explored. A series of parametric studies were performed in which the influence of stratigraphy on stability was investigated. Both circular and noncircular shear surfaces were assumed in the stability analyses. A study also was performed to investigate the effects of bathymetry on the stability of a deep water submerged slope. In particular, the effects of uncertainty in the bathymetry on the evaluation of slope stability were examined. In these studies, shear strengths were characterized assuming both "drained" cases ( $c = 0$ ) and "undrained" cases ( $\phi = 0$ ).

## **Table of Contents**

<b>List of Tables</b>	<b>xii</b>
<b>List of Figures</b>	<b>xiii</b>
<b>1. Slope Stability in Deep Water</b>	<b>1</b>
<b>2. Variables and Uncertainties in Sea-Floor Stability and Shear Strengths</b>	<b>5</b>
<b>2.1 Introduction</b>	<b>5</b>
<b>2.2 Back Analysis</b>	<b>5</b>
<b>2.2.1 Advantages of Back Analyses</b>	<b>7</b>
<b>2.2.2 Disadvantages of Back Analyses</b>	<b>7</b>
2.2.2.1 Mechanics	8
2.2.2.2 Number of Unknown Strength Parameters	8
2.2.2.3 Three Dimensional Effects	12
<b>2.3 Variability of Shear Strength</b>	<b>12</b>
2.3.1 Variability of Shear Strength in the Vertical Direction	13
2.3.2 Variability of Shear Strength in the Lateral Direction	19
<b>2.4 Uncertainty in Bathymetry Measurements</b>	<b>19</b>

<b>2.5 Conclusions</b>	<b>25</b>
<b>3. Effects of Variability of Shear Strength in the Vertical Direction on Slope Stability</b>	<b>27</b>
<b>3.1 Introduction</b>	<b>27</b>
<b>3.2 Variables</b>	<b>28</b>
<b>3.3 Dimensionless Variables</b>	<b>28</b>
<b>3.4 Stability Calculations</b>	<b>30</b>
<b>3.5 Shear Strength</b>	<b>30</b>
<b>3.6 Case 1, Constant Strength Cohesion Soil</b>	<b>31</b>
<b>3.6.1 Procedure for Detecting Stability with Thin, Weak Seam</b>	<b>31</b>
<b>3.6.2 Verification of Dimensionless Parameters</b>	<b>33</b>
<b>3.6.3 Results</b>	<b>35</b>
<b>3.7 Case 2 - Cohesion Increasing Linearly with Depth</b>	<b>38</b>
<b>3.7.1 Variables</b>	<b>39</b>
<b>3.7.2 Procedure for Detecting Stability with Thin, Weak Seam</b>	<b>39</b>
<b>3.7.3 Verification of Dimensionless Parameters</b>	<b>41</b>
<b>3.7.4 Results</b>	<b>43</b>
3.7.4.1 Circular Shear Surfaces	43
3.7.4.2 Noncircular Shear Surfaces	48
<b>3.8 Case 3 - Friction Angle is Constant</b>	<b>51</b>

3.8.1 Variables	53
3.8.2 Procedure for Detecting Stability with Thin, Weak Seam	53
3.8.3 Verification of Dimensionless Parameters	55
3.8.4 Results	57
3.8.4.1 Circular Shear Surfaces	57
3.8.4.2 Noncircular Shear Surfaces	60
3.9 Conclusions	64
4. Variation of Back-Calculated Shear Strength and Slope Stability Assuming Infinite Slope Conditions	67
4.1 Introduction	67
4.2 Description of Profiles in Pigmy Basin	69
4.3 Variability in Shear Strength from Back Analyses	71
4.4 Variability in Stability from Forward Analyses	73
4.5 Conclusions	80
5. Spatial Variability of Shear Strength in the Lateral Direction	81
5.1 Introduction	81
5.2 The Scale of Fluctuation	82
5.3 Evaluation of the Scale of Fluctuation	82



5.3.1 Correlation Coefficients	84
5.3.1.1 Formal Description and Properties of the Correlation Coefficient	84
5.3.1.2 Calculations for the Correlation Coefficient	85
5.3.1.3 Computer Program	93
5.3.2 Scale of Fluctuation Models	93
5.3.3 Results	95
5.3.4 Calculation of the Autocorrelation Distance	99
5.4 Propagation of Errors Associated in Calculating the Scale of Fluctuation	102
5.4.1 Sources of Error	103
5.4.2 Monte Carlo Simulation	104
5.4.3 Results	106
5.5 Conclusion	110
6. Characterizing Stability along the Length of an Irregular Slope	112
6.1 Introduction	112
6.2 Slope Stability	113
6.3 Cross-Section C-C	113
6.4 Searching Method Restricting Lateral Coordinate of the Center of the Circle	113
6.4.1 Description of Search Method	116

6.4.2 Results for Searching Method Restricting Lateral Coordinate of the Center of the Circle	121
6.5 Searching Method with Shear Surface Restricted to Pass Beneath the Center Point	124
6.5.1 Cohesionless Soil	127
6.5.2 Cohesive and Frictional Soil	136
6.6 Conclusion	137
7. Summary, Conclusions, and Recommendations for Future Work	141
7.1 Summary and Conclusions	141
7.2 Recommendations for Future Work	143
Appendix A Back-Calculated Nonlinear Shear Strength "Resistance" Envelope	145
A.1 Introduction	145
A.2 Variables	147
A.3 Stability Analysis	151
A.4 Methodology	151
A.4.1 Determine Combinations of $c'$ and $\phi'$ Which Produce a Factor of Safety Equal to One	Error! Bookmark not defined.
A.4.2 Determine Minimum Shear Strength Envelope	152
A.4.3 Determine Normalized Nonlinear "Resistance Envelope"	156

<b>A.5 Verification of Dimensionless Variables</b>	<b>158</b>
<b>A.5.1 Effect of Slope Height</b>	<b>158</b>
<b>A.5.2 Unit Weight</b>	<b>163</b>
<b>A.6 Illustrative Example Calculations</b>	<b>167</b>
<b>A.6.1 Forward Analyses</b>	<b>167</b>
<b>A.6.2 Back Analysis</b>	<b>169</b>
<b>A.7 Conclusion</b>	<b>171</b>
<b>Appendix B Source Code for Computer Program VARREDF</b>	<b>172</b>
<b>Appendix C Users Manual For VARREDF</b>	<b>175</b>
<b>C.1 Input</b>	<b>175</b>
<b>C.2 Output</b>	<b>175</b>
<b>References</b>	<b>178</b>
<b>Vita</b>	<b>182</b>

## List of Tables

Table 2.1 Autocorrelation distances for shear strength in the vertical direction (after Lacasse and Nadim, 1996).....	18
Table 2.2 Autocorrelation distances for shear strength in the horizontal direction (after Lacasse and Nadim, 1996).....	20
Table 2.3 Multibeam echo sounder system characteristics.....	22
Table 3.1 Results for verification of dimensionless parameters for Case 1 - constant strength cohesive soil.....	36
Table 3.2 Results for verification of dimensionless parameters for Case 2 - cohesion increasing linearly with depth .....	42
Table 3.3 Results for verification of dimensionless parameters for Case 3 - friction angle is constant.....	56
Table 5.1 Example input of lateral coordinates and the corresponding shear strength.....	88
Table 5.2 Shear strength pairs put into bins corresponding to distances between lateral coordinates.....	89
Table 5.3 Expected values of shear strength pairs for the second bin (20m - 40m).....	91
Table 5.4 Frequency distribution for the difference between the maximum and the minimum value of the scale of fluctuation for each of the 80 simulations.....	107
Table A.1 Table showing that unique values for the dimensionless quantities $c'/(\gamma H)$ and $\tan \phi'$ are necessary to produce a factor of safety equal to unity.....	150
Table A.2 Combinations of $c'$ and $\phi'$ and the corresponding factors of safety used in the analyses.....	153
Table C.1 Data input format for VARREDF.....	176
Table C.1 Data output format for VARREDF.....	177

## List of Figures

Figure 2.1 Nonlinear shear strength behavior for London clay(after Bishop et al. 1965).....	10
Figure 2.2 Variation of shear strength in the vertical direction measured using a vane shear device on cored samples (after Bryant et al. 1983).....	14
Figure 2.3 Variation of shear strength in the vertical direction (after Bea et al. 1983).....	15
Figure 2.4 Variation of undrained shear strength in the vertical direction (from drop cores taken in the Gulf of Mexico, Bryant et al., 1995).....	17
Figure 2.5 Geometry of footprints for Sea Beam .....	24
Figure 3.1 Variables defining slope geometry with thin seam.....	29
Figure 3.2 Slope and shear strength variables for Case 1 - constant strength cohesive soil.....	32
Figure 3.3 Results for the location of the critical shear strength for Case 1 - constant strength cohesive soil with $\beta = 15$ degrees and $c_{seam}/c_{slope} = 1/2$ ..	37
Figure 3.4 Slope and shear strength variables for Case 2 - cohesion increases linearly with depth .....	40
Figure 3.5 Combinations of $t/H$ and $d/H$ where seam effects stability for Case 2 - cohesion increases linearly with depth with $\beta = 15$ degrees .....	44
Figure 3.6 Effect of slope angle on the combinations of $t/H$ and $d/H$ where seam effects stability for Case 2 - cohesion increases linearly with depth with $c_{seam}/(c_z*d) = 1/2$ .....	46
Figure 3.7 Effect of slope angle on the combinations of $t/H$ and $d/H$ where seam effects stability for Case 2 - cohesion increases linearly with depth with $c_{seam}/(c_z*d) = 1/3$ .....	47
Figure 3.8 Effect of shape of shear surface on the combinations of $t/H$ and $d/H$ where seam effects stability for Case 2 - cohesion increases linearly with depth with $\beta = 30$ degrees and $c_{seam}/(c_z*d) = 1/3$ .....	49

Figure 3.9 Comparison of factors of safety using circular and noncircular shear surfaces for Case 2 - cohesion increases linearly with depth with $\beta = 15$ degrees and $c_{seam}/(c_z \cdot d) = 1/2$ .....	52
Figure 3.10 Slope and shear strength variables for Case 3 - friction angle is constant.....	54
Figure 3.11 Combinations of $t/H$ and $d/H$ where seam effects stability for Case 3 - friction angle is constant with $\beta = 15$ degrees.....	58
Figure 3.12 Combinations of $t/H$ and $d/H$ where seam effects stability for Case 3 - friction angle is constant with $\beta = 30$ degrees.....	59
Figure 3.13 Effect of shape of shear surface on the combinations of $t/H$ and $d/H$ where seam effects stability for Case 3 - friction angle is constant with $\beta = 15$ degrees and $c_{seam}/(c_z \cdot d) = 1/3$ .....	61
Figure 3.14 Effect of shape of shear surface on the combinations of $t/H$ and $d/H$ where seam effects stability for Case 3 - friction angle is constant with $\beta = 15^\circ$ and $c_{seam}/(c_z \cdot d) = 1/2$ .....	62
Figure 3.15 Effect of shape of shear surface on the combinations of $t/H$ and $d/H$ where seam effects stability for Case 3 - friction angle is constant with $\beta = 15$ degrees and $c_{seam}/(c_z \cdot d) = 1/3$ .....	63
Figure 4.1 Bathymetry chart of Pigmy Basin in the Gulf of Mexico, with 50 meter contours.....	68
Figure 4.2 Plan view of cross-sections A-A, B-B, and C-C in Pigmy Basin with 20 meter contours.....	70
Figure 4.3 Profile of cross-sections A-A, B-B, and C-C.....	72
Figure 4.4 Variation of $\phi'$ along cross-section A-A assuming a factor of safety equal to unity.....	74
Figure 4.5 Variation of $\phi'$ along cross-section B-B assuming a factor of safety equal to unity.....	75
Figure 4.6 Variation of $\phi'$ along cross-section C-C assuming a factor of safety equal to unity.....	76
Figure 4.7 Variation of factor of safety along cross-section A-A assuming cohesionless soil.....	77
Figure 4.8 Variation of factor of safety along cross-section B-B assuming cohesionless soil.....	78

Figure 4.9 Variation of factor of safety along cross-section C-C assuming cohesionless soil.....	79
Figure 5.1 Simple triangular correlation structure.....	83
Figure 5.2 Example of the cross-sectional geometry and shear strengths used in the analyses.....	86
Figure 5.3 Correlation coefficient versus normalized distance.....	94
Figure 5.4 Correlation coefficients versus length for cross-section C-C in Pigmy Basin, Gulf of Mexico.....	97
Figure 5.5 Comparison of four different correlation functions to the correlation coefficients using a scale of fluctuation equal to 275 m.....	98
Figure 5.6 Results of the calculated correlation coefficients and the exponential correlation function using a scale of fluctuation equal to 250 m, 325 m, and 400 m .....	100
Figure 5.7 Illustration of the determination of autocorrelation distance from the scale of fluctuation.....	101
Figure 5.8 Frequency distribution for the scale of fluctuation based on 80 Monte Carlo simulations.....	109
Figure 6.1 Soil densities for drop cores 4 and 8 in Pigmy Basin (after Bryant et al., 1995).....	114
Figure 6.2 Cross-section C-C with horizontal extensions .....	115
Figure 6.3 Example of search method restricting lateral coordinate of the center of the circle.....	117
Figure 6.4 Twenty-six vertical lines spaced 152.4 meter apart used for restricting the circular shear surface centers .....	118
Figure 6.5 Example of subdividing radius around local minimum factor of safety.....	120
Figure 6.6 Comparison of factors of safety using infinite slope and restricted center for cross-section C-C assuming cohesionless soil.....	122
Figure 6.7 Figurative example of result for the variation in the factor of safety for cross-section C-C for the search method using restricted centers .....	123
Figure 6.8 Example of accepted and rejected shear surfaces based on criteria restricting location of shear surface relative to lateral coordinate of center.....	126

Figure 6.9 Variation in factors of safety with location using location (infinite slope) or center point (circle) using infinite slope, restricted center, and restricted center and restricted shear surface extent for cross-section C-C assuming cohesionless soil .....	128
Figure 6.10 Relationship between subtended angle ( $\theta$ ) and the slope angle ( $\beta$ )...	129
Figure 6.11 Relationship between subtended angle ( $\theta$ ), the slope angle ( $\beta$ ), and the relative slide depth $d/l$ .....	130
Figure 6.12 Comparison of circle crossing beneath center with circle not passing beneath center.....	132
Figure 6.13 Influence of depth to length of circle on the factor of safety for cohesionless soil .....	134
Figure 6.14 Minimum factor of safety for slope using results from infinite slope and the modified search method restricting the lateral extent of the circle	135
Figure 6.15 Variation in factor of safety with the center point (circle) using the restricted center and restricted shear surface extent along cross-section C-C for a soil containing both friction and cohesion.....	138
Figure 6.16 Results showing how the addition of cohesion smoothes the variation in the factor of safety along an irregular slope.....	139
Figure A.1 Representation of resistance envelope suggested by Casagrande (1950)	Error! Bookmark
Figure A.2 Slope geometry and variables.....	148
Figure A.3 Linear shear strength envelopes corresponding to $F = 1.00$ and $H = 30.5$ m for $\gamma = 15.7$ kN/m <sup>3</sup> and $\beta = 30$ degrees.....	154
Figure A.4 Minimum shear strength envelope for $H = 30.5$ m, $\gamma = 15.7$ kN/m <sup>3</sup> and $\beta = 30$ degrees .....	155
Figure A.5 "Resistance envelope" for $H = 30.5$ m, $\gamma = 15.7$ kN/m <sup>3</sup> and $\beta = 30$ degrees .....	157
Figure A.6 Linear shear strength envelopes corresponding to $F = 1.00$ and $H = 12.2$ m for $\gamma = 15.7$ kN/m <sup>3</sup> and $\beta = 30$ degrees.....	159
Figure A.7 Linear shear strength envelopes corresponding to $F = 1.00$ and $H = 106.7$ m for $\gamma = 15.7$ kN/m <sup>3</sup> and $\beta = 30$ degrees.....	160
Figure A.8 Minimum shear strength envelopes for each slope height for $\gamma = 15.7$ kN/m <sup>3</sup> and $\beta = 30$ degrees .....	161



Figure A.9 "Resistance envelope" independent of slope height for $\gamma = 15.7 \text{ kN/m}^3$ and $\beta = 30$ degrees.....	162
Figure A.10 Minimum shear strength envelopes for each unit weight for $H = 106.7$ m and $\beta = 30$ degrees.....	164
Figure A.11 "Resistance envelope" independent of unit weight for $H = 106.7$ m and $\beta = 30$ degrees.....	165
Figure A.12 "Resistance Envelope" for $\beta = 30$ degrees.....	166
Figure A.13 Resistance envelope and linear envelope for forward analysis example	168
Figure A.14 Resistance envelope and linear envelope for back analysis example	170

## **1. Slope Stability in Deep Water**

Slope stability is a problem in deep water. Bathymetry data from Pigmy Basin in the Gulf of Mexico reveals slopes steeper than 50 degrees are present and suggests that slope stability may be a problem. In fact, samples recovered from piston cores indicate soil may be slumping from the basin walls onto the basin floor. The slumping process raises questions about overall stability in the region. In particular, instability is a problem for oil production facilities located in the Gulf of Mexico. Foundations for oil platforms may be located on or near slopes. In addition, pipelines associated with the production of oil may have routes which bring them on or near slopes. Both of these underwater facilities are subject to damage from landslides associated with instability. In order to assess stability several variables used in stability analyses must be quantified. These variables include shear strength, stratigraphy, and bathymetry.

Shear strength information for soil in deep water is both difficult and expensive to acquire. Standard sampling techniques used on land cannot be employed in deep water. Specialized techniques and tools developed for the purpose of recovering samples in deep water are costly. Pressure relief caused by bringing samples to the surface may cause cavitation, which, in turn, may cause disturbance in the sample. A discussion of the factors which make obtaining shear strength information in the offshore environment difficult and expensive is given by Hoeg (1983), Richards and Zuidberg (1986), and Doyle (1994).

An alternative to measuring shear strength properties directly is to infer shear strength through back-calculation. Shear strengths can be back-calculated if slope stability is known. In back-calculation, also termed “back analyses”, the factor of safety is assumed to be known, i.e. the factor of safety is assumed to be one. Stability calculations are performed and the shear strength required to produce a factor of safety equal to unity is determined. Back-calculation of shear strength in this manner avoids the difficulties and expense of acquiring samples for laboratory testing. However, back-calculations can be difficult and may lead to inconclusive results. The advantages and disadvantages of back-calculating shear strength are discussed further in Chapter 2.

Shear strength varies in the vertical direction. Variation of shear strength in the vertical direction is shown in Chapter 2. In addition, a series of deterministic, parametric stability studies was performed to understand how variability of shear strength in the vertical direction effects stability. Variability of shear strength in the vertical direction was modeled by introducing a thin seam of weak material within an otherwise uniform slope. The effects from the location of the seam within the slope, the thickness of the seam and the shear strength of the seam relative to the shear strength of the rest of the slope were quantified. Both “undrained” and “drained” shear strength representations were used for the soils. Also, both circular and noncircular shear surfaces were considered and compared in the analyses. Results are presented in Chapter 3.

Shear strength also varies in the lateral direction. Variability of shear strength in the lateral direction is shown in Chapter 2. The variability of both shear strength and stability along three cross-sections was examined using infinite slope analysis procedures for three irregular slope profiles obtained from bathymetry data for Pigmy Basin in the Gulf of Mexico (Bryant et al., 1995). The results are shown in Chapter 4

Results from the investigation of variability in shear strength along the length of a slope were used to determine the correlation structure of shear strength in the lateral direction. The results for the correlation structure of shear strength in the lateral direction are presented in Chapter 5. Also presented in Chapter 5 is an examination of the effect from the uncertainty in the method used to obtain the slope profile on the outcome of the correlation structure. A random error was associated with the method used to obtain the slope profile from the bathymetry data. The effects of this error on the variability of the back-calculated shear strength in the lateral direction was modeled using Monte Carlo simulations.

The variation in stability for one of the slopes profiles in Pigmy Basin analyzed in Chapter 4 was reevaluated using a method of slices and circular shear surfaces. The results are presented in Chapter 6. A comparison between the results previously obtained using infinite slope procedures and the results obtained using circular shear surfaces is made. Based on the results of the comparison, a method for systematically determining the minimum factor of safety along the cross-section of an irregular slope was developed. The method varies slightly depending on whether the soil has either

cohesive and frictional properties or is cohesionless. The method and results are presented in Chapter 6.

A summary of this thesis is presented in Chapter 7. In addition, conclusions based on the work presented in this thesis and recommendations for future work are also presented in Chapter 7.

## **2. Variables and Uncertainties in Sea-Floor Stability and Shear Strengths**

### **2.1 Introduction**

Shear strength is one of the most important properties for assessing slope stability, and it may be difficult and expensive to measure directly in deep water. Difficulties in measuring shear strength of soils in deep water can be avoided by using back analyses techniques. An overview of back-calculating shear strengths along with some advantages, disadvantages, and limitations associated with the approach is presented in this chapter.

The variability of shear strength is discussed in this chapter. Spatial variability of shear strength in the vertical and lateral directions can be investigated through soil borings or inferred either through geophysical methods or from existing stability conditions. Variability of shear strength in the vertical and lateral directions is also obtained from cone penetration resistance measurements.

Bathymetry is an important parameter needed for assessing slope stability. The uncertainty in bathymetry measurements is discussed in this chapter. Bathymetry is usually measured using acoustic waves. Uncertainty is inherent in the measurements of bathymetry taken by sonar due to resolution and accuracy constraints.

## 2.2 Back Analysis

Slope failures provide a useful opportunity to back-calculate shear strength. In order to back-calculate shear strength, a single value or range of values for the factor of safety must be known. In general, the factor of safety is assumed to be equal to one for a failed slope. Shear strength can then be determined through back analyses using the information regarding the factor of safety. The factor of safety is defined by,

$$F = \frac{s}{\tau} \quad (1)$$

where  $F$  is the factor of safety,  $s$  is the available shear strength, and  $\tau$  is the shear strength required for static equilibrium.

The process of back-calculating shear strengths begins by assuming a value for shear strength. Stability analyses are performed and the factor of safety is calculated. The shear strength parameters that will result in the desired factor of safety (unity), for the shear surface used in the analyses, can be calculated using the values for both the calculated factor of safety,  $F$  and the assumed shear strength parameters,  $c_{\text{assumed}}$  and  $\phi_{\text{assumed}}$  by

$$c_{F=1} = \frac{c_{\text{assumed}}}{F} \quad (2)$$

$$\phi_{F=1} = \frac{\phi_{\text{assumed}}}{F} \quad (3)$$

If stability is reanalyzed using  $c_{F=1}$  and  $\phi_{F=1}$  the resulting factor of safety will be unity.

Calculating shear strength through back analyses has both advantages and

disadvantages compared to measuring shear strength directly in either the laboratory or in the field. A procedure which can be used to back-calculate shear strength is presented in Appendix A from work previously performed by Casagrande (1950).

#### **2.2.1 Advantages of Back Analyses**

Duncan and Stark (1992) discuss the advantages of back-calculating shear strength as opposed to using conventional laboratory or field testing methods to determine shear strength. They point out that the problem of sample disturbance is avoided, scale effects in the laboratory, such as sample size and length of the shear surface do not influence results, and times to failures are typically not hurried as they might be in the laboratory. Duncan and Stark also site several cases where back-calculated shear strengths are in good agreement with results from laboratory testing. However, they indicate that in order for the shear strengths from back analyses and laboratory testing to be in good agreement the soil conditions must be simple and conditions at failure must be accurately known. Advantages of using back analyses as opposed to direct measurements to determine shear strength make back-calculations of shear strength especially attractive for slopes in deep water.

#### **2.2.2 Disadvantages of Back Analyses**

Disadvantages of back-calculating shear strengths include effects of assumptions required to make the problem statically determinate (mechanics of method of slices procedures), the existence of more unknown values ( $c$  and  $\phi$ ) than available



equations (equation for factor of safety), and quantifying the uncertainties caused by using two-dimensional analyses for three-dimensional problems. Each of these difficulties will be discussed in the following sections.

#### 2.2.2.1 Mechanics

Method of slices used to solve slope stability problems require that assumptions be made regarding one or more of the unknown forces and their locations in order for the problem to be made statically determinant. A thorough discussion into these two issues is beyond the scope of this paper, however, a brief discussion on these matters follows.

Fredlund and Krahn (1977) performed comparative analyses using six different method of slices techniques used for stability analyses. Variations in the calculated factor of safety were determined using the six different techniques. Fredlund and Krahn compared factors of safety calculated by the ordinary method, simplified Bishop method, Spencer's method, Janbu's simplified method, Janbu's rigorous method and the Morgenstern-Price method. The authors found that for a simple slope there was an eight percent difference between the highest and lowest value of the factor of safety and for a more complex slope there was an 11 percent difference between the highest and lowest value of the factor of safety. Similar values have been reported by Duncan and Wright (1980). Once the mechanics have been solved and a method to perform the stability analyses has been selected, a separate problem exists which involves having too many unknown shear strength parameters to solve for using the available slope stability equations.

#### 2.2.2.2 Number of Unknown Strength Parameters

The shear strength expressed in terms of the Mohr-Coulomb equation and total stresses is given by

$$s = c + \sigma \tan \phi \quad (1)$$

where  $s$  is the shear strength,  $c$  is the cohesion,  $\sigma$  is the total normal stress, and  $\phi$  is the angle of internal friction. Similarly the shear strength in terms of effective stress is given by

$$s = c' + \sigma' \tan \phi' \quad (2)$$

where  $c'$  is the effective cohesion,  $\sigma'$  is the effective normal stress, and  $\phi'$  is the effective stress angle of internal friction.

In general, a problem associated with back-calculating shear strengths lies in the fact that there is only one factor of safety associated with two unknown quantities  $c$  and  $\phi$  (or  $c'$  and  $\phi'$ ). Thus, with the exception of two special cases, cohesion equal to zero or friction angle equal to zero ( $c = 0$  or  $\phi = 0$ ), the problem requires that two values be solved for one factor of safety.

The problem of an excess of unknown values is further complicated if the shear strength envelope is nonlinear. Shear strengths of many soils are more accurately represented by a nonlinear shear strength envelope, particularly if the range of stress is large. Laboratory measurements presented by Bishop, Webb, and Lewin (1965) show such a nonlinear trend for shear strength. Figure 2.1 shows a nonlinear shear strength envelope for London clay under drained triaxial compression. More recent work performed by Stark and Eid (1994) indicate that the drained residual envelopes for

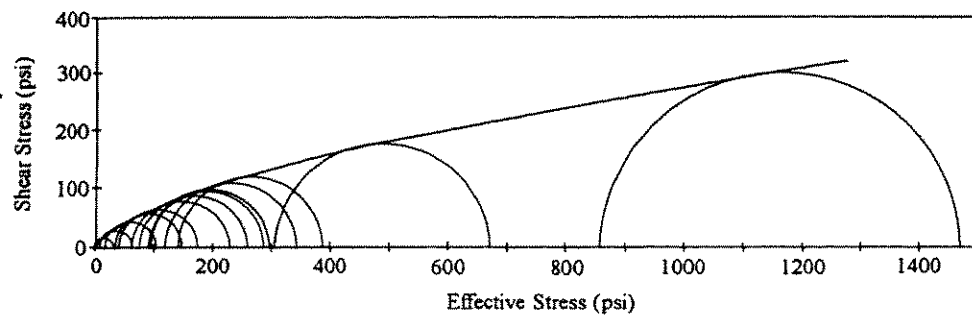


Figure 2.1 Nonlinear shear strength behavior for London clay(after Bishop et al. 1965)

several clays and shales are nonlinear. Duncan et al. (1978) suggest representing a nonlinear shear strength envelope for effective stress in the form,

$$s = c' + \sigma' \tan \left[ \phi'_0 + \Delta\phi' \ln \left( \frac{\sigma'}{\sigma^*} \right) \right] \quad (2)$$

where  $\sigma^*$  is a “normalizing” effective (reference) stress,  $\Delta\phi'$  is the change in the effective stress friction angle due to the change in effective normal stress and  $\phi'_0$  is the effective stress secant friction angle when the effective normal stress is equal to the normalizing stress. If such a nonlinear envelope is used to describe the shear strength, there are three unknown shear strength parameters:  $c'$ ,  $\phi'_0$  and  $\Delta\phi'$ . There is again a problem back-calculating shear strength because there are three unknown values and only one factor of safety.

Duncan and Stark (1992) attempted to back-calculate unique values for shear strength parameters  $c'$  and  $\phi'$  from a series of slope stability failures. The slope failures were located in the same geographic region and occurred within the same soil type. In theory, a unique combination of  $c$  and  $\phi$  can be back-calculated if the location of the shear surface within the slope is known. However, Duncan and Stark indicate that knowledge regarding the location of the failure surface does not help resolve the problem of too many unknowns because of effects of progressive failure and heterogeneity of shear strength within the slope. In conclusion, Duncan and Stark determined that back-calculating unique values for shear strength parameters  $c'$  and  $\phi'$  is not possible for most

cases and suggest that a value be assumed for  $\phi'$ , based on judgment and experience, and then a corresponding value for  $c'$  can be back-calculated.

#### 2.2.2.3 Three Dimensional Effects

Seed et al. (1990), Stark and Poeppel (1994), and Byrne et al. (1992) performed comparative analyses using both two-dimensional and three-dimensional slope stability analysis procedures. All three sets of investigators independently analyzed stability for Kettleman Hills landfill. Seed et al. determined it is possible that the maximum two-dimensional cross-section overestimated the factor of safety compared to the three-dimensional analyses in some cases. Byrne et al. determined the three-dimensional analyses produced higher values for the factor of safety than the two-dimensional analyses for some cases. Finally, Stark and Poeppel, using peak and residual shear strengths for different parts of the failure surface determined that in some cases the three-dimensional factor of safety is greater than the two-dimensional factor of safety and in other cases the two-dimensional factor of safety is greater than the three-dimensional factor of safety. From the findings of the three sets of researchers it remains unclear if a two-dimensional back analyses will overestimate or underestimate shear strength.

A probabilistic procedure which accounts for the effects of the uncertainty associated with the mechanics of the procedure of slices (Section 2.2.2.1) and two-versus three-dimensional effects on back-calculated shear strength is given by Gilbert et al. (1996). Gilbert et al. avoid the problem of the number of known quantities for one

factor of safety (Section 2.2.2.2) by assuming a range in values for the factor of safety to determine back-calculated shear strength parameters.

## **2.3 Variability of Shear Strength**

Variability of shear strength should be accounted for in evaluating stability in deep water. Shear strengths usually vary spatially in both the vertical and lateral directions. The following sections show the variability of shear strength in the vertical and lateral directions.

### **2.3.1 Variability of Shear Strength in the Vertical Direction**

Variation of shear strength in the vertical direction is perhaps more important for foundation design than it is for pipelines, especially if the foundation is a pile foundation which extends vertically versus pipelines which extend laterally. Figure 2.2 shows undrained shear strength as a function of depth, for an offshore soil in the Gulf of Mexico taken during leg 96 of the Deep Sea Drilling Project from Bryant et al. (1983). In general, the trend is for the shear strength to increase with increasing depth below the surface. However, large fluctuations of shear strength occur locally. For example, the data in Figure 2.2 show a sharp decrease in shear strength of more than a factor of two at a depth of about 56 meters. Such an abrupt change in shear strength may indicate a transition between two soil types.

The shear strength measurements shown in Figure 2.3 were reported by Bea et al. (1983). The data again show similar trends in the variation of undrained shear

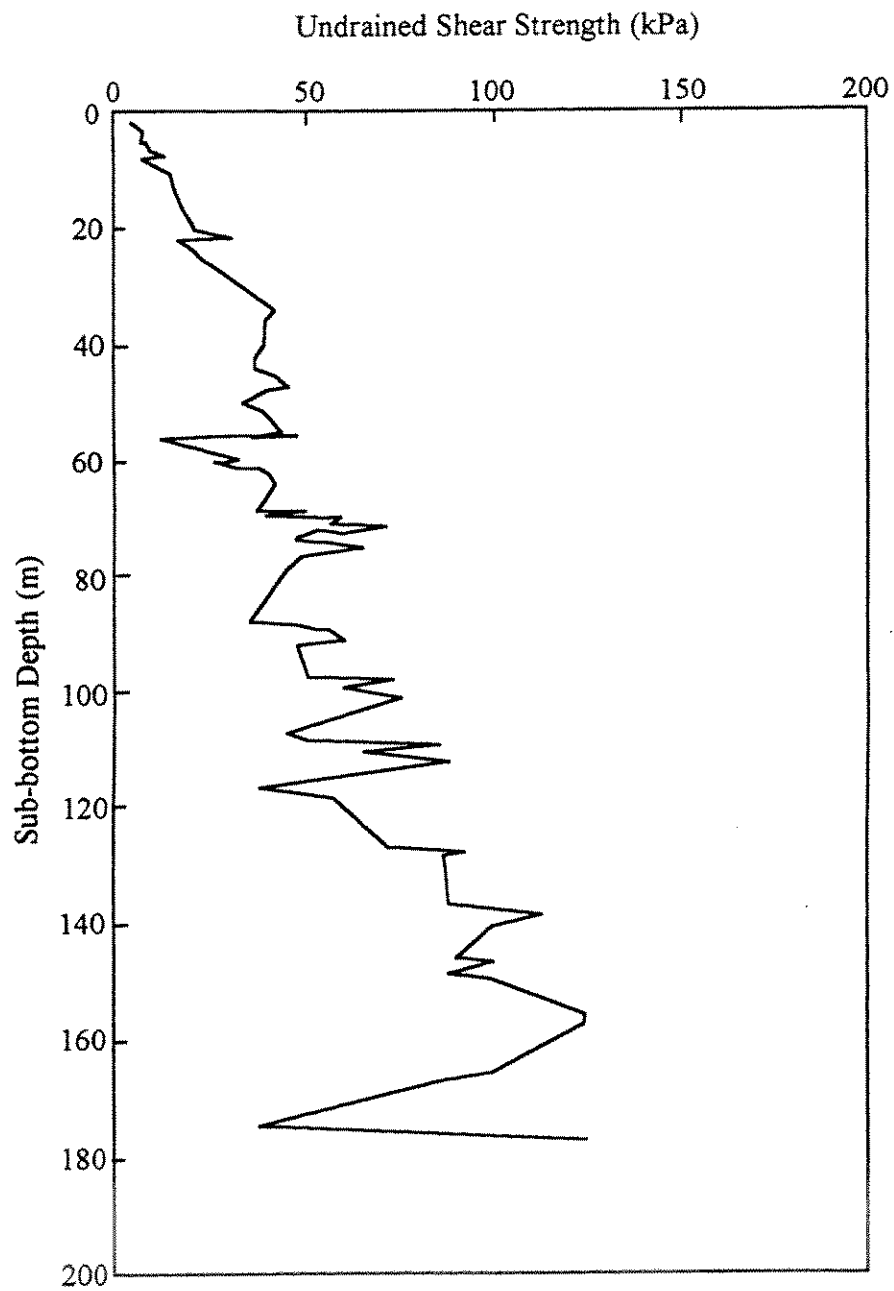


Figure 2.2 Variation of shear strength in the vertical direction measured using a vane shear device on cored samples (after Bryant et al. 1983)

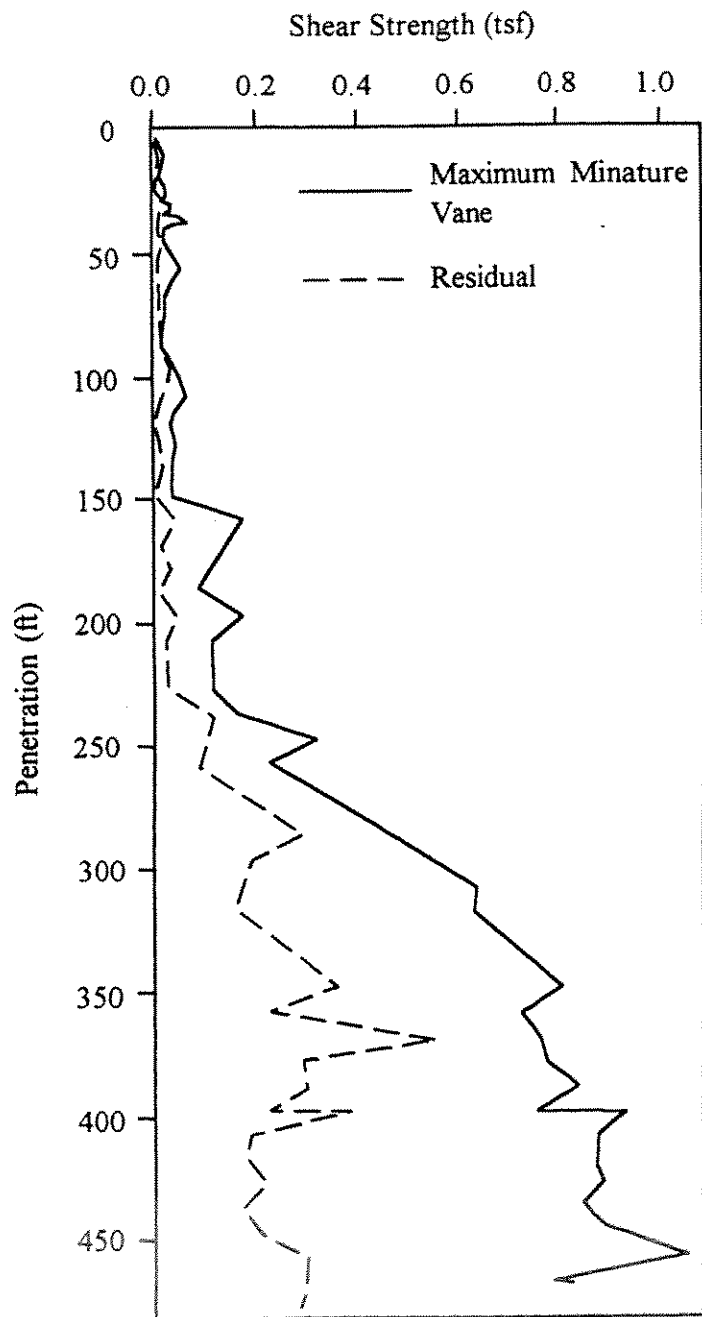


Figure 2.3 Variation of shear strength in the vertical direction (after Bea et al. 1983)



strength as a function of depth. Shear strength measurements in Figure 2.3 were performed for an offshore soil in the Mississippi delta. Again, the general trend is for the shear strength to increase with depth and for variability to occur at the local level.

Shear strength data are shown in Figure 2.4 from measurements taken using a vane shear device on a sample recovered from a drop core in Pigmy basin in the Gulf of Mexico from Bryant et al. (1995). Large variations of shear strength in the vertical direction can be seen shown in this figure over a distance of only three meters particularly at depths between 1.9 and 2.3 meters.

Figures 2.2 and 2.3 show variations in shear strength over a large range in depths while Figure 2.4 shows similar variation but at a much smaller scale. Thus, there are different scales of fluctuation depending upon the scale of the measurements. Variability of shear strength in the vertical direction can be quantified by a parameter such as the autocorrelation distance. The autocorrelation distance is an indicator of the distance in which a variable is correlated. The variable in this case is shear strength. As an example, if the shear strength changes (increases or decreases) as the distance between two points increases then the correlation between the shear strength of the soil decreases as the distance between the points increases. If the autocorrelation distance is large, one would expect a smaller variation in shear strength over a given distance compared to the variation in shear strength if the autocorrelation distance was smaller. Shown in Table 2.1 are autocorrelation distances for shear strength in the vertical

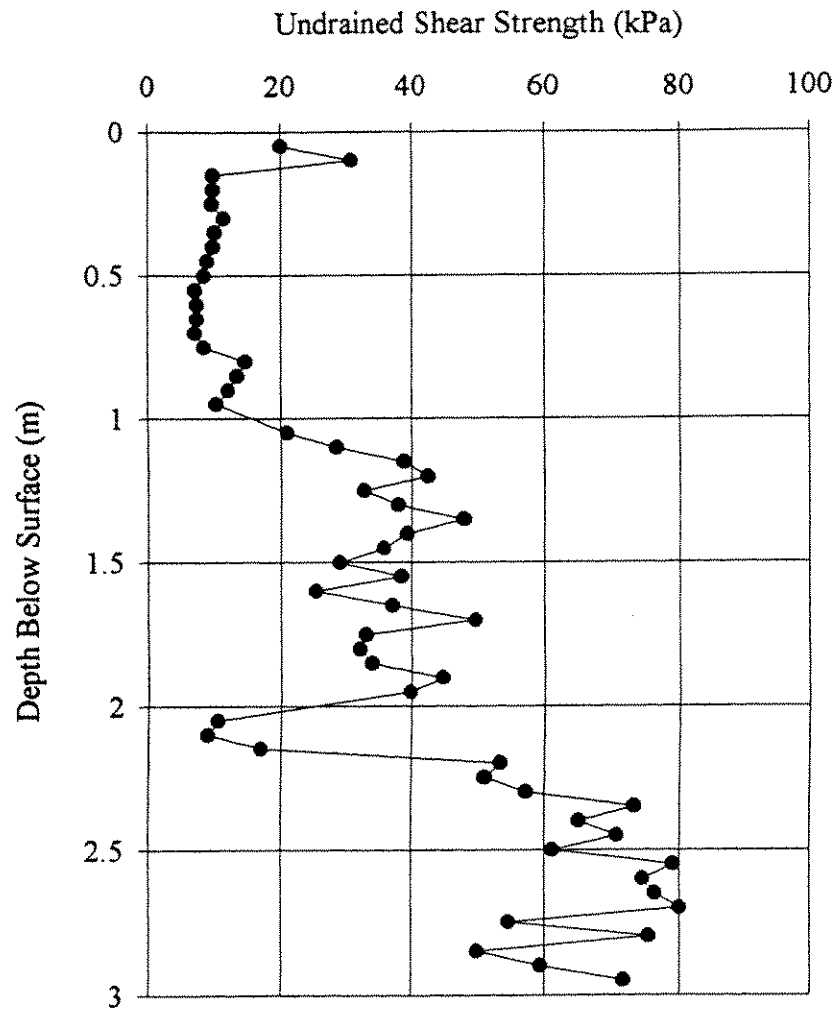


Figure 2.4 Variation of undrained shear strength in the vertical direction (from drop cores taken in the Gulf of Mexico, Bryant et al., 1995)

Table 2.1  
Autocorrelation distances for shear strength in the vertical direction (after Lacasse and Nadim ,1996)

Soil Type	Autocorrelation Distance (meters)	Reference
Clean sand	3	Alonzo and Krizek (1975)
Mexico Clay	1	Alonzo and Krizek (1975)
Clay	1	Vanmarcke (1977)
Sensitive Clay	2	Chiasson et al. (1995)
Silty clay	1	Lacasse and Lamballerie (1995)

direction which were summarized by Lacasse and Nadim (1996). Shear strength was inferred from the results of cone penetration tests

### **2.3.2 Variability of Shear Strength in the Lateral Direction**

Variation of shear strength in the lateral direction is perhaps more important for pipelines than it is for the design of foundations since pipelines cover significant lateral distances compared to most, but not all foundations. Soil adjacent to a boring may be expected to have similar properties to those measured on samples obtained from the boring. However, the soil in an adjacent valley or canyon some further distance away may have a completely different set of properties than the properties measured in the sample from the boring. Somewhere between the boring and the adjacent valley or canyon the soil properties change. The change or changes in soil properties may be gradual or abrupt. Table 2.2 indicate autocorrelation distances for shear strength (from cone penetration tests) in the lateral direction for several offshore soils and a clay from work summarized by Lacasse and Nadim (1996). The results shown in Tables 2.1 and 2.2 indicate spatial variability of shear strength exists in both the vertical and lateral directions and that over a short distance a higher degree of variability in shear strength would be expected in the vertical direction.

### **2.4 Uncertainty in Bathymetry Measurements**

On land slope geometry is generally considered known and with low uncertainty.

Technology has existed for many years that can and is used to acquire

Table 2.2  
Autocorrelation distances for shear strength in the horizontal direction (after Lacasse  
and Nadim, 1996)

Soil Type	Autocorrelation Distance (meters)	Reference
Offshore soils	30	Høeg and Tang (1976); Tang (1979)
Offshore sand	14-38	Keaveny et al. (1989)
Silty clay	5-12	Lacasse and Lamballerie (1995)

accurate measurements of slope geometry (topography). The accuracy possible for measuring slope geometry on land far exceeds the resolution required for stability analyses given the uncertainties in measuring other parameters such as shear strength and pore water distribution. In contrast, measurement of bathymetry in deep water can have uncertainties not normally associated with measurements of slope geometry on land. Because of the uncertainty in bathymetry measurements in deep water there is greater uncertainty in stability in deep water than on land.

Bathymetry in deep water is measured by acoustical soundings. The two devices most commonly used to measure bathymetry in deep water are Sea Beam and SeaMARC II. Information about the two devices including the manufacturer of the devices is presented in Table 2.3 (after Tyce, 1986). A thorough description of Sea Beam is given by de Moustier and Kleinrock (1986), and for Sea Beam and SeaMARC II by Tyce (1986), and Davis et al. (1986) among others.

Sea Beam is a hull mounted multibeam echo sounder which produces bathymetry maps in real time. A multibeam echo sounder uses a series of emitters and receivers to measure bathymetry. Sea Beam has 20 emitters. The area, or "footprint," from the 20 transmitters is a single beam  $2\frac{2}{3}$  degrees wide along (parallel to) the track of the ship and 54 degrees wide across (perpendicular to) the track of the ship. The transmitting beam is adjusted for the pitch of the ship and is orientated such that the sonar pulse is released in the vertical direction. The receiving beams form 16 discrete beams 20 degrees wide along-track and  $2\frac{2}{3}$  degrees wide across-track. The receiving

Table 2.3  
Multibeam echo sounder system characteristics

	Sea Beam	SeaMARC II
Date introduced	1976	1982
Manufacturer	General Instruments Corporation	Hawaii Institute of Geophysics and International Submarine Institute
Tow depth	Hull mounted	50 - 100 m
Water depths	> 10 km	> 10 km
Cross track resolution (5 km water depth)	14 m	5 m
Along track resolution (5 km water depth)	233 m	175 m
Bathymetry accuracy (5 km water depth)	150 m	10 - 50 m

beam is 20 degrees along-track to account for a  $\pm 10$  degree pitch of the ship at the time of reception of the return beam, i.e. the receiving beam is not adjusted for the pitch of the ship. Figure 2.5 illustrates the geometry of the beam footprints. Figure 2.5 is only meant as an indication of the overall geometry. The actual footprints are elliptical in shape and the size of the footprint increases the further the footprint is towards the outer edge. SeaMARC II is a shallow towed multibeam echo sounder which collects both bathymetry and long range imagery information. This device uses the same technology to measure bathymetry.

The return signal from each of Sea Beam's 20 emitters is picked up by the 40 receivers which form 16 discrete footprints. From this information the maximum elevation of the seafloor can be determined by measuring the travel time of the wave from the source to the bottom and back to the receiver and knowing the speed of compression waves in sea water. However, the location of the maximum seafloor elevation within each footprint can not be determined since each footprint is composed of one wave. Thus, as the seafloor becomes increasingly deeper there becomes an increasingly larger possible area in which the measured maximum seafloor elevation may be located. In simple terms, there is only one data point measured from each of the 16 footprints on the seafloor for each set of impulse signals emitted. Each measured data point is associated with a latitude and longitude as well as an elevation. Using a series of these points contours are drawn and the bathymetry charts made. Bathymetry charts are made in the same fashion by acoustical measurements taken by SeaMARC II.



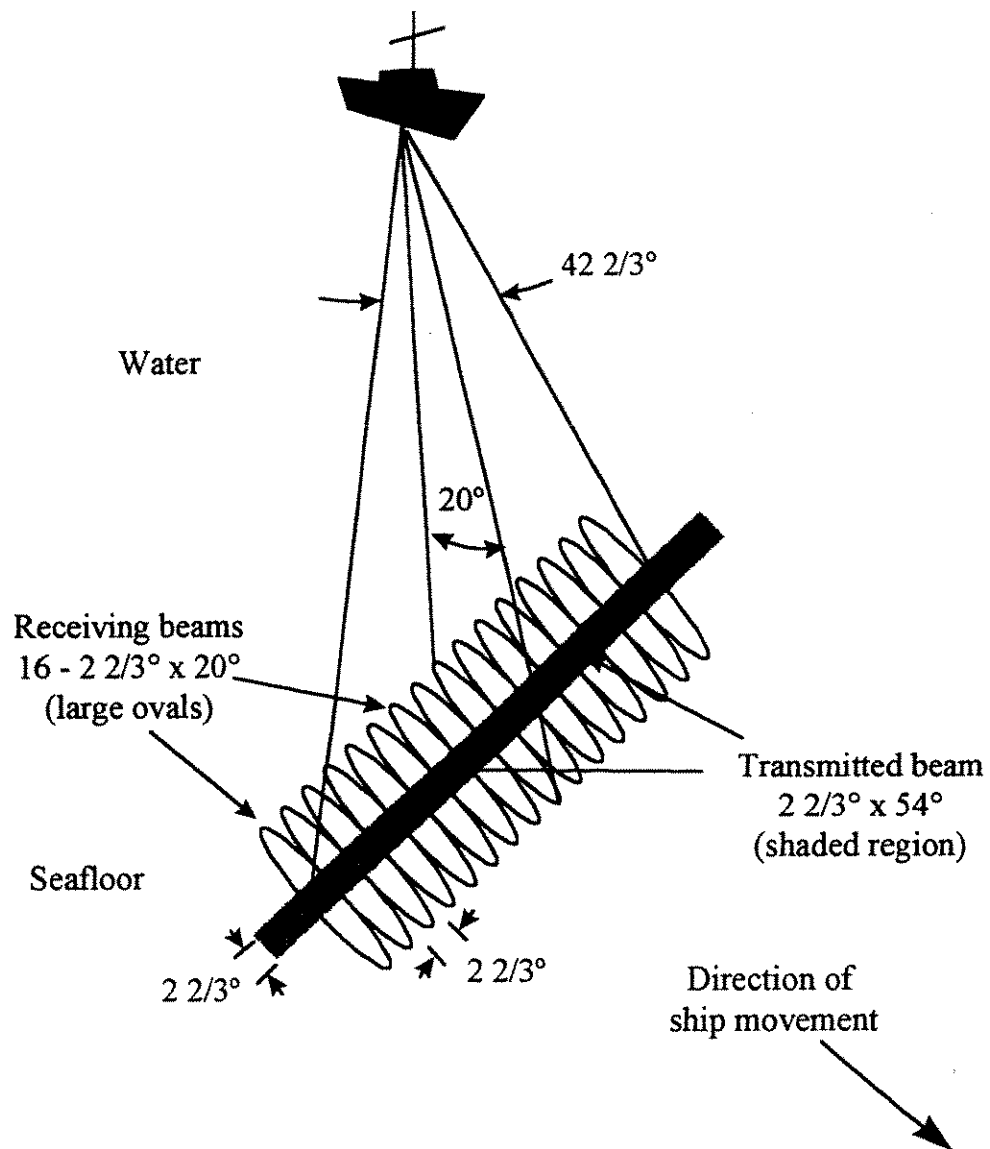


Figure 2.5 Geometry of footprints for Sea Beam

The primary difference between how bathymetry information is determined using Sea Beam and SeaMARC II is in the number of receiving beams. SeaMARC II uses one pair of receivers to determine the angle which the transmitted beam is reflected from the sea floor as compared to the 40 receivers used by Sea Beam for the same measurements. Because SeaMARC II uses only two receivers it is more prone than Sea Beam to errors associated with multiple echoes created on the sea floor.

The uncertainty in the location of the measured point within each footprint is described by the resolution in the measurement. The resolution in bathymetry data measured can be determined by the beam geometry and the length of the water column. The across-track and along-track resolution for Sea Beam and SeaMARC II are shown in Table 2.3 for a water depth of 5 km. There is also uncertainty associated with the depth of the measured data point which is described by accuracy. The accuracy of bathymetry measurements in 5 km of water is shown in Table 2.3 for both Sea Beam and SeaMARC II. The uncertainty in bathymetry data comes from the resolution and accuracy of bathymetry measurements.

## **2.5 Conclusions**

Two important parameters for the assessment of slope stability, shear strength and bathymetry, are discussed in this chapter. It was shown that back-calculations can be performed to obtain shear strength information which avoids the difficulties and expenses required to directly measure shear strength. However, back-calculating shear strength may lead to inconclusive results unless the soil conditions are either purely

cohesionless ( $c = 0$ ) or purely cohesive ( $\phi = 0$ ). Typical variability of shear strength in the vertical and lateral directions has been shown. The variability of shear strength in the vertical direction will be explored further in Chapter 3. Variability of shear strength in the lateral direction will be investigated in Chapters 4 and 5. Also, uncertainty in bathymetry information has been illustrated by examining resolution and accuracy in bathymetry measurements for two bathymetric measuring devices. Slope profiles obtained using bathymetry charts are used in Chapters 4, 5, and 6.

### 3. Effects of Variability of Shear Strength in the Vertical Direction on Slope Stability

#### 3.1 Introduction

The effects of variability of shear strength in the vertical direction on slope stability are examined in this chapter. Numerous sets of slope stability calculations were performed in which a thin, weak layer of soil in an otherwise uniform slope was used to represent variability of shear strength in the vertical direction. Parametric studies were performed where the depth to the seam, representation of shear strength ( $c = 0$ ;  $\phi = 0$ ), relative values of shear strength of the seam and the surrounding soil, slope angle, and shape of the assumed potential shear surface were varied to investigate the thickness of the seam required to just affect stability. Results are presented in dimensionless form in charts.

Three representations of shear strength were used. For the first two representations the shear strength was represented by cohesion with the angle of internal friction equal to zero. These two shear strength representations correspond to the familiar " $\phi = 0$ " case which is applicable to shear strength during undrained, "short-term" loading of saturated soils. For the third representation, shear strength was represented by an angle of internal friction with cohesion equal to zero. This " $c = 0$ " representation of shear strength is an appropriate representation of shear strength for drained, "long-term" loading

The effects of the assumed shape for the shear surface in the slope stability calculations was also investigated for two of the shear strength representations. Both circular and noncircular shear surfaces were used for this purpose. Slope angles of 15 degrees and 30 degrees were examined.

### 3.2 Variables

The variables defining the slope geometry are shown in Figure 3.1. Dimensions consist of the slope height ( $H$ ), the depth beneath the surface of the slope to the top of the seam ( $d$ ), and the thickness of the seam ( $t$ ). The inclination of the slope face is measured from the horizontal and designated as an angle,  $\beta$ . The seam was assumed to be parallel to the face of the slope. Thus,  $\beta$  also describes the inclination of the portion of the seam beneath the slope. The unit weight of soil, ( $\gamma$ ) was assumed to be constant and the same for both the seam and surrounding material.

### 3.3 Dimensionless Variables

Dimensionless variables were used to reduce the number of analyses that needed to be performed. The dimensionless variables used for the geometry are  $t/H$  and  $d/H$ . The validity of the dimensionless variables is investigated and the results presented in the following sections.

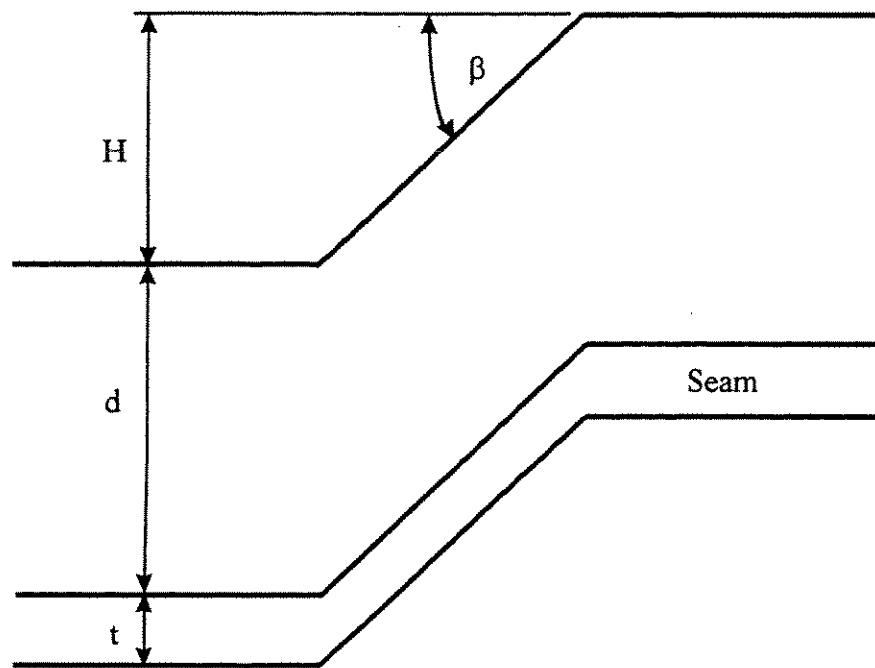


Figure 3.1 Variables defining slope geometry with thin seam

### 3.4 Stability Calculations

The slope stability program UTEXAS3 (Wright, 1991) was used to calculate the factor of safety. The factor of safety,  $F$ , was calculated by Spencer's (1967) limit equilibrium method of slices procedure and is defined as

$$F = \frac{s}{\tau} \quad (1)$$

where,  $s$  is the available shear strength of the soil and  $\tau$  is the shear strength required for static equilibrium.

All the slopes were assumed to be fully submerged. To account for submergence in the analyses buoyant unit weights were used and pore water pressures were set to zero.

### 3.5 Shear Strength

Three representations of shear strength were used for these studies. For the first representation of shear strength, the strength was represented entirely by cohesion and was assumed to be constant, independent of depth within a particular stratum. In the second case the shear strength was also represented by cohesion, but the cohesion was assumed to increase linearly with depth below the surface from a value of zero at the surface. In both cases the shear strength for the seam was assumed to be constant and different contrasting strengths were assumed for the seam. For the third representation of shear strength, the strength was represented entirely by "friction" and the angle of internal friction was assumed to be constant within each stratum. Different shear

strength contrasts (different friction angles) were used for the strength of the seam and the slope.

### 3.6 Case 1, Constant Strength Cohesion Soil

For this first case the strength of both the slope and the seam were assumed to be constant and represented by values of cohesion ( $\phi = 0$ ). The variables describing the slope geometry have previously been defined and are shown again in Figure 3.2 with the variables which describe the shear strength. The ratio of the cohesion in the seam to the cohesion of the surrounding soil,  $c_{\text{seam}}/c_{\text{slope}}$ , was used as a dimensionless parameter.

#### 3.6.1 Procedure for Detecting Stability with Thin, Weak Seam

For each slope the factor of safety of the slope without the seam was calculated first. For a purely cohesive soil the factor of safety can be expressed as

$$F = N_o \frac{c}{\gamma H} \quad (2)$$

where,  $N_o$  is a dimensionless stability number. The value of  $N_o$  depends on the slope angle and the depth to any significantly firmer stratum below the slope. If the slope angle is less than 53 degrees and the firm stratum is infinitely deep  $N_o$  has a value of 5.53 (Janbu 1954), i.e.

$$F = 5.53 \frac{c}{\gamma H} \quad (3)$$

If the slope is steeper than 53 degrees or the depth to a much stronger foundation layer is not infinite then the value of  $N_o$  depends upon both the slope angle and the depth to the



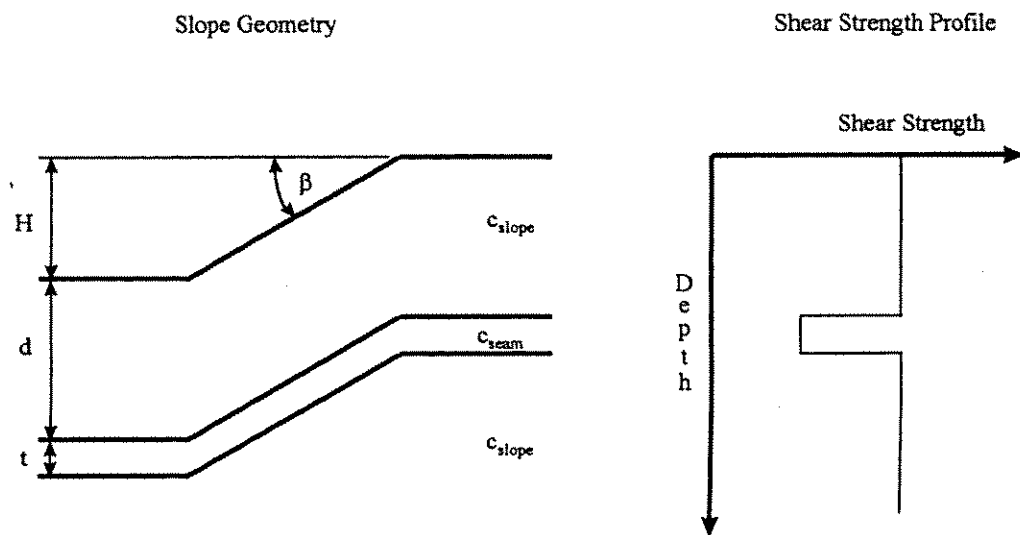


Figure 3.2 Slope and shear strength variables for Case 1 - constant strength cohesive soil

foundation layer. For the analyses presented in this chapter, slope angles less than 53 degrees were used and the depth to the foundation was considered infinite. Thus, Equation 3 was used to calculate the factor of safety for the slope without the seam.

For a slope without a significantly firmer stratum at depth, the most critical potential shear surface will tend to go infinitely deep. Thus, introducing a seam of lower shear strength soil will always effect stability since the potential shear surface will pass through the seam.

Of interest in this investigation was the minimum thickness of the seam required to cause the critical circular shear to pass into, but not below, the seam. For example, for a thin seam at a given depth the critical circle may pass through the seam and continue on to significant depths. However, as a progressively larger seam thickness is considered, there will exists a seam thickness such that the critical circle passes into, but not below, the seam. This seam thickness is termed the "critical" seam thickness for the given depth and shear strength conditions. The process of varying the seam thickness was repeated for various depths of the seam.

### **3.6.2 Verification of Dimensionless Parameters**

To verify the uniqueness of the various dimensionless parameters used, a series of stability calculations was performed where values for individual quantities in the dimensionless variables were changed. The effects from the changes of these variables on the dimensionless thickness ratio ( $t/H$ ) required to cause the critical shear surface to be confined to the seam were investigated. Values for the dimensionless parameters

( $d/H$  and  $c_{seam}/c_{slope}$ ) were kept constant while the magnitudes of the individual variables were changed. The variables  $H$ ,  $\gamma$ ,  $c_{seam}$  and  $c_{slope}$  were changed.

The verification calculations are summarized in Table 3.1. The values for  $d/H$  and  $c_{seam}/c_{slope}$  for each set of data were kept constant and the effects of the values of the changed parameters on the critical seam thickness were determined. The first set of values (first row) in the table represent the base parameters used for further comparison. For this set of geometry and shear strength parameters the critical seam thickness is 17.1 ft and  $t/H$  is 0.43. The second set of values (second row) illustrates the effect of increasing the slope height. The third set illustrates the effect of changing the magnitude of the shear strengths; and the fourth and final set illustrates the effect of changing unit weight. In all cases, the ratio  $t/H$  was unaffected by the changes in the values of the variables. The factor of safety shown in Table 3.1 for each case is different due to the changes in the values of the variables defining the factor of safety. However, the values for the dimensionless ratio,  $N_o = \frac{F}{c_{seam} / \gamma H}$  for all four cases are the same. These results verify that the absolute value of slope height, shear strength, and unit weight do not affect the critical seam thickness ratio,  $t/H$  as long as  $\frac{c_{seam}}{c_{slope}}$  is constant.

### 3.6.3 Results

Figure 3.3 shows the relationship between the dimensionless critical seam thickness,  $t/H$ , for different dimensionless depth factors,  $d/H$ . The results are for a slope

Table 3.1  
Results for verification of dimensionless parameters for Case 1 - constant strength  
cohesive soil

H ft	d ft	d/H	c <sub>seam</sub> psf	c <sub>slope</sub> psf	c <sub>seam</sub> / c <sub>slope</sub>	γ pcf	t ft	t/H	Factor of safety	F/ (c <sub>seam</sub> /γH)
40	20	0.5	400	800	0.5	100	17.1	0.43	1.106	11.06
120	60	0.5	400	800	0.5	100	51.7	0.43	0.369	11.07
40	20	0.5	700	1400	0.5	100	17.1	0.43	1.936	11.06
40	20	0.5	400	800	0.5	30	17.1	0.43	3.688	11.06

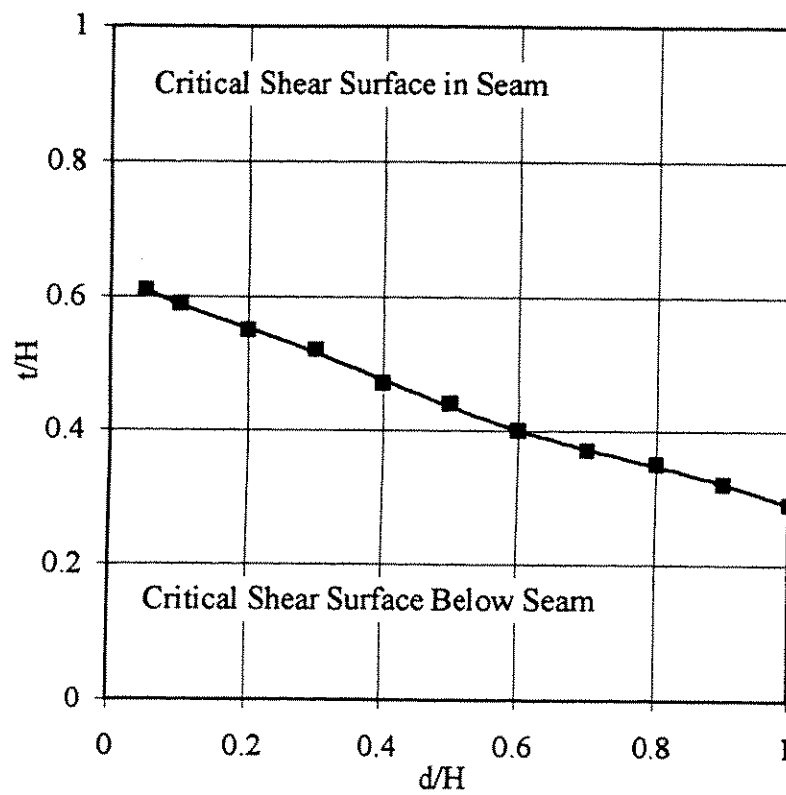


Figure 3.3 Results for the location of the critical shear strength for Case 1 - constant strength cohesive soil with  $\beta = 15$  degrees and  $c_{seam}/c_{slope} = 1/2$

angle of 15 degrees and a dimensionless strength ratio,  $c_{\text{seam}}/c_{\text{slope}}$  of one-half.

Combinations of  $t/H$  and  $d/H$  represented by points along the line represent conditions of seam thickness and depth where the critical seam thickness is "captured by the seam", i.e. the critical shear surface passes into, but not below, the seam. With no seam it will be recalled that the critical shear surface goes infinitely deep. Combinations of  $t/H$  and  $d/H$  which plot above the curve in Figure 3.3 represent conditions where the critical shear surface passes into, and not below, the seam and the factor of safety is less than the factor of safety calculated for the critical seam thickness. Combinations of  $t/H$  and  $d/H$  which plot below the curve in Figure 3.3 represent conditions where the critical shear surface passes through the seam, continuing to a lower depth, and the factor of safety is still less than the factor of safety for a homogeneous slope with no seam. The results presented in Figure 3.3 indicate that for deeper seams the thickness required to "capture" the critical shear surface is reduced.

### 3.7 Case 2 - Cohesion Increasing Linearly with Depth

For the second case the soil strength was again assumed to be purely cohesive, but the cohesion increases linearly with depth from a value of zero at the surface of the slope. The seam thickness required to just affect stability was determined for various depths of the seam. The effect of the slope angle on the seam thickness required to affect stability was also investigated. Both circular and noncircular shear surfaces were used. The effect of the assumed potential critical shear surface on the seam thickness required to just affect stability and on the factor of safety is examined.

### 3.7.1 Variables

The variables describing the slope geometry for Case 2 are shown again in Figure 3.4 along with the variables which describe the shear strength. The shear strength (cohesion) for the seam is assumed to be a constant. The cohesion of the surrounding soil increases linearly with depth at the rate,  $c_z$ , from a value of zero at the surface. The dimensionless variables  $t/H$  and  $d/H$  are again used. The ratio of the shear strength of the seam to the shear strength of the soil immediately above the seam,  $c_{seam}/(c_z * d)$ , is used as a dimensionless shear strength ratio.

### 3.7.2 Procedure for Detecting Stability with Thin, Weak Seam

For each slope the factor of safety without the seam was calculated first. For a linear increase in shear strength with depth from zero at the surface, the factor of safety can be calculated from an infinite slope analysis and is expressed by

$$F = \frac{2c_z}{\gamma} \operatorname{cosec}(2\beta) \quad (4)$$

which indicates that  $F$  does not depend on the depth of the critical shear surface.

Equation 4 was used to calculate the factor of safety for the slope without a seam.

The critical potential shear surface for a homogeneous slope without a seam tends to be very shallow and becomes tangent to the slope face, regardless of the value of  $c_z$  provided the cohesion at the surface is zero. Unlike Case 1, where a weaker seam in the slope will always affect stability because the critical shear surface passes through

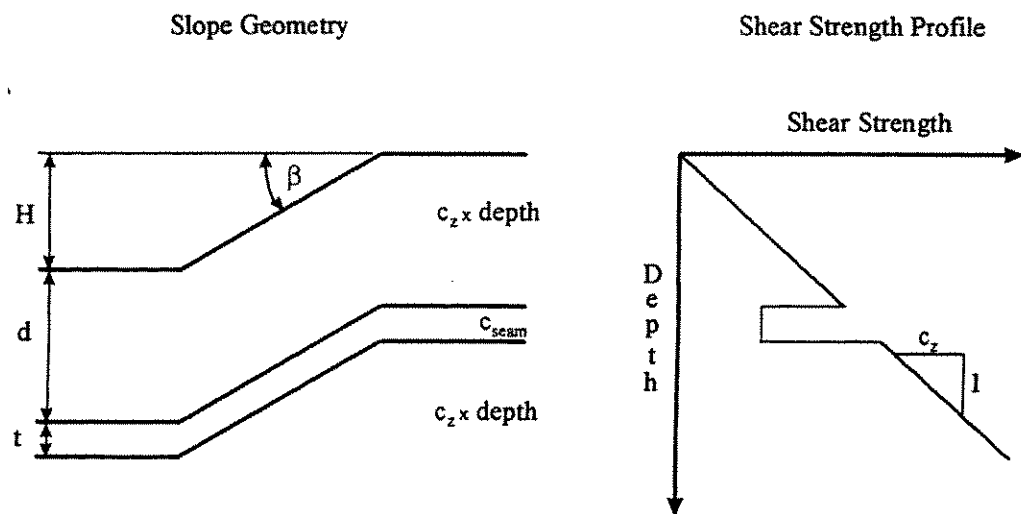


Figure 3.4 Slope and shear strength variables for Case 2 - cohesion increases linearly with depth



the seam, it is possible in the second case that a seam of weaker material may exist, but not effect the stability since the critical shear surface may be located much shallower.

Of interest in this investigation was the thickness of the seam required for the factor of safety for the slope with the seam to be equal to the factor of safety for the homogeneous slope, without the seam, and for the critical shear surface to pass into the seam. Analyses were performed using various depths to the seam, shear strength ratios, slope angles and shapes for the critical shear surface.

### 3.7.3 Verification of Dimensionless Parameters

To confirm the uniqueness of a solution for a given set of dimensionless parameters ( $t/H$ ,  $d/H$ , and  $c_{seam}/(c_z*d)$ ) a series of slope stability calculations was performed where values for individual components of the dimensionless variables were changed. Values for the dimensionless parameters were kept constant while the magnitude of the individual quantities were changed. The values for the variables  $H$ ,  $\gamma$ ,  $c_{seam}$  and  $c_z$  were changed.

The results from the confirmation study are summarized in Table 3.2. The dimensionless ratios  $d/H$  and  $c_{seam}/(c_z*d)$  were kept constant while the values of  $H$ ,  $c_{seam}$ , and  $c_z$  were varied. The effects of changing the values of the individual variables on the seam thickness required to just affect stability were then determined for each combination of values. The first set of values (first row) in Table 3.2 are the "base" parameters used for further comparison described later. With this set of values the seam thickness required to just effect stability is 0.28 ft and  $t/H$  is 0.007. The second set of

Table 3.2  
Results for verification of dimensionless parameters for Case 2 - cohesion increasing linearly with depth

H ft	d ft	d/H	c <sub>seam</sub> psf	c <sub>z</sub> psf	c <sub>seam</sub> / (c <sub>z</sub> *d)	γ pcf	t ft	t/H	Factor of safety	F/ (c <sub>z</sub> d/γH)
40	20	0.5	100	10	0.5	100	0.28	0.007	0.400	8.00
120	60	0.5	300	10	0.5	100	0.85	0.007	0.400	8.00
40	20	0.5	100	15	0.5	100	0.28	0.007	0.600	8.00
40	20	0.5	100	10	0.5	30	0.28	0.007	1.333	8.00

values (second row in Table 3.2) illustrates the effect of increasing the slope height. The third set of values illustrates the effect of changing the magnitude of the shear strengths. The fourth and final set of values illustrates the effect of changing unit weight. In all cases the required seam thickness expressed by the dimensionless ratio  $t/H$  was unaffected by the changes in the values of the variables. As noted in Table 3.2, the factor of safety for some cases is different. However, the dimensionless ratio  $\frac{F}{c_z d / \gamma H}$ , is the same for all sets of data. The results shown in Table 3.2 verify that the absolute value of slope height, shear strength, and unit weight do not effect the results for the critical seam thickness ratio,  $t/H$ , provided  $\frac{c_{seam}}{c_z d}$  remains constant.

### 3.7.4 Results

Slope stability calculations were performed for the second case using both circular and noncircular shear surfaces. Results are presented separately below.

#### 3.7.4.1 Circular Shear Surfaces

Figure 3.5 depicts combinations of  $d/H$  and  $t/H$  where the seam first begins to influence stability. Results are shown for normalized shear strength ratios,  $c_{seam}/(c_z * d)$ , equal to 1/2, 1/3, 1/5 and 1/10. All analyses were performed with circular shear surfaces and a slope angle of 15 degrees.

Combinations of  $t/H$  and  $d/H$ , shown in Figure 3.5, which lie to the left and above the curves correspond to cases where the critical shear surface will be in the seam

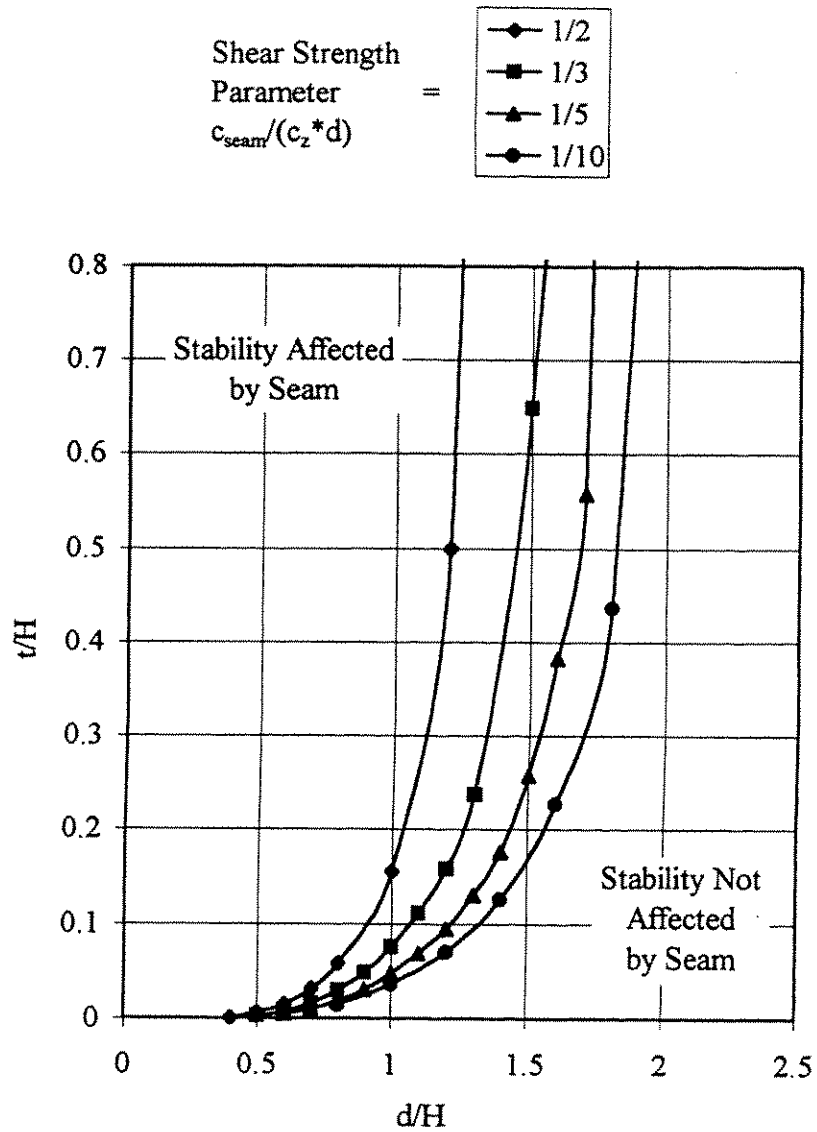


Figure 3.5 Combinations of  $t/H$  and  $d/H$  where seam effects stability for Case 2 - cohesion increases linearly with depth with  $\beta = 15$  degrees

and the factor of safety will be less than the factor of safety for a homogeneous slope without the seam. For these conditions the seam will affect stability. Conversely, combinations of the  $t/H$  and  $d/H$  which lie to the right of and below the curves represent conditions where the critical shear surface lies above the seam and the factor of safety is equal to the factor of safety for a homogeneous slope without the seam. For these configurations the seam does not influence stability.

Figure 3.5 indicates that for a given value of  $c_{seam}/(c_z*d)$ , the seam thickness required to influence stability increases as the depth of the seam increases. However, for each  $c_{seam}/(c_z*d)$ , there exists a "transition" depth at which the seam will not influence the stability regardless of the thickness of the seam. This transition depth is represented by the vertical portions of the curves in Figure 3.5. This result is reasonable considering the preference of the critical shear surface to be tangent to the face of the slope. As the depth to the seam increases, the thickness of the seam must also increase to draw the critical shear surface into the seam and eventually the seam reaches a depth where regardless of the thickness of the seam the critical shear surface will not pass into the seam. At very low values of  $d/H$ , the value of  $t/H$  approaches zero. No dimensionless seam thickness less than  $t/H$  equal to 0.000025, (thickness of one one-thousandths of a foot for a 40 feet high slope) was examined in this study.

The effect of slope angle on the seam thickness required to affect stability is shown in Figures 3.6 and 3.7 for  $c_{seam}/(c_z*d)$  equal to  $1/2$  and  $1/3$ , respectively. Curves are shown for slope angles of 15 degrees and 30 degrees. Again, for points which lie

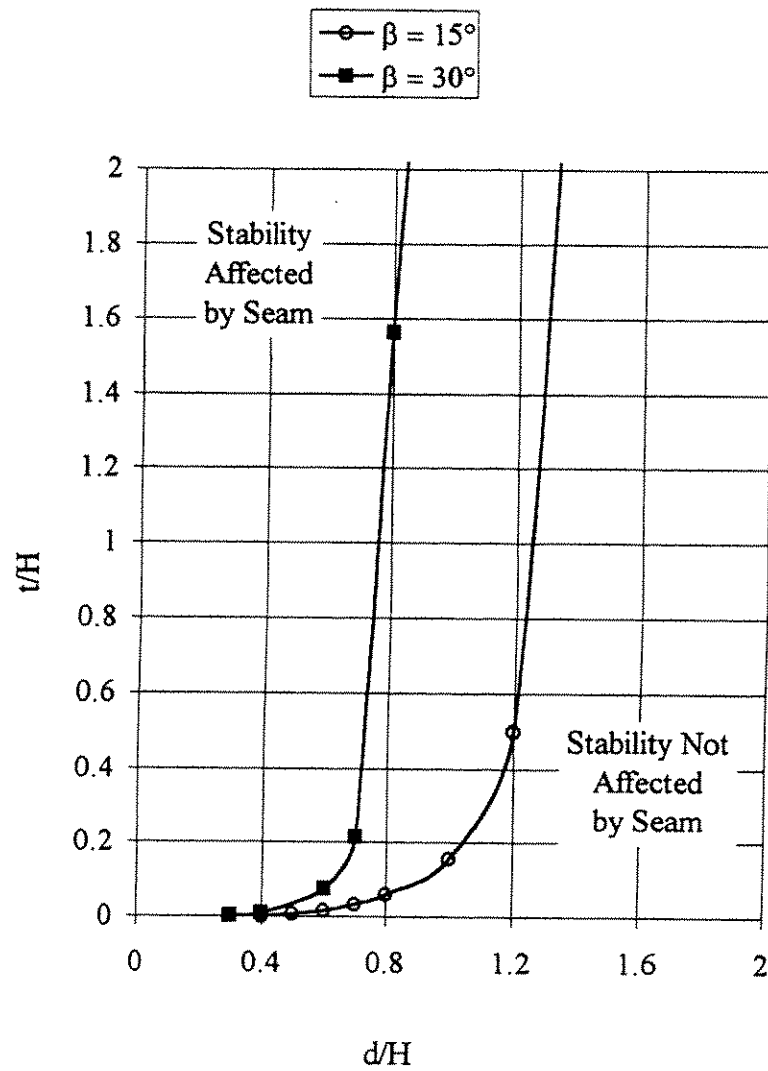


Figure 3.6 Effect of slope angle on the combinations of  $t/H$  and  $d/H$  where seam effects stability for Case 2 - cohesion increases linearly with depth with  $c_{seam}/(c_z \cdot d) = 1/2$

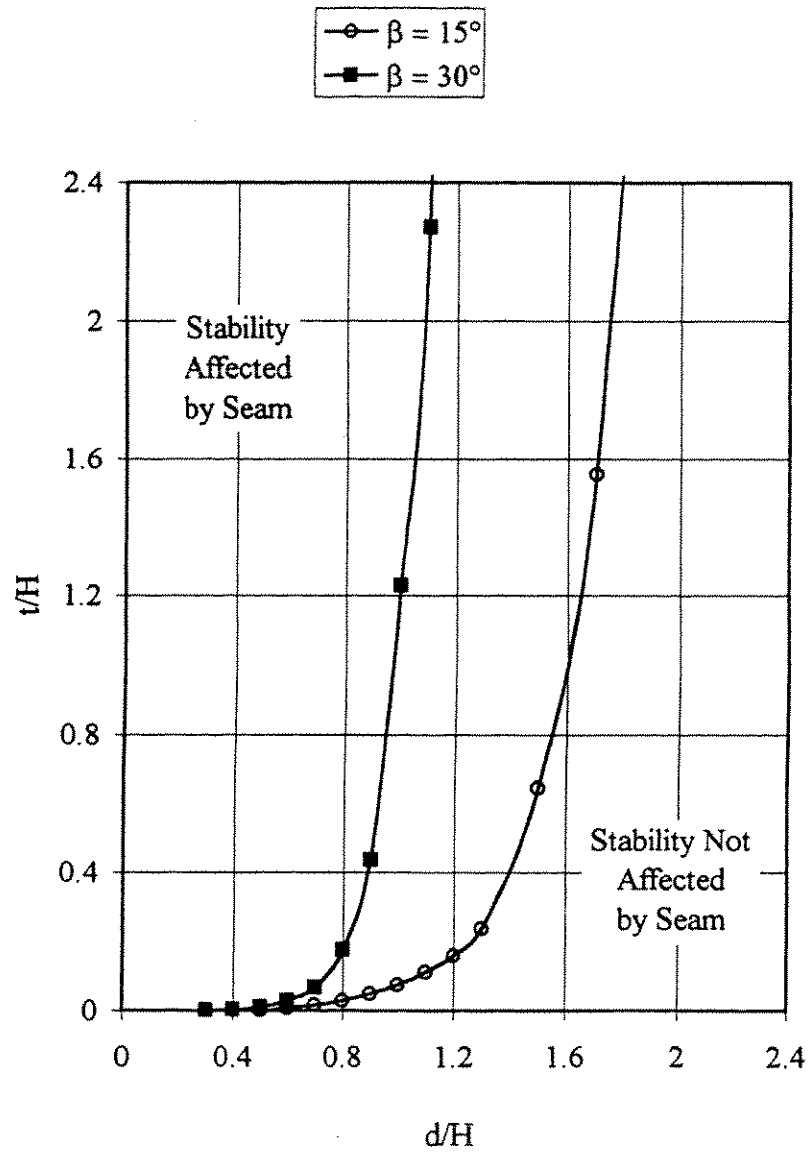


Figure 3.7 Effect of slope angle on the combinations of  $t/H$  and  $d/H$  where seam effects stability for Case 2 - cohesion increases linearly with depth with  $c_{seam}/(c_z \cdot d) = 1/3$

above and to the left of the curves, the critical shear surface will be in the seam and the factor of safety will be less than the factor of safety for a homogeneous slope without the seam. For these conditions, the seam will effect stability. Conversely, combinations of  $t/H$  and  $d/H$  which lie to the right of and below a set of data represent conditions where the factor of safety is not affected by the seam and the critical shear surface lies above the seam, tangent to the slope face. For a given seam thickness, the depth to the seam required to just effect stability is less for the 30 degree slope compared to the 15 degree slope.

#### 3.7.4.2 Noncircular Shear Surfaces

Computations also were performed using noncircular shear surfaces. Again, the seam thickness required to just effect stability was determined for various depths of the seam.

The results for the seam thickness required to just affect stability determined using both circular and noncircular shear surfaces are shown in Figure 3.8 with  $c_{seam}/(c_z*d)$  equal to 1/3 and a slope angle of 30 degrees. Combinations of dimensionless seam thickness ( $t/H$ ) and seam depth ( $d/H$ ) which plot to the left of and above the curves in Figure 3.8 will affect stability and those to the right of and below will not affect stability. The relationship between  $d/H$  and  $t/H$  for the noncircular shear surface is similar in shape to the relationship for circular shear surfaces; however, the curve for noncircular shear surfaces lies to the right of the curve for circular shear surfaces. This indicates that the thickness of the seam required to just affect stability, for a given  $d/H$ ,



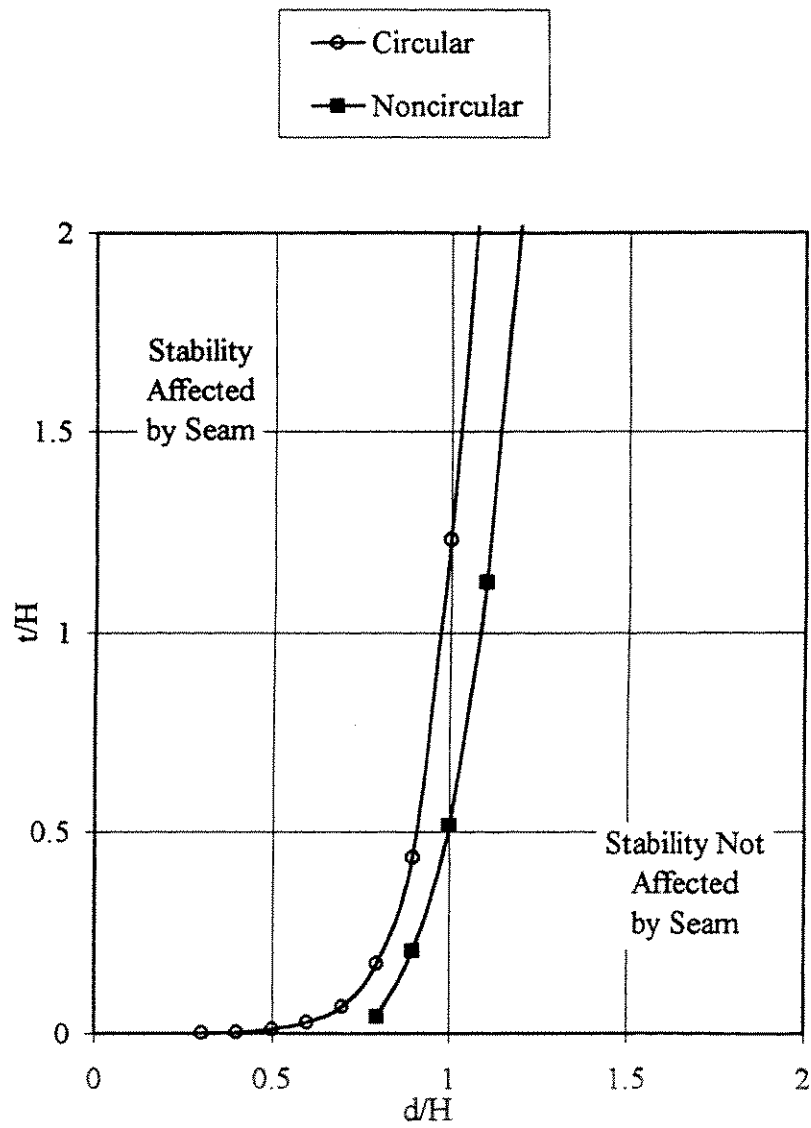


Figure 3.8 Effect of shape of shear surface on the combinations of  $t/H$  and  $d/H$  where seam effects stability for Case 2 - cohesion increases linearly with depth with  $\beta = 30$  degrees and  $c_{seam}/(c_z \cdot d) = 1/3$

is smaller when noncircular shear surfaces are considered compared to circular shear surfaces. This result is reasonable. A circular shear surface cannot pass through as much of the seam as a noncircular shear surface due to constraints in geometry.

The results shown in Figure 3.8 suggest that there are three regions that can be defined. The first region lies to the left and above the curve for the circular shear surfaces. In this region the weaker seam will influence stability regardless of the shape of the shear surface. The second region is the region between the two curves for the circular and noncircular shear surfaces. In this region analyses assuming a circular shear surface would indicate the seam does not affect stability while analyses assuming a noncircular shear surface would indicate the seam does influence stability. The third region lies below and to the right of the curve for the noncircular shear surface. In this region the seam will not influence stability regardless of the assumed shape of the shear surface.

It is possible that different values for the factor of safety may be calculated depending on whether the shear surface is circular or noncircular. However, the results shown in Figure 3.8 do not quantify the difference between the factors of safety calculated assuming a circular and noncircular shear surface. To understand the impact of the assumed shape of the shear surface on the factor of safety, comparisons were made for slopes with identical geometry and material properties. A seam thickness was selected which corresponds to the seam thickness required to just affect stability assuming a circular shear surface for a given depth. The factors of safety for this

geometry were calculated using circular and noncircular shear surfaces. Figure 3.9 compares the factor of safety calculated in this manner for a slope with a slope angle of 15 degrees, and  $c_{seam}/(c_z*d)$  equal to one-half. The critical seam thickness required to affect stability assuming a circular shear surface for each  $d/H$  is given on Figure 3.9. The units on the abscissa are the dimensionless ratio  $d/H$  and the units on the ordinate are the dimensionless ratio  $F_{noncircular}/F_{critical-circular}$ . For a seam depth equal to 40 percent of the slope height ( $d/H = 0.4$ ) the factor of safety using a noncircular shear surface is 70 percent of the value obtained using a circular shear surface. However, at  $d/H$  equal to 1 the factors of safety are more similar, with the factor of safety for a noncircular shear surface being 94 percent of the value for a circular shear surface. The results shown in Figure 3.9 indicate the shape of the shear surface is more important for shallow seams compared to deeper seams.

### 3.8 Case 3 - Friction Angle is Constant

For the third case, the shear strengths were represented as entirely frictional ( $c = 0$ ). The seam thickness required to just affect stability was determined for various depths of the seam.. The effects of the slope angle and relative strength ratio ( $\tan\phi'_{seam}/\tan\phi'_{slope}$ ) on the critical seam thickness was also investigated. Both circular and noncircular shear surfaces were used in the analyses.



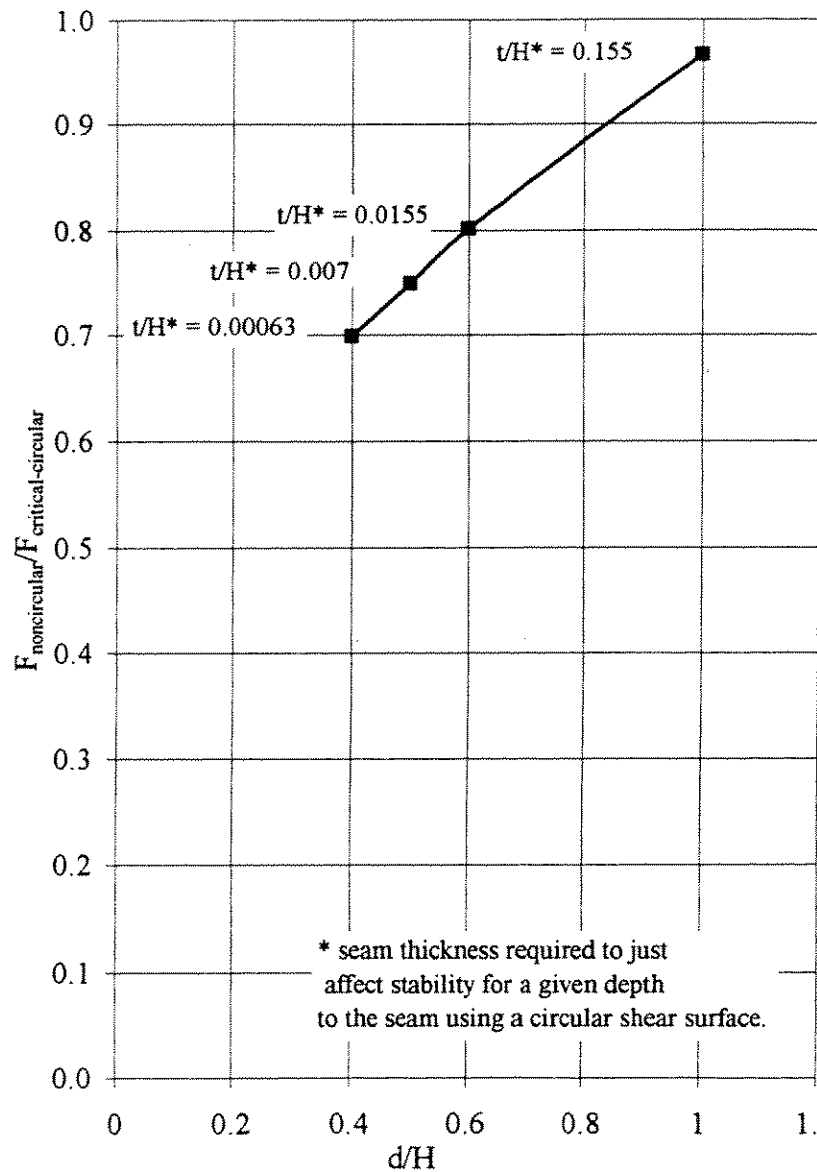


Figure 3.9 Comparison of factors of safety using circular and noncircular shear surfaces for Case 2 - cohesion increases linearly with depth with  $\beta = 15$  degrees and  $c_{\text{seam}} / (c_z \cdot d) = 1/2$

### 3.8.1 Variables

The variables describing the slope geometry have previously been defined and are shown again in Figure 3.10 along with the variables used to describe the shear strength of the soil. The effective stress friction angles,  $\phi'_{\text{seam}}$  and  $\phi'_{\text{slope}}$  for the seam and surrounding soil, respectively, are assumed to be a constant. The dimensionless variables  $t/H$  and  $d/H$  are used to describe the geometry and the ratio,  $\tan\phi'_{\text{seam}}/\tan\phi'_{\text{slope}}$ , is used to describe the relative shear strengths.

### 3.8.2 Procedure for Detecting Stability with Thin, Weak Seam

For each combination of slope angle ( $\beta$ ) and effective stress friction angle ( $\phi'_{\text{slope}}$ ), the factor of safety without the seam was calculated first. For this case of a cohesionless soil, the factor of safety can be calculated from an infinite slope analysis and is given by

$$F = \frac{\tan \phi'}{\tan \beta} \quad (5)$$

which indicates that  $F$  does not depend on the depth of the critical shear surface. As in Case 2, the critical potential shear surface tends to be very shallow and becomes tangent to the slope face. Because the critical shear surface is tangent to the face of the slope it is possible that a seam of weaker material can exist but have no influence on stability.

Of interest in this investigation was the thickness of the seam required such that the factor of safety for the slope with the seam is equal to the factor of safety for the

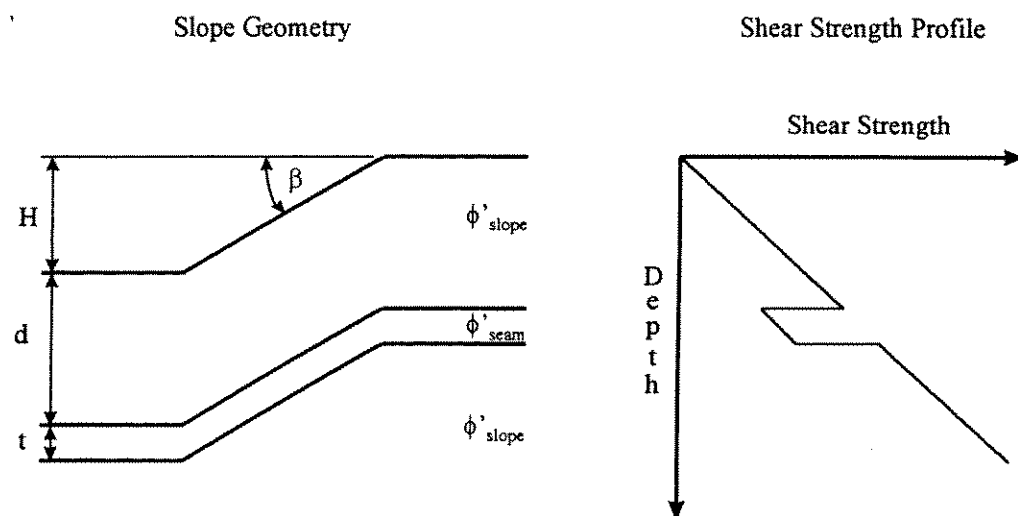


Figure 3.10 Slope and shear strength variables for Case 3 - friction angle is constant

homogeneous slope without the seam, and the potential shear surfaces is "captured" by the seam. Analyses were performed using several depths for the seam, shear strength ratios, slope angles and shapes for the critical potential shear surface.

### 3.8.3 Verification of Dimensionless Parameters

To validate the uniqueness of the dimensionless parameters used in the analyses, a series of stability calculations was performed where values for individual terms in the expression for the dimensionless variables were changed. The effects of the changes in the values on the dimensionless thickness ratio ( $t/H$ ), were investigated. Values for the dimensionless parameters ( $d/H$  and  $\tan\phi'_{\text{seam}}/\tan\phi'_{\text{slope}}$ ) were kept constant while the values of individual variables  $H$ ,  $\gamma$ ,  $\phi'_{\text{slope}}$  and  $\phi'_{\text{seam}}$  were changed.

Results from the verification study are summarized in Table 3.3. The dimensionless ratios  $d/H$  and  $\tan\phi'_{\text{seam}}/\tan\phi'_{\text{slope}}$  were kept constant while  $H$ ,  $\tan\phi'_{\text{seam}}$ , and  $\tan\phi'_{\text{slope}}$  were varied. The effects of changing the individual variables on the seam thickness required to just affect stability were then determined for each combination of values. The first set of values (first row) in Table 3.3 represent the "base" parameters used for comparison later. For this set of values the critical seam thickness is 0.38 ft corresponding to  $t/H$  of 0.0095. The second set of values (second row) in Table 3.3 examine the effect of slope height. The third set of values is used to examine the effect of changing the shear strengths. The fourth and final set are used to explore the effect of changing the unit weight of soil. In all cases the ratio  $t/H$  remained unaffected by the



Table 3.3  
Results for verification of dimensionless parameters for Case 3 - friction angle is constant

H ft	d ft	d/H	$\phi_1$ psf	$\phi_2$ psf	$\tan\phi'_{\text{seam}} / \tan\phi'_{\text{slope}}$	$\gamma$ pcf	t ft	t/H	Factor of safety	F/ $\tan\phi'_{\text{seam}}$
40	20	0.5	16.1	30	0.5	100	0.38	0.010	2.155	7.47
120	60	0.5	16.1	30	0.5	100	1.14	0.010	2.155	7.47
40	20	0.5	26.6	45	0.5	100	0.38	0.010	3.732	7.45
40	20	0.5	16.1	30	0.5	30	0.38	0.010	2.155	7.47

changes. As noted in Table 3.3, the factor of safety for some cases is different.

However, the dimensionless ratio  $\frac{F}{\tan \phi'_{\text{slope}}}$ , shown in the last column of Table 3.3, is

the same for all sets of data. These results indicate that the absolute value of slope height, shear strength, and unit weight do not effect the results for the critical seam

thickness as long as  $\frac{\tan \phi'_{\text{seam}}}{\tan \phi'_{\text{slope}}}$  remains constant.

### 3.8.4 Results

Slope stability calculations for the third, and final, case were also performed using both circular and noncircular shear surfaces. Results are presented separately below.

#### 3.8.4.1 Circular Shear Surfaces

Figures 3.11 and 3.12 present curves showing combinations of  $t/H$  and  $d/H$  where stability is first affected by the seam for slope angles of 15 and 30 degrees, respectively. Curves are shown for values of  $\tan \phi'_{\text{seam}}/\tan \phi'_{\text{slope}}$  equal to 3/4, 1/2, and 1/3. Combinations of  $t/H$  and  $d/H$ , shown in Figures 3.11 and 3.12 which lie to the left and above the curves correspond to cases where the critical shear surface will be in the seam and the factor of safety will be less than the factor of safety for a homogeneous slope without the seam. For these conditions, the seam will influence stability. Conversely, combinations of the  $t/H$  and  $d/H$  which lie to the right of the curves

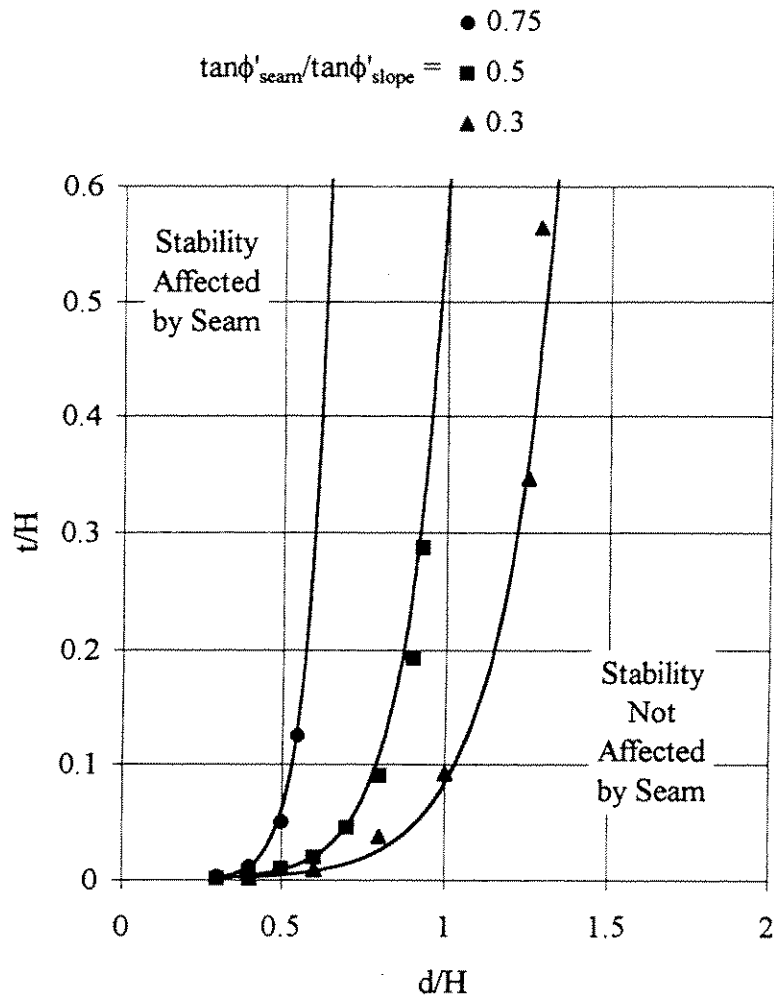


Figure 3.11 Combinations of  $t/H$  and  $d/H$  where seam effects stability for Case 3 - friction angle is constant with  $\beta = 15$  degrees

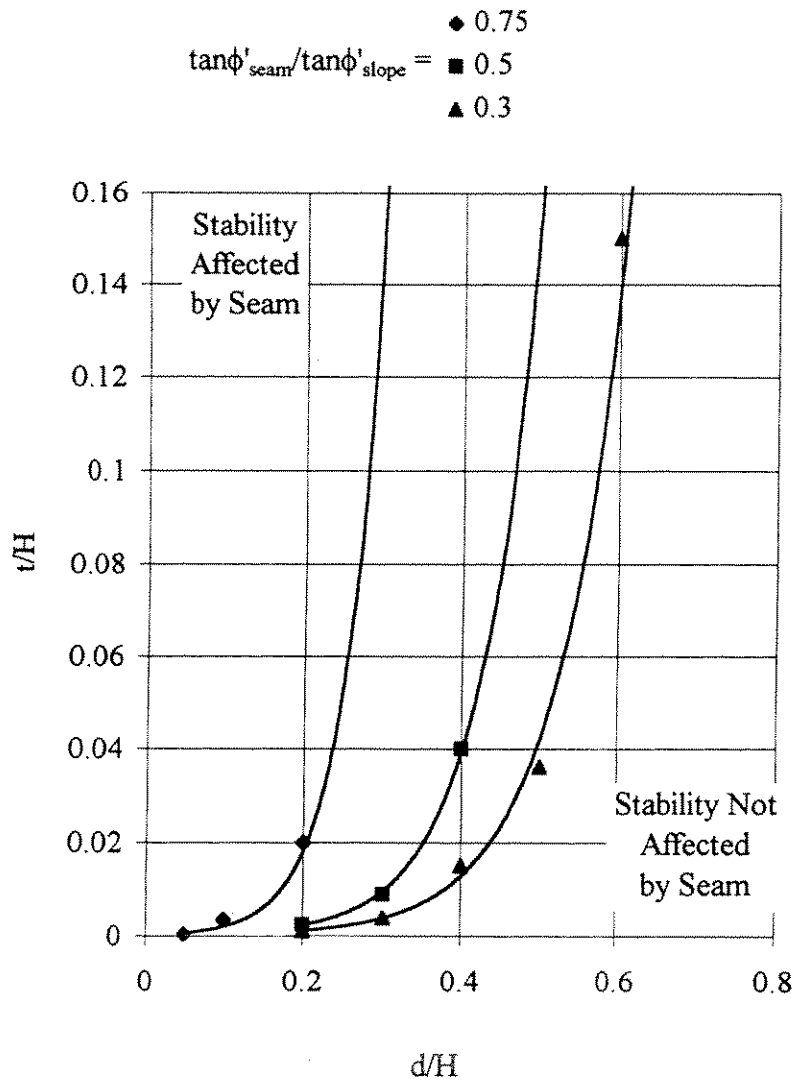


Figure 3.12 Combinations of  $t/H$  and  $d/H$  where seam effects stability for Case 3 - friction angle is constant with  $\beta = 30$  degrees

represent conditions where the critical shear surface lies above the seam and the factor of safety is not affected by the seam.

As for the previous case where the cohesion increased linearly with depth, the thickness of the seam required to affect stability increases as the depth to the seam increases. The results presented in Figures 3.11 and 3.12 indicate that for a given  $d/H$ , the seam thickness required to affect stability increases as  $\tan\phi'_{\text{seam}}/\tan\phi'_{\text{slope}}$  increases. This result is reasonable considering that the critical shear surface will be tangent to the face of the slope. As the contrast between the strength of the seam ( $\phi'_{\text{seam}}$ ) and the strength of the surrounding soil ( $\phi'_{\text{slope}}$ ) gets smaller, the seam thickness at a given depth will have to increase in order for the critical shear surface to pass into the seam.

#### 3.8.4.2 Noncircular Shear Surfaces

Computations were also performed using noncircular shear surfaces and the seam thickness required to just affect stability was determined for various depths of the seam.

The results of computations with circular and noncircular shear surfaces are compared in Figures 3.13, 3.14 and 3.15 for  $\tan\phi'_{\text{seam}}/\tan\phi'_{\text{slope}}$  equal to 3/4, 1/2, and 1/3 respectively and a slope angle of 15 degrees. Again, stability will be affected by the seam if  $t/H$  and  $d/H$  lie to the left and above the curves shown.

In all cases, the seam thickness required to just affect stability is less for noncircular shear surfaces compared to circular shear surfaces. As in the previous case

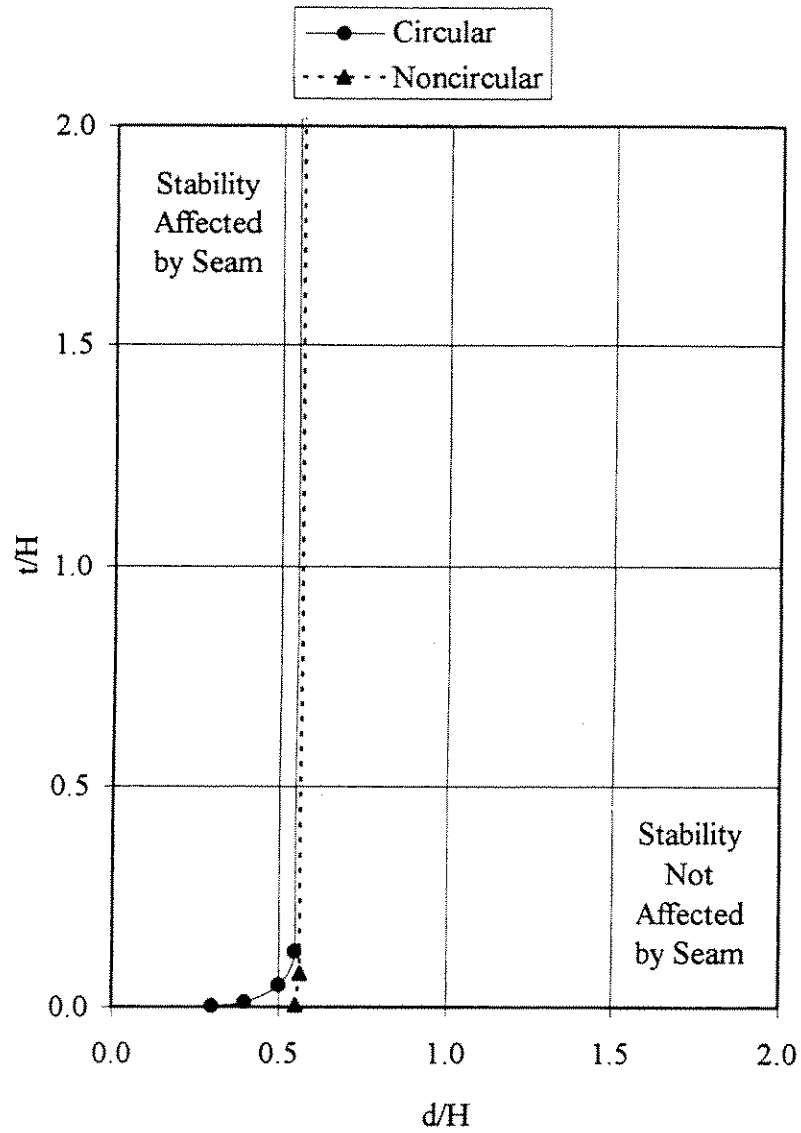


Figure 3.13 Effect of shape of shear surface on the combinations of  $t/H$  and  $d/H$  where seam effects stability for Case 3 - friction angle is constant with  $\beta = 15$  degrees and  $c_{seam}/(c_z * d) = 1/3$

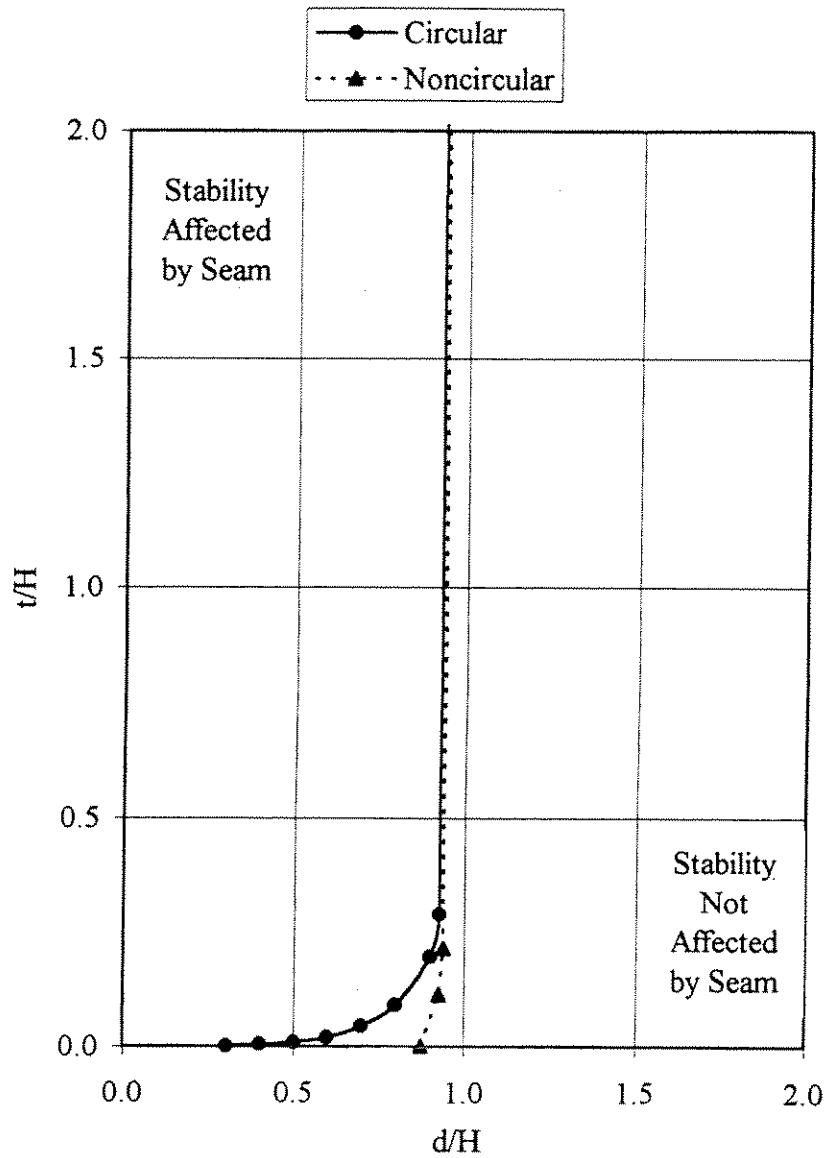


Figure 3.14 Effect of shape of shear surface on the combinations of  $t/H$  and  $d/H$  where seam effects stability for Case 3 - friction angle is constant with  $\beta = 15^\circ$  and  $c_{\text{seam}}/(c_z \cdot d) = 1/2$

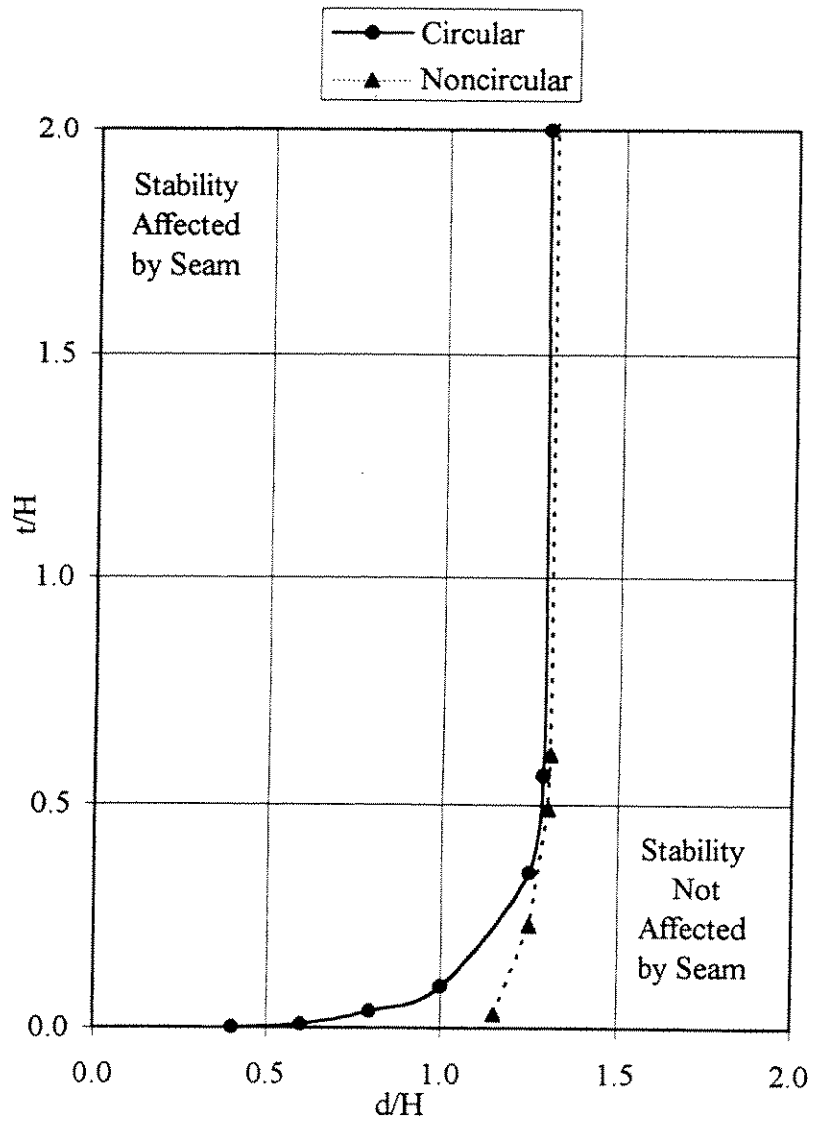


Figure 3.15 Effect of shape of shear surface on the combinations of  $t/H$  and  $d/H$  where seam effects stability for Case 3 - friction angle is constant with  $\beta = 15$  degrees and  $c_{seam}/(c_z * d) = 1/3$



where undrained shear strength increased linearly with depth, there are three regions where stability can be defined depending upon the shape of the shear surface. The first region lies to the left and above the curve obtained for the circular shear surfaces. In this region the seam will affect stability regardless of the shape of the shear surface. The second region lies between the two curves obtained for circular and noncircular shear surfaces. In this region analyses assuming a circular shear surface would indicate the seam does not affect stability while analyses assuming a noncircular shear surface would indicate the seam does influence stability. The third region lies below and to the right of the curve for the noncircular shear surface and here the seam will not affect stability regardless of the shape of the shear surface.

Figures 3.13, 3.14 and 3.15 indicate that for each value of  $\tan\phi'_{\text{seam}}/\tan\phi'_{\text{slope}}$  the seam thickness required to influence stability increases as the depth of the seam increases. However for each  $\tan\phi'_{\text{seam}}/\tan\phi'_{\text{slope}}$  there exists a "transition" depth of seam at which the seam will not influence stability regardless of the thickness of the seam. This transition depth is and is represented by the vertical portions of the curves in Figures 3.13, 3.14, and 3.15.

### 3.9 Conclusions

A series of parametric studies was performed to examine the effects of variability in shear strength in the vertical direction on stability. A thin seam of weak material was used to represent the variability. Several simple variations in shear

strength were examined and the effect of the depth to the seam, slope angle, ratio of shear strength of the seam and slope, and the shape of the shear surface were examined. Dimensionless variables were used to present the results. Several conclusions can be drawn depending on how the shear strength is characterized.

The first case considered was for a purely cohesive ( $\phi = 0$ ) soil with constant strength. In this case a seam of weaker soil will affect stability regardless of the depth of the seam. The results from the computations indicate that as the depth to the seam increases the thickness of the seam required for the shear surface to become "captured" by the seam decreases.

The second case also considered the shear strength to be purely cohesive ( $\phi = 0$ ), but the cohesion increased linearly with depth from a value of zero at the surface. It was found that:

- (1) the thickness of the seam required to affect stability increased as the depth to the seam increased,
- (2) the thickness of the seam required to affect stability for a given depth of seam decreased as the contrast between the shear strengths of the seam and the surrounding soil increased,
- (3) the thickness of the seam required to affect stability for a given depth of seam increased as the slope angle increased,

- (4) a smaller seam thickness is required to affect stability for a given depth of seam if noncircular shear surfaces are considered rather than circular shear surfaces, and
- (5) the shape of the shear surface influences the factor of safety more for shallow seams than for deeper seams.

The third and final case considered was for a cohesionless ( $c' = 0$ ) soil. The results for this case were similar to those for Case 2 however, comparisons of the factor of safety using circular and noncircular shear surfaces were not made as they were for the case where cohesion increases linearly with depth.

For the two cases (Cases 2 and 3) where shear strength increases linearly with depth it was shown that it is possible for seams of weak soil to exist and not have an effect on stability. The thickness of the seam required to not influence stability depends on the depth of the seam, the slope angle, the contrast in shear strength between the seam and surrounding soil, and the shape of the shear surface. There also exists a "threshold" depth where stability will not be affected by a seam regardless of the thickness of the seam. The threshold depth is a function of the slope angle, shape of the assumed shear surface, and shear strength contrast between the seam and surrounding soil. These two conclusions may be useful in probabilistic approaches that attempt to define the effects of vertical variability of shear strength on slope stability. For example, if the depth to the seam is uncertain but greater than the depth where it

influences the factor of safety, uncertainty in the depth and thickness of the seam are not important.

#### **4. Variation of Back-Calculated Shear Strength and Slope Stability Assuming Infinite Slope Conditions**

##### **4.1 Introduction**

The effects of bathymetry on the variability of both back-calculated shear strength and forecast stability are explored in this chapter for a submarine slope in Pigmy Basin. Pigmy Basin, shown in Figure 4.1, is an intraslope basin located in the Gulf of Mexico. Pigmy Basin is approximately 250 square kilometers in area and lies beneath from 1500 meters to 2200 meters of water. Slope geometry was obtained from bathymetric data. The bathymetric data were retrieved through a World Wide Web site developed and maintained by Bryant et al. (1995). The bathymetric data at this Web site are based on bathymetry information originally compiled by NOAA (1992).

Three slope profiles were selected and slope geometry was determined from the bathymetry information. Both variability of shear strength through back analyses and variation of slope stability through forward analyses were determined using the slope profiles.

The variability of shear strength along the cross-section of each slope was investigated first and was determined by back analyses using infinite slope procedures. The factor of safety was assumed to be constant along the entire cross-section of the slope and the shear strength parameter  $\phi'$  (effective stress friction angle) was back-calculated.

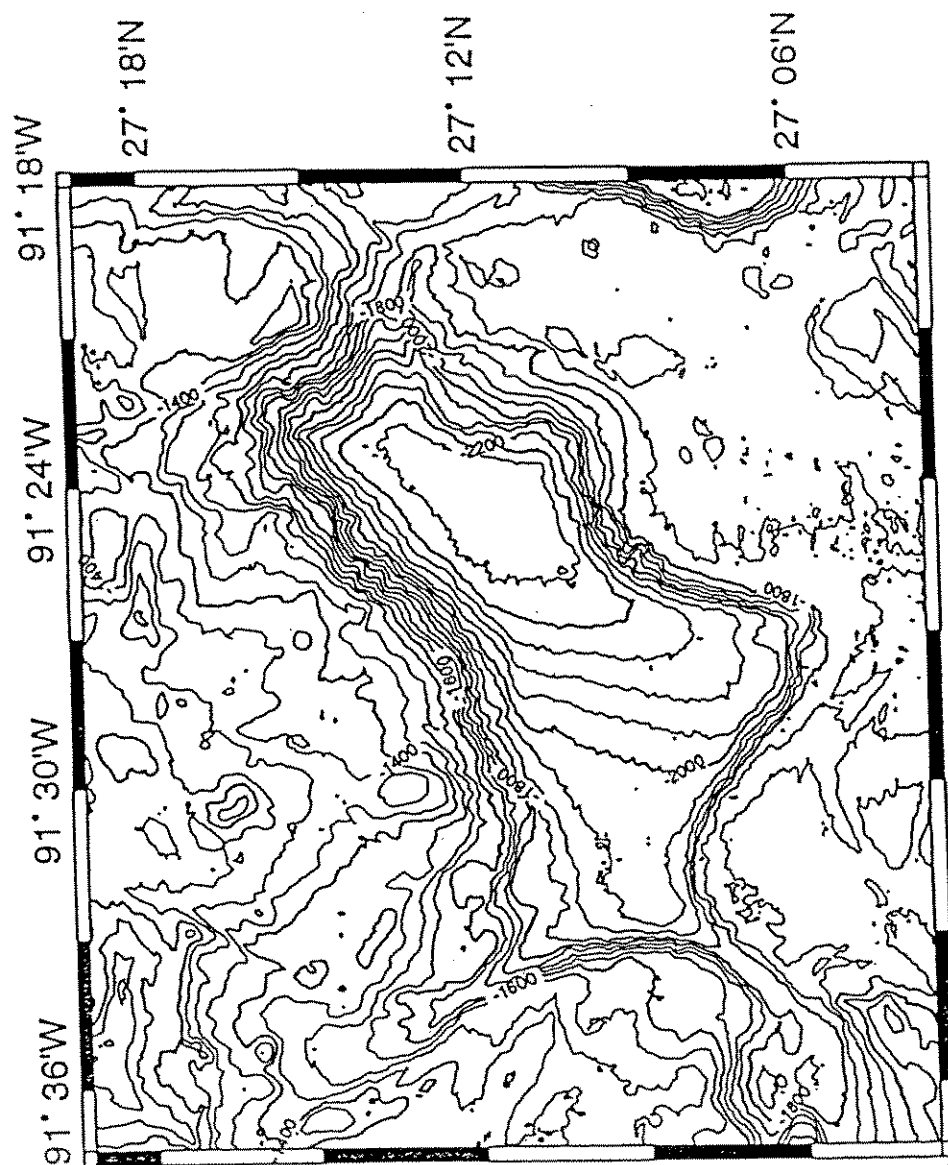


Figure 4.1 Bathymetry chart of Pigmy Basin in the Gulf of Mexico, with 50 meter contours

The variability in the factor of safety along slopes was also calculated using infinite slope procedures. The effective stress friction angle ( $\phi'$ ) was assumed to be constant along the entire cross-section and the factor of safety was calculated. The soil was assumed to have no cohesion and the shear strength was expressed in terms of an effective stress friction angle  $\phi'$ . This characterization of shear strength is believed to be representative of "drained" (long term) strength of many normally consolidated and lightly over consolidated clays.

#### **4.2 Description of Profiles in Pigmy Basin**

The three slope profiles selected are identified in Figure 4.2 which shows Pigmy basin in plan view. The latitude and longitude near the center of the slope are approximately  $27^{\circ}14'N$  and  $91^{\circ}26'W$  respectively. Each of the three profiles covers a distance of approximately 4000 meters parallel to the slope with a change in elevation of 760 meters. The water depths range from 2240 to 1480 meters. This area of Pigmy basin was chosen because of the steep slopes and irregularity in the bathymetry. The steepest portions of the slopes are approximately 25, 35, and 35 degrees for cross-sections A-A, B-B, and C-C respectively. The average slope, represented by the slope of a straight line drawn from the toe of the slope to the crest of the slope, is 11 degrees.

Topographic information was obtained by scaling the distances between 10 meter contour intervals on a figure similar to Figure 4.2. The scale of the figure used to measure distances between contour intervals was 710 meters per inch. Scaling the

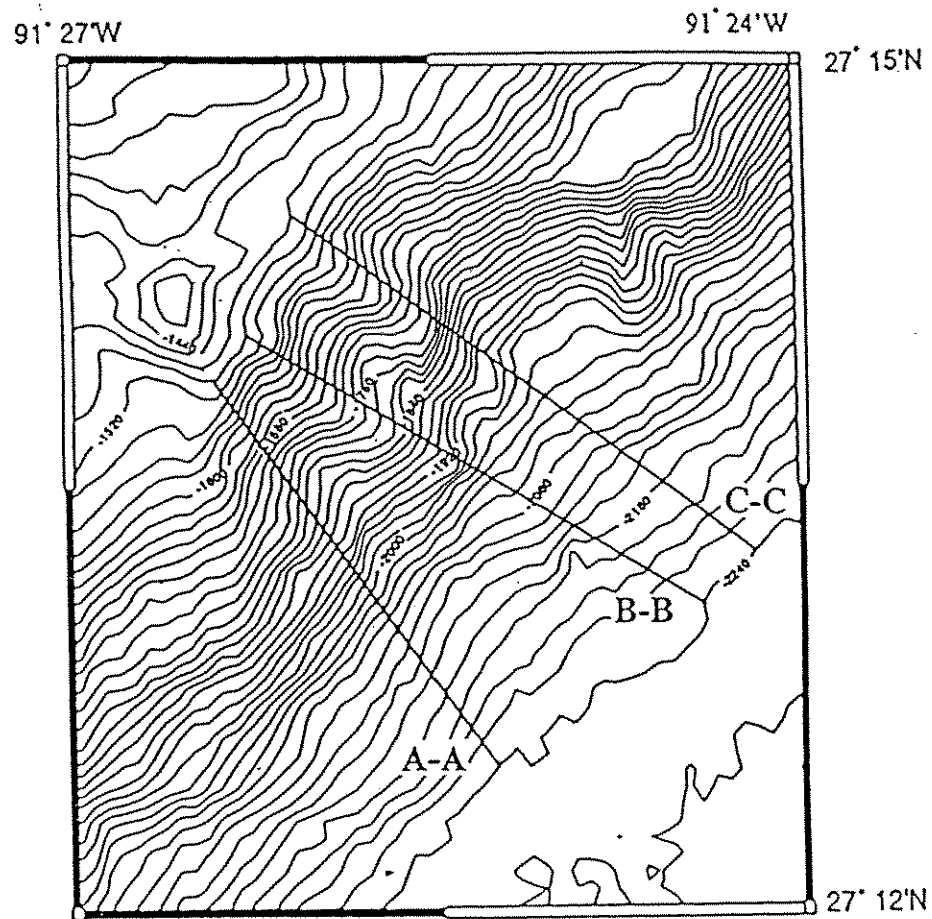


Figure 4.2 Plan view of cross-sections A-A, B-B, and C-C in Pigmy Basin with 20 meter contours



distances between contour intervals provided the horizontal distance relative to the beginning of the cross-section and the elevation at points where each contour crossed the line of the cross-section. The data points determined from scaling distances off the contour plot were used to construct the three profiles shown in Figure 4.3. The simple arithmetic average slope angle obtained by averaging the slope angles between each pair of contour lines on the cross-section is 16 degrees.

#### **4.3 Variability in Shear Strength from Back Analyses**

Two-dimensional analyses were performed to back-calculate the variability of shear strength for each of the three slope profiles. The soil was assumed to be cohesionless ( $c' = 0$ ), and the effective stress friction angle  $\phi'$  was assumed to be constant over each linear segment, i.e. between points represented by the original contours. The factor of safety was assumed to be unity everywhere along the slope. No excess pore water pressures were assumed, i.e. the soil was assumed to be fully consolidated and drained during shear.

The factor of safety was calculated assuming an infinite slope thus,

$$F = \frac{\tan \phi'}{\tan \beta} \quad (1)$$

where  $\phi'$  is the effective stress angle of internal friction and  $\beta$  is the slope angle measured from the horizontal. Equation 1 was used to calculate  $\phi'$  for each segment of the slope, assuming a factor of safety equal to one. Thus, the effective stress friction angle was equal to the slope angle ( $\phi' = \beta$ ).

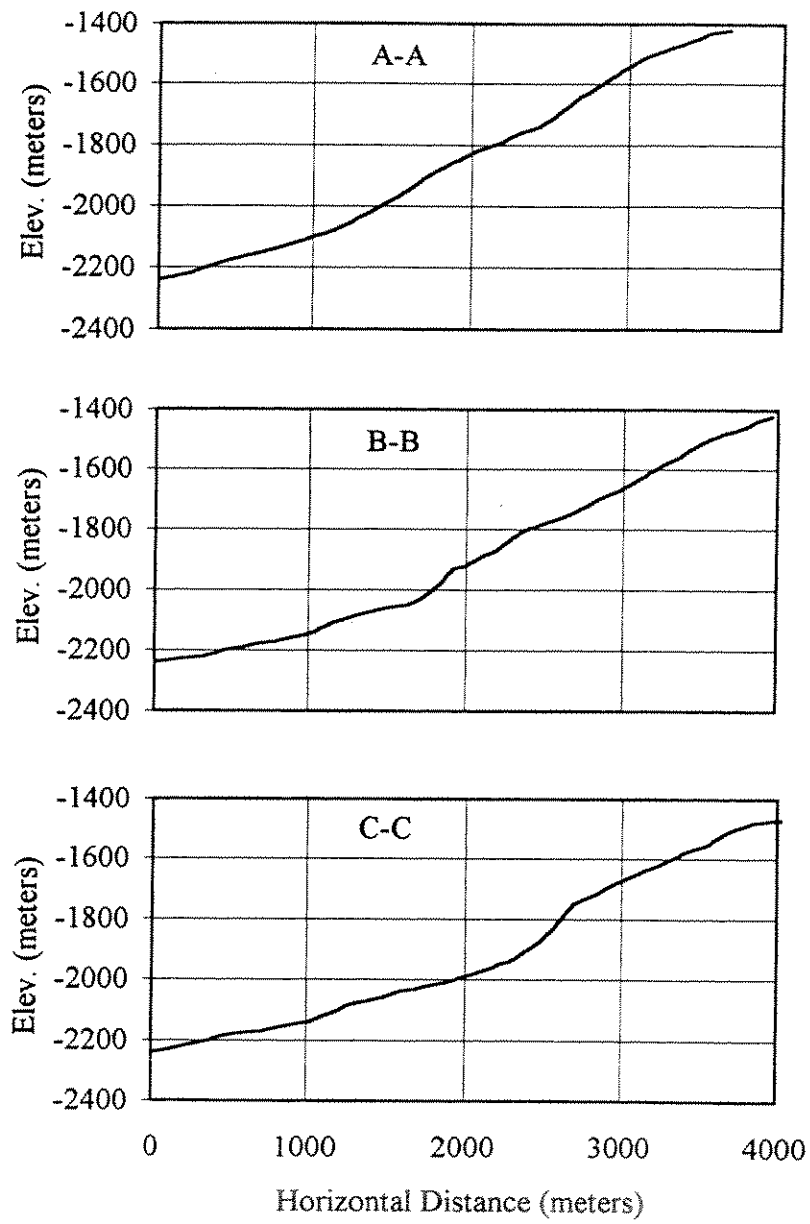


Figure 4.3 Profile of cross-sections A-A, B-B, and C-C

The calculated shear strength along the slopes is shown in Figures 4.4, 4.5, and 4.6 for cross-sections A-A, B-B, and C-C respectively. Each figure indicates a large variation in  $\phi'$  along the cross-section of the slope, particularly for cross-sections B-B and C-C.

#### 4.4 Variability in Stability from Forward Analyses

Stability analyses were also performed to calculate the factor of safety for the three irregular slope profiles shown in Figure 4.3 using an assumed shear strength. The soil was assumed to be cohesionless and  $\phi'$  was assumed to be 16 degrees. This angle (16 degrees) represents the approximate average slope angle calculated in the previous analyses presented earlier in Figures 4.4, 4.5 and 4.6. This friction angle was chosen so that the nominal average value for the factor of safety would be near unity. The effective stress friction angle  $\phi'$  was assumed to be constant everywhere along the slope. No excess pore water pressures were assumed. The factor of safety was calculated using Equation 1.

The variation of the factor of safety along the three slopes are shown in Figures 4.7, 4.8, and 4.9 for cross-sections A-A, B-B, and C-C respectively. Each figure indicates a large variation in the factor of safety along the slope, particularly for cross-sections B-B and C-C.

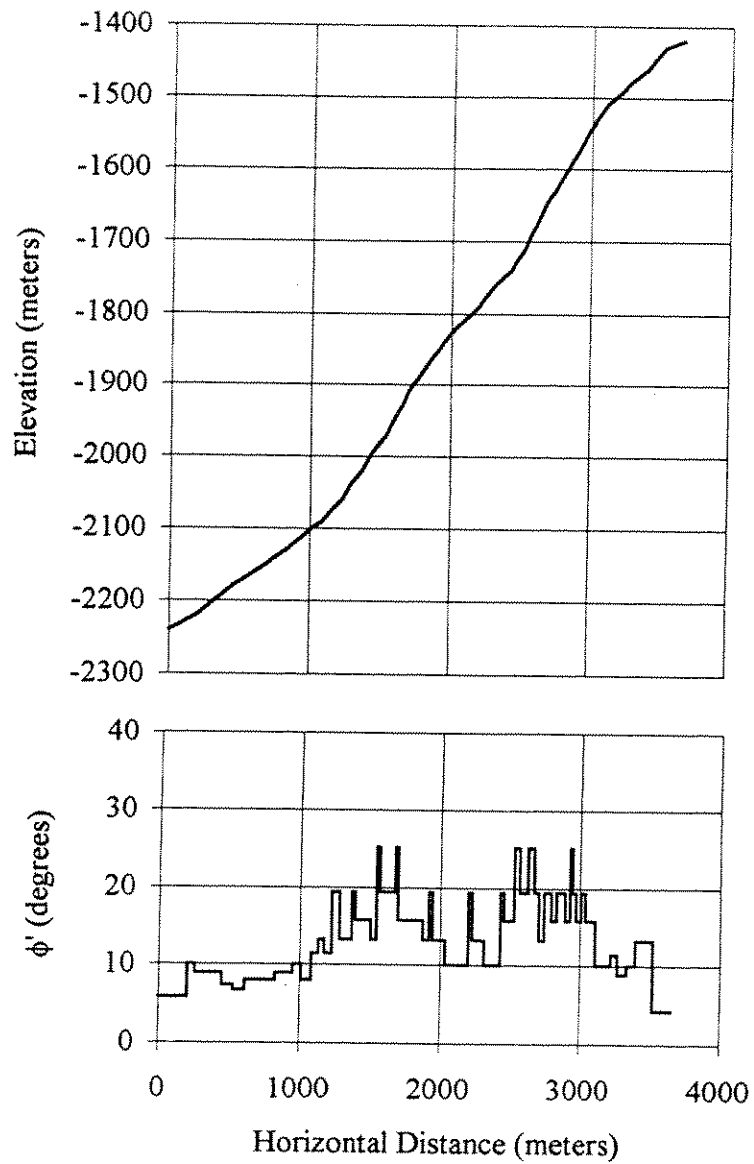


Figure 4.4 Variation of  $\phi'$  along cross-section A-A assuming a factor of safety equal to unity

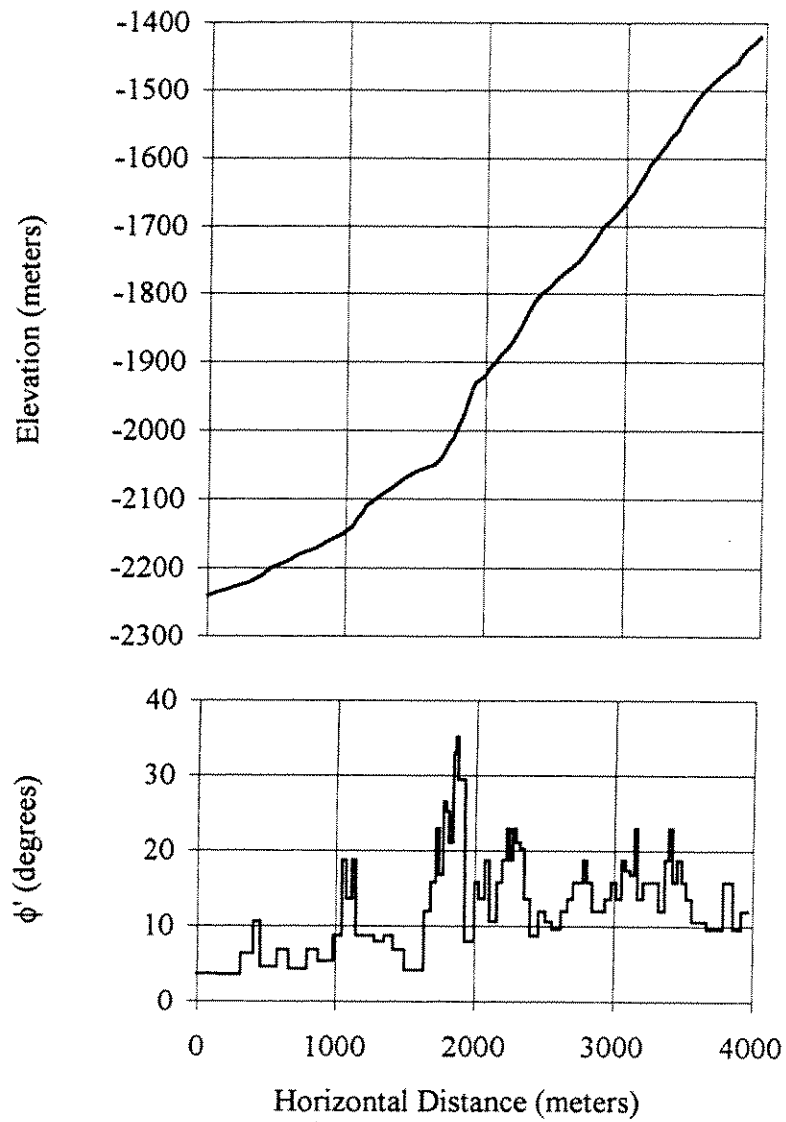


Figure 4.5 Variation of  $\phi'$  along cross-section B-B assuming a factor of safety equal to unity

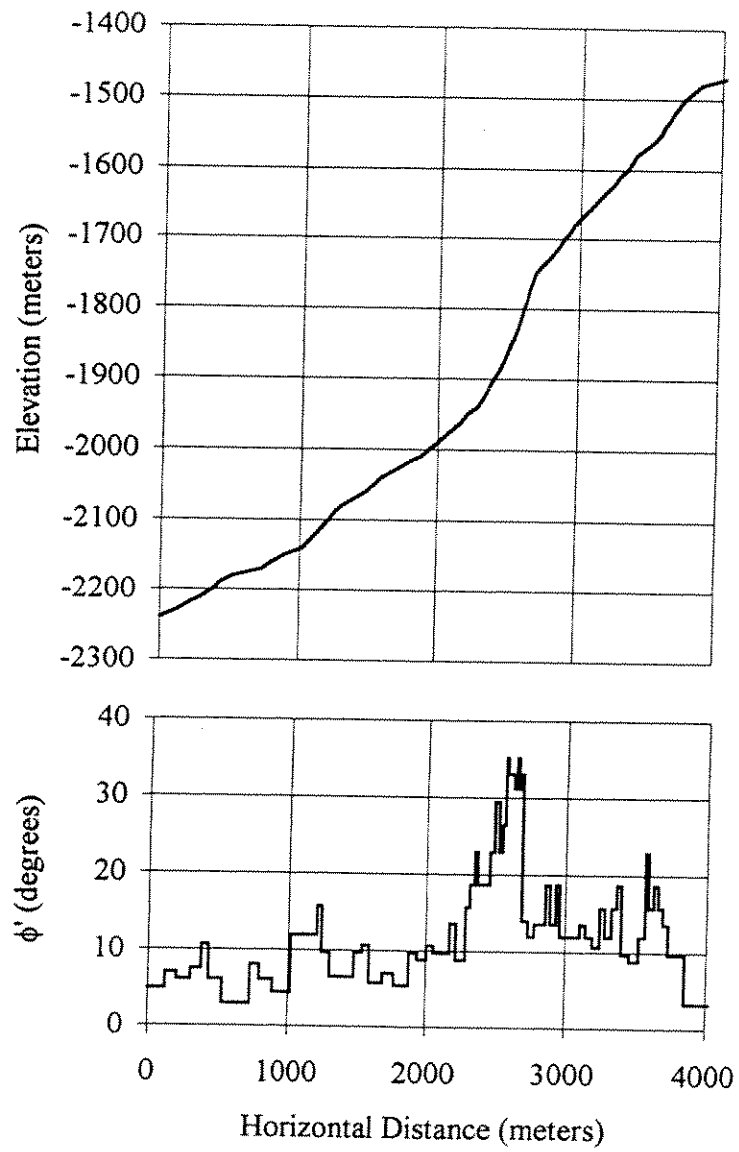


Figure 4.6 Variation of  $\phi'$  along cross-section C-C assuming a factor of safety equal to unity

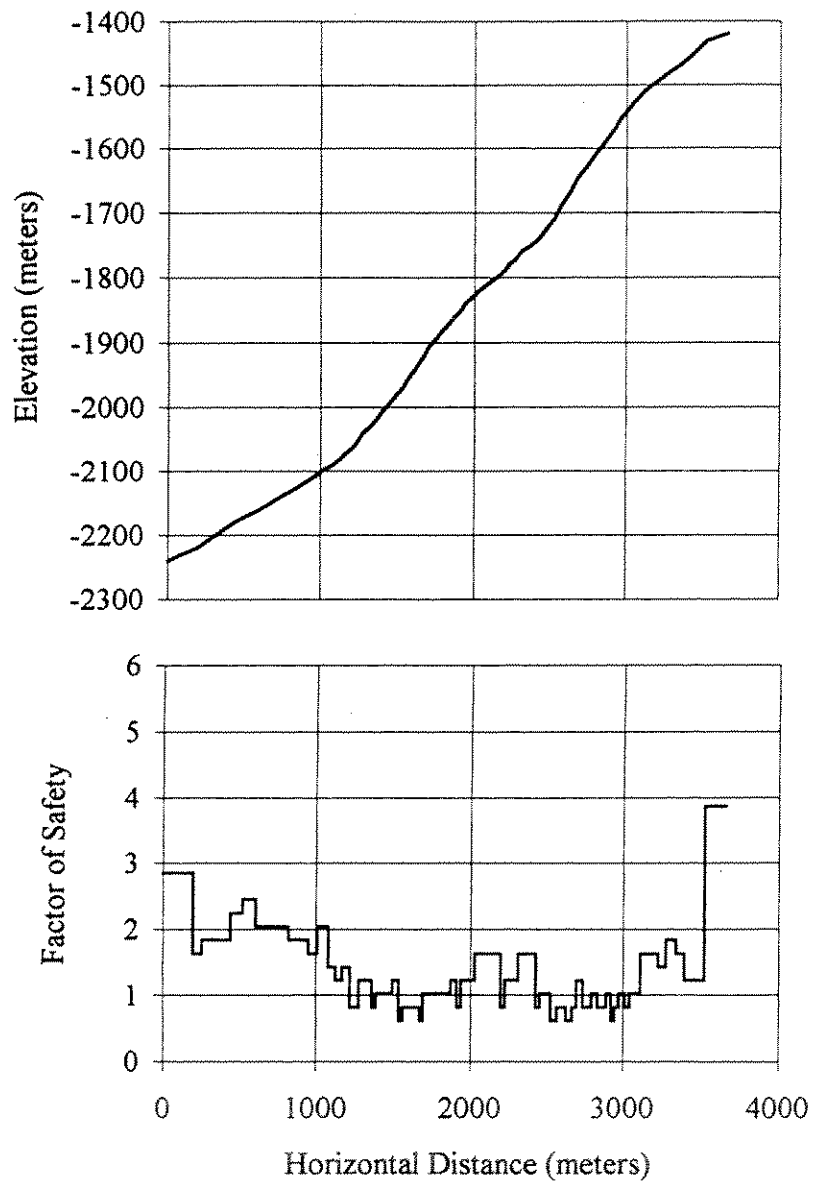


Figure 4.7 Variation of factor of safety along cross-section A-A assuming cohesionless soil

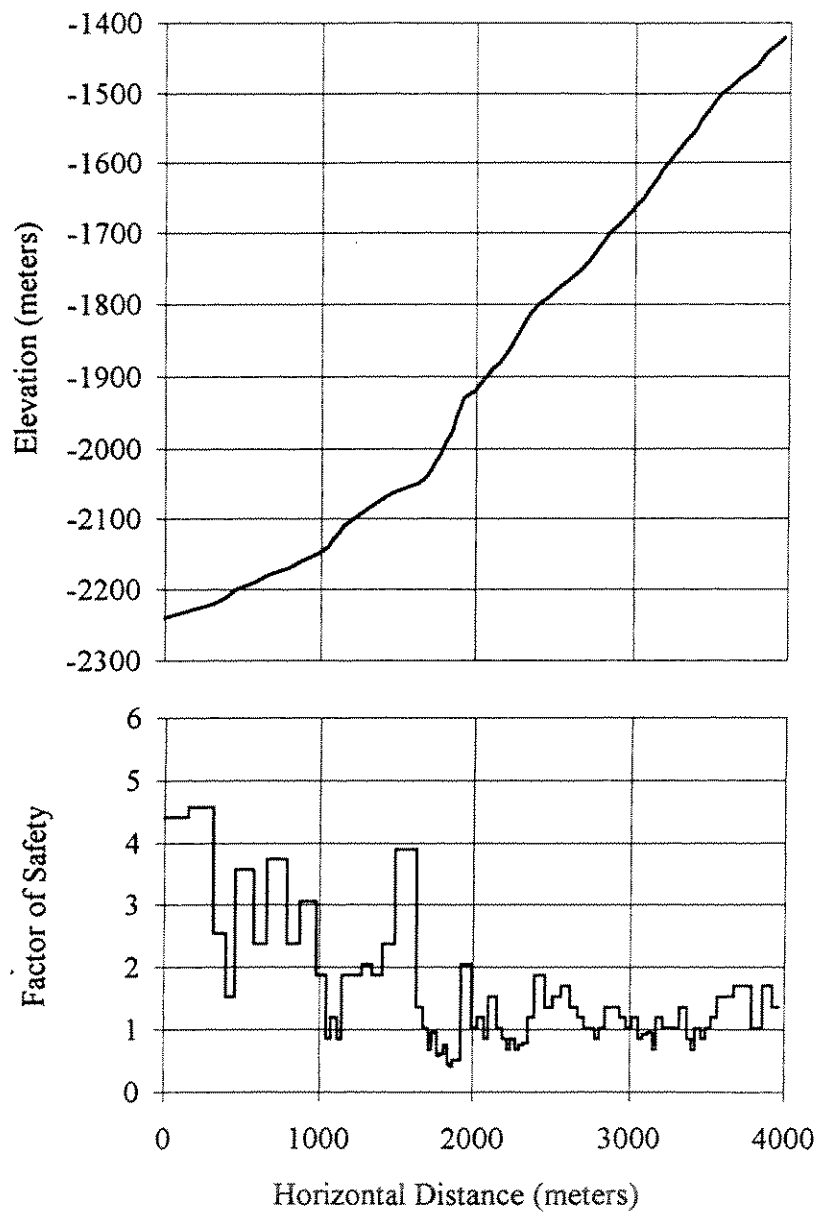


Figure 4.8 Variation of factor of safety along cross-section B-B assuming cohesionless soil



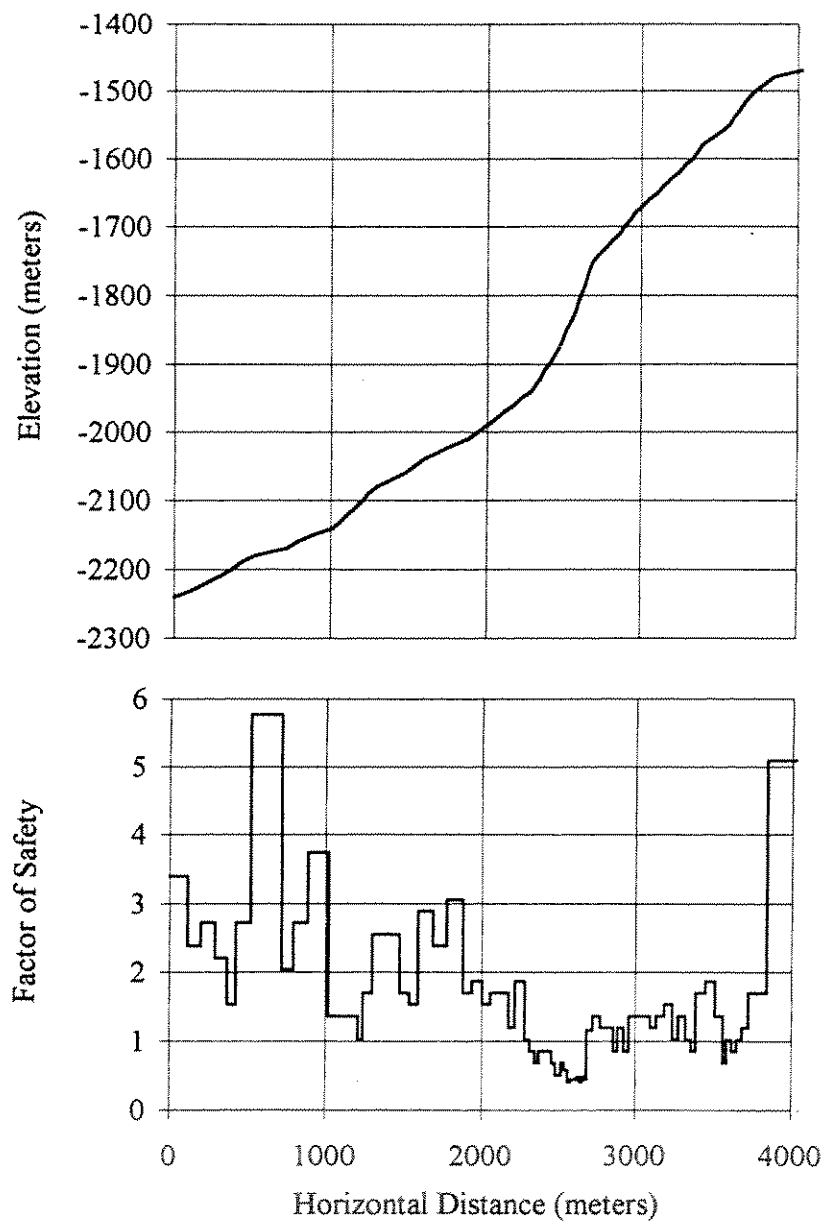


Figure 4.9 Variation of factor of safety along cross-section C-C assuming cohesionless soil

#### 4.5 Conclusions

Some of the apparent variability in shear strength and stability along the slopes may be artificial due to the assumptions used to perform the calculations, such as assuming that the factor of safety (F) or effective stress friction angle ( $\phi'$ ) were constant along the entire slope. By assuming the values of F and  $\phi'$  are constant along the slope the corresponding calculated variations in effective stress friction angle and factor of safety, respectively, probably represent the maximum variation that might be expected to occur. The variability in shear strength implied by the results shown in Figures 4.4, 4.5, and 4.6 is explored further in Chapter 5.

## 5. Spatial Variability of Shear Strength in the Lateral Direction

### 5.1 Introduction

The calculations presented in Chapter 4 suggest that the shear strength may be highly variable laterally along the slope profile. Actual measurements of shear strength at various sites on land and offshore show that over a given distance shear strength can vary either abruptly or gradually. If a single stratum of soil is considered, shear strength measurements from samples taken a short distance apart in the horizontal direction may tend to be similar in comparison to shear strength measurements at distances further apart in the horizontal direction. Thus, two values for shear strength would be expected to be highly correlated if the distance between the samples is small while, shear strengths would be expected to be correlated less if the distance between the samples is large. This change in correlation of shear strength measurements as the horizontal distance between the measurements changes can be referred to as a "correlation structure". A correlation structure describes how a variable, such as shear strength, might be expected to change spatially or temporally.

A correlation structure for shear strength in the lateral direction is calculated in this chapter using the cross-section designated C-C, presented in Chapter 4. Instead of using direct measurements of shear strength at various locations along cross-section C-C, shear strengths inferred from back analyses using slope stability are used. The variation of shear strength for cross-section C-C was presented in Chapter 4. The

correlation structure for the shear strength in the lateral direction will be characterized by a single statistical parameter called the "scale of fluctuation" (Vanmarcke, 1983).

## 5.2 The Scale of Fluctuation

The scale of fluctuation is a measure of the spatial or temporal interval over which a variable is correlated. For the investigation in this chapter, the scale of fluctuation can be defined as a measure of the distance over which the shear strength is correlated. An example of a simple linear correlation structure is shown in Figure 5.1. The correlation structure is defined by the series of points representing values for the correlation coefficient  $\rho(\tau)$  at different lateral distances  $\tau$ . The correlation coefficient for the correlation structure shown in Figure 5.1 starts at a value of one (perfectly correlated), for a lateral distance of zero, and gradually decreases to a value of zero (statistically independent) for lateral distances of 80 meters. In the context of this chapter, the correlation structure can be used to describe the correlation coefficient  $\rho(\tau)$  for shear strength between two samples separated by some lateral distance  $\tau$ .

## 5.3 Evaluation of the Scale of Fluctuation

The scale of fluctuation was calculated for the slope geometry and back-calculated shear strengths determined in Chapter 4 for cross-section C-C. The scale of fluctuation was determined by first calculating the correlation coefficients between pairs of shear strengths separated by some distance,  $\tau$ . The correlation coefficients can then be used to define the correlation structure. Once the correlation structure is determined

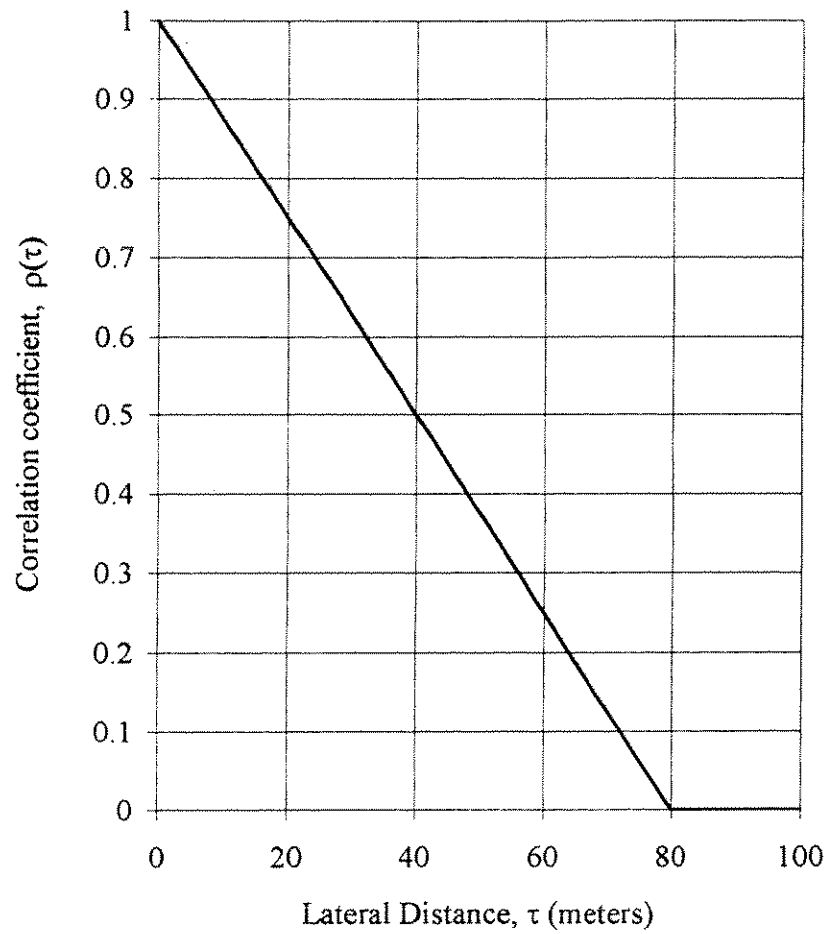


Figure 5.1 Simple triangular correlation structure

several different models for the scale of fluctuation can be fit to the results to establish which model fits the data the best. Each of the models can be defined by a single variable called the scale of fluctuation. The following sections define and describe, using an example, the procedure used to determine the scale of fluctuation.

### 5.3.1 Correlation Coefficients

The mathematical expression used to calculate the correlation coefficients is presented along with a formal explanation and several properties of correlation coefficients. An example is presented to show how the correlation coefficients are calculated and the scale of fluctuation is evaluated. Finally, a brief description of a computer program VARREDF, which was developed to calculate the correlation coefficients, is presented.

#### 5.3.1.1 Formal Description and Properties of the Correlation Coefficient

The correlation coefficient is calculated by

$$\rho(\tau) = \frac{\text{COV}(X, Y)}{\sigma_X \sigma_Y} \quad (2)$$

where  $\rho(\tau)$  is the correlation coefficient,  $\text{COV}(X, Y)$ , covariance between  $X$  and  $Y$ , and  $\sigma_X$  and  $\sigma_Y$  are the variances of  $X$  and  $Y$ , respectively. For the case being investigated in this chapter,  $\text{COV}(X, Y)$  is the variance between pairs of shear strength separated by a distance  $\tau$ , and  $\sigma_X$  and  $\sigma_Y$  are the variances of individual components of the pairs of shear strengths.

If the correlation coefficient between shear strength measurements separated by some distance  $\tau$  is equal to unity (perfectly correlated), then the values for the shear strength measurements are positively, linearly related. If the correlation coefficient is equal to zero then the values for the shear strength measurements are statistically independent. If the correlation coefficient is equal to negative one then the values for the shear strength measurements are negatively, linearly related. A property of the correlation coefficient is that its value must lie between minus one and plus one. The calculations of the variances necessary to solve for the correlation coefficients can be determined for either discrete or continuous data.

#### 5.3.1.2 Calculations for the Correlation Coefficient

The correlation coefficients were calculated using discrete values for distance since the slope geometry was determined from bathymetry charts at discrete locations. Recall that the method used to determine values from the bathymetry charts led to irregularly spaced coordinates dictated by contour intervals. Only the points scaled from the bathymetry charts were used for this investigation. The values for the back-calculated shear strengths, determined in Chapter 4 assuming infinite slope procedures, are constant for each segment of the slope (see Figure 4.3). Since the shear strength for each segment is constant, the midpoint of each segment will be used to determine distances. Figure 5.2 illustrates a simple example of a cross-section and shear strengths associated with each point (midpoint) defining the cross-section. The points in Figure 5.2 represent the points scaled from the bathymetry charts. Straight lines are assumed

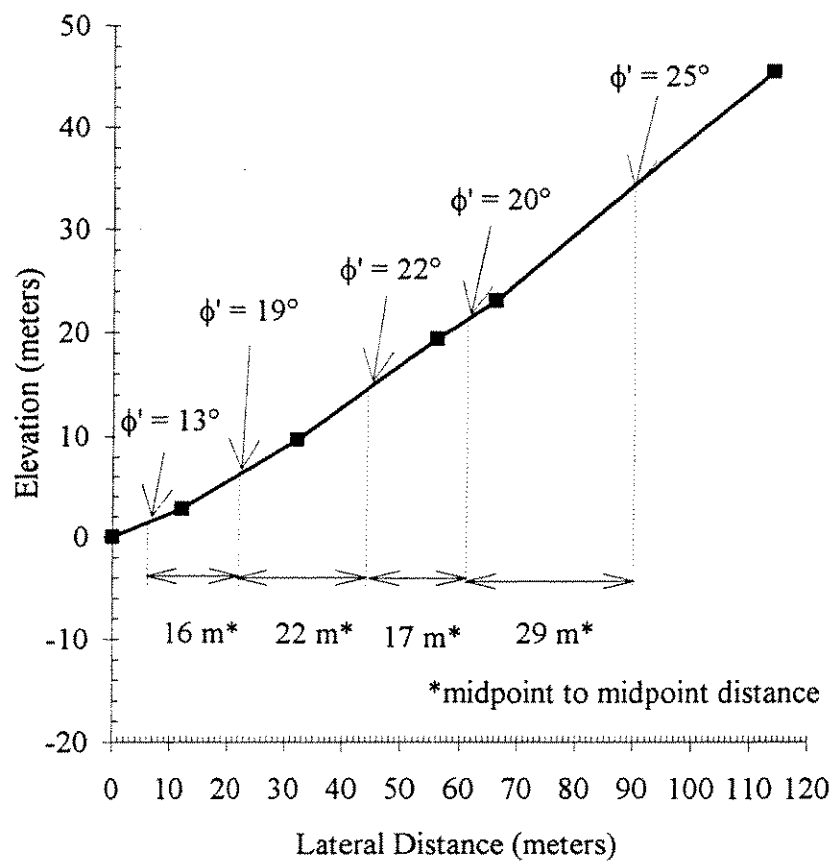


Figure 5.2 Example of the cross-sectional geometry and shear strengths used in the analyses



between the scaled points. The lateral distance between successive midpoints and the shear strength associated with each midpoint (interval) are shown on Figure 5.2. The effective stress friction angle  $\phi'$  is set equal to the angle ( $\beta$ ) of the segment containing the midpoint (based on assuming infinite slope conditions and  $F = 1.0$ ). Table 5.1 lists the lateral coordinates of the midpoint of each segment and the associated effective stress friction angle for the example slope shown in Figure 5.2.

The first step in calculating the correlation coefficients is to determine the distance from each point to every other point. For the example set of data listed in Table 5.1, the distance between the first point and the second is 16 meters, first and third is 38 meters, first and fourth is 55 meters, first and fifth is 88 meters, second and third is 22 meters and so on up to the fourth and fifth point (29 meters). Associated with each distance between two points are two values for  $\phi'$ , one at the left endpoint  $\phi'_l$  and one at the right endpoint  $\phi'_r$ . Next, each pair of effective stress friction angles ( $\phi'_l$  and  $\phi'_r$ ) is "grouped" together with other pairs of effective stress friction angles separated by similar distances. This grouping is necessary because of the discrete nature of the data. The individual groups where data are to be placed are referred to as "bins". For this example, five bins, each 20 meters wide, were chosen. The bin number and the corresponding distances for the bin can be seen in the heading of Table 5.2. In the first bin, pairs of effective stress friction angles corresponding to the distance between the two endpoints which fall in the range from 0 to 20 meters are placed, in the second bin, pairs of effective stress friction angles corresponding to the distance between

Table 5.1  
Example input of lateral coordinates and the corresponding shear strength

Lateral coordinate of midpoint of each segment (meters)	Shear strength, $\phi'$ (degrees)
6	13
22	19
44	22
61	20
90	25

Table 5.2  
Shear strength pairs put into bins corresponding to distances between lateral coordinates

Bin 1	Bin 2	Bin 3	Bin 4	Bin 5
0-20 (meters)	20-40 (meters)	40-60 (meters)	60-80 (meters)	80-100 (meters)
13, 19	13, 22	13, 20	19, 25	13, 25
22, 20	19, 22	22, 25		
	19, 20			
	20, 25			

two endpoints that fall in the range from 20 to 40 meters are placed, and so on. For the example, the lateral distance between the first and the second point was previously determined to be 16 meters, thus, the respective shear strength parameters 13 and 19 degrees ( $\phi'_l$  and  $\phi'_r$ ) are placed in the first bin (first row, first column) of Table 5.2. The lateral distance between the first and the third point is 38 meters, thus, the respective shear strength parameters 13 and 22 degrees are placed in the second bin (first row, second column). The lateral distance between the first and the fourth point is 55 meters, thus, the respective shear strength parameters 13 and 20 degrees are placed in the third bin (first row, third column). This process is repeated for each combination of distances between pairs of points. The results of "grouping" the data in bins are shown in Table 5.2. In the actual analyses several different sizes for the bins were analyzed.

Once the data are separated into the appropriate bins, the right hand side of Equation 2 can be evaluated. The covariance of the pairs of shear strengths,  $COV(\phi_r, \phi_l)$  for all the data in each bin is calculated as follows

$$COV(\phi_r, \phi_l) = E(\phi_r \times \phi_l) - E(\phi_r) \times E(\phi_l) \quad (3)$$

where  $\phi_l$  and  $\phi_r$  the pairs of effective stress friction angles in the bin for the left and right side of a segment, respectively, and the  $E(\bullet)$  operator is the expected value or mean value of the corresponding effective stress friction angles within the bin. For the example problem, Equation 3 is used to calculate  $COV(\phi_r, \phi_l)$  for the second bin (20-40 meters). The four sets of data for the second bin (from Table 5.2) are shown in Table 5.3. The product of  $\phi'_l$  and  $\phi'_r$  is shown in the third column of Table 5.3. The last row

Table 5.3  
Expected values of shear strength pairs for the second bin (20 m - 40 m)

	$\phi'_l$ (degrees)	$\phi'_r$ (degrees)	$\phi'_l * \phi'_r$ (degrees <sup>2</sup> )
Pair 1	13	22	286
Pair 2	19	22	418
Pair 3	19	20	380
Pair 4	20	25	500
Expected Value	17.75	22.25	396

of Table 5.3 shows the expected values (average) for  $\phi_l$ ,  $\phi_r$ , and the product of  $\phi_l$  and  $\phi_r$ . Using the expected values shown in the last row of Table 5.3, the covariance of the pairs of shear strength values for the second bin can be calculated using Equation 3, i.e.  $COV(\phi_r, \phi_l) = 396 - (22.25 \times 17.75) = 1.0625$ . The value for  $COV(\phi_r, \phi_l)$  is in "degrees squared".

Next, the variance for the friction angles on the left side of the segments,  $\phi_l$ , in the bin is calculated by

$$\sigma_l^2 \cong \frac{1}{n} \sum_{i=1}^n (\phi_i - \bar{\phi}_l)^2 \quad (4)$$

the summation is evaluated for the "n" values of  $\phi_l$  in the bin and  $\bar{\phi}_l$  is the average friction angle on the left side of a segment within the bin. The variance of the friction angle on the right side of the segments,  $\phi_r$ , in the bin is calculated using Equation 4 and replacing the "l" subscripts for the left end of a segment with "r" for the right end of a segment. For the example problem, the standard deviations (square root of variance) of  $\phi_l$  and  $\phi_r$  in the second bin are 2.77 and 1.79 degrees, respectively.

Finally, the correlation coefficient for each bin is calculated using Equation 2 and the results from Equations 3 and 4 for each bin respectively. For the example problem, the value for the correlation coefficient can now be determined for the second bin using Equation 2, i.e.  $COV(\phi_r, \phi_l) = 1.0625 / (2.77 \times 1.79) = 0.21$ . In the actual analyses the correlation coefficient is calculated for each bin using a computer program developed for this purpose. The computer program is described in the next section.

#### 5.3.1.3 Computer Program

The computer program, VARREDF, was written in the FORTRAN programming language to do the calculations required to define the correlation coefficient. A listing of the source code for VARREDF is presented in Appendix B and a users guide is presented in Appendix C. The algorithm is similar to the procedure described in the previous section to calculate the correlation coefficient for the example problem.

The user defined input to VARREDF consists of pairs of lateral coordinates and the corresponding shear strength parameter  $\phi'$ . In addition, the size and number of bins are input by the user. The values for the correlation coefficient for each bin are then computed and output.

#### 5.3.2 Scale of Fluctuation Models

Once the correlation coefficient is determined there are several models which can be fit to the results of the correlation coefficient to determine the scale of fluctuation. Each model is a function of the scale of fluctuation. Several common models for the correlation functions are (1) uniform, (2) triangular, (3) exponential, and (4) Gaussian. The differences among these models for the correlation coefficient can be seen in Figure 5.3. On the vertical axis is the correlation coefficient  $\rho(\tau)$  and on the horizontal axis is the normalized distance  $\tau/\theta$  where  $\tau$  is the lateral distance between

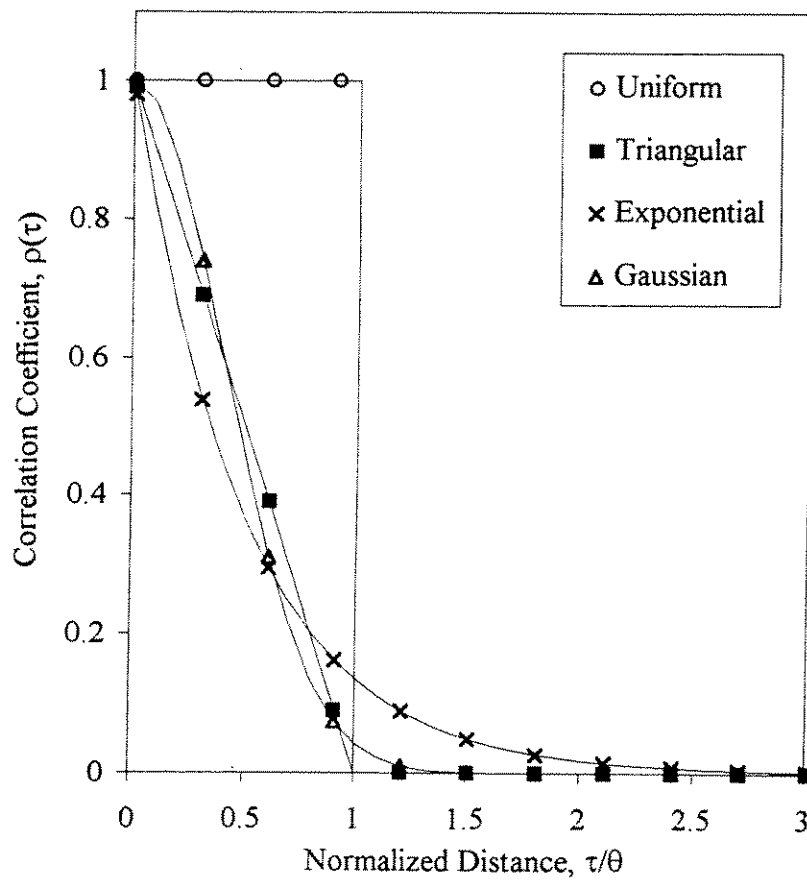


Figure 5.3 Correlation coefficient versus normalized distance



points and  $\theta$  is the scale of fluctuation. The difference between the various correlation models is negligible for values of  $\tau/\theta$  greater than 2.5.

The distance  $\tau$  corresponding to each bin is the average length that the bin extends, i.e. for the example problem the average length for the extent of the second bin is 30 meters  $[(20 \text{ m} + 40 \text{ m})/2]$ . The results for the correlation coefficient determined for the second bin can be plotted on a figure similar to Figure 5.3 and the scale of fluctuation can be evaluated. Recall that the value for the correlation coefficient for the example problem is 0.21. The normalized distance  $\tau/\theta$  on Figure 5.3 corresponding to a value of 0.21 for the correlation coefficient is approximately 0.8 (using the triangular model). Thus, the scale of fluctuation, ( $\theta$ ), using only information from the second bin, can be calculated, i.e.  $\theta = 30 \text{ m}/0.8 = 37.5 \text{ m}$ . In the actual analyses the values for the correlation coefficients are determined for each bin and plotted on a figure similar to Figure 5.3 where the scale of fluctuation can be evaluated.

### 5.3.3 Results

The size chosen for the bins influences the number of sets of shear strength data within each bin. For example, if the bin size is as large as the length of the slope then only one bin will be used. Thus, only one value can be calculated for the correlation coefficient, making it difficult to define the scale of fluctuation. Conversely if the bins are chosen to be too small, there will be a large number of empty or near empty bins which may lead to statistically insignificant results. It is desirable to avoid choosing bin

sizes that are either too large or too small. Several different bin sizes were tried and eventually a bin size of 30 meters was chosen. For the data set used in these calculations, a bin size of 30 meters led to approximately 50 sets of data per bin.

Seventy-two sets of lateral coordinates and shear strengths for cross-section C-C were used as input into VARREDF; these values were determined from the calculations presented in Chapter 4. The calculated values for the correlation coefficients are shown in Figure 5.4. The results indicate that as the distance between two points on the slope increases the correlation between expected values for  $\phi'$  decreases. Also shown on Figure 5.4 is the number of pairs of data points used to calculate the correlation coefficient within each "bin".

Several correlation models were fit to the correlation coefficient data. A comparison of the correlation functions using a value for the scale of fluctuation of 275 meters is shown in Figure 5.5. It can be observed that the uniform correlation model over-predicts the calculated values, especially at smaller lateral distances, and the triangular and Gaussian correlation functions over predict the values at smaller distances and under predict the correlation coefficients at larger distances, shown on Figure 5.5. The exponential correlation functions appear to fit the data well. Thus, the exponential correlation model was chosen over the other models to be used to calculate the scale of fluctuation. The correlation coefficient using an exponential correlation function is expressed by

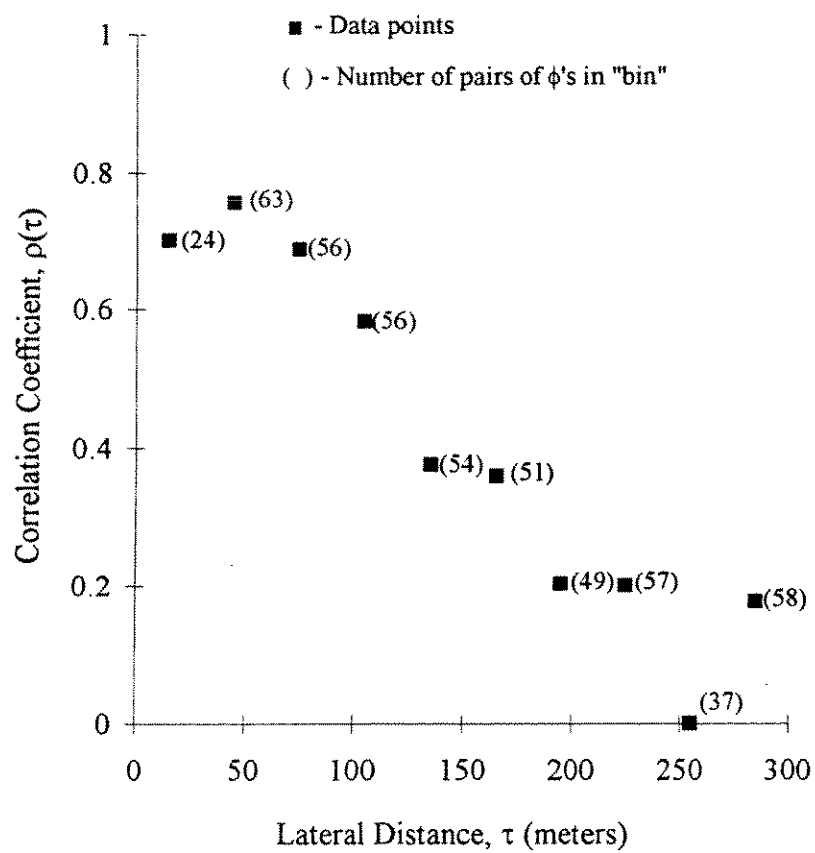


Figure 5.4 Correlation coefficients versus length for cross-section C-C in Pigmy Basin, Gulf of Mexico

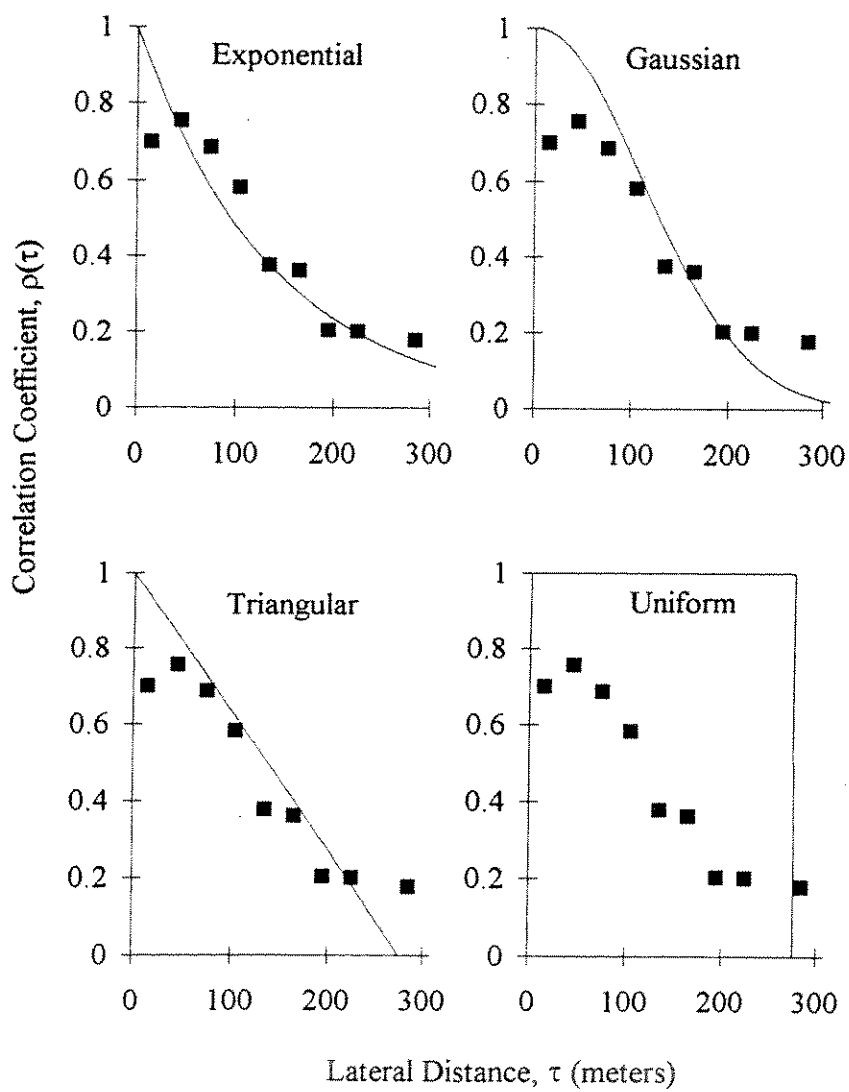


Figure 5.5 Comparison of four different correlation functions to the correlation coefficients using a scale of fluctuation equal to 275 m

$$\rho(\tau) = \exp\left[\frac{-2|\tau|}{\theta}\right] \quad (5)$$

where  $\tau$  is the distance between points.

Figure 5.6 shows the data for the correlation coefficients and the exponential correlation function using values of 250, 325, and 400 meters for the scale of fluctuation. The values of 250 and 400 meters represent upper and lower bound for the scale of fluctuation and were chosen to represent the upper and lower bounds of the data by examination, i.e. curves were fit by eye to represent the bounds. A value of 325 meters was chosen to represent scale of fluctuation and was determined as the average of the upper and lower bounds.

#### 5.3.4 Calculation of the Autocorrelation Distance

The autocorrelation distance, like the scale of fluctuation, can be a useful parameter for describing the correlation structure for a variable using a single variable. The autocorrelation distance is defined as the distance at which the correlation coefficient is equal to  $1/e$ , where  $e$  is the base of the natural logarithm. Figure 5.7 shows the correlation structure developed using the exponential correlation model and values of 250 and 400 meters for the scale of fluctuation. A horizontal line located at  $\rho(\tau)$  equal to  $1/e$  is shown on Figure 5.7. The distance,  $\tau$ , where the  $\rho(\tau)$  is equal to  $1/e$ , represents the autocorrelation distance for the particular value for the scale of fluctuation (Vanmarcke, 1983). The autocorrelation distances for the scale of fluctuation equal to 250 and 400 meters are 125 and 200 meters, respectively (Figure 5.7).

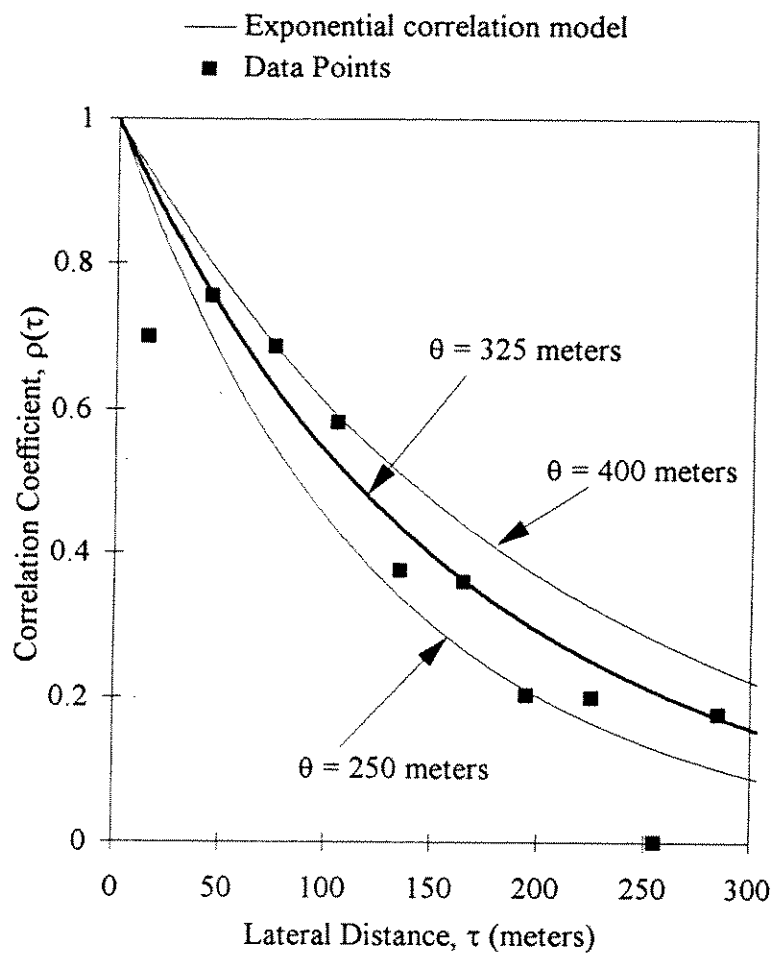


Figure 5.6 Results of the calculated correlation coefficients and the exponential correlation function using a scale of fluctuation equal to 250 m, 325 m, and 400 m

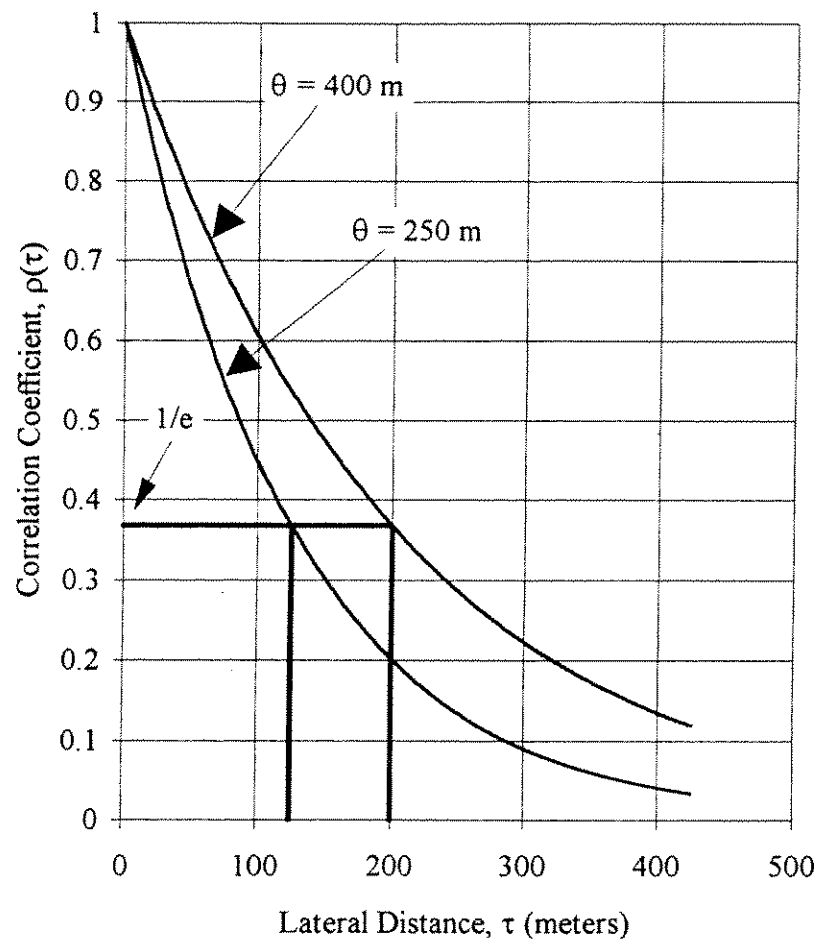


Figure 5.7 Illustration of the determination of autocorrelation distance from the scale of fluctuation

The values calculated for the autocorrelation distances for effective stress friction angles in the lateral direction (125 and 200 meters) are significantly larger than the values reported in Chapter 2 for shear strength in the lateral direction (14 to 38 meters). The primary reason for the differences between the values of the autocorrelation distances calculated in this chapter and those reported in Chapter 2 is likely due to the differences in the scale of the measurements used to determine the autocorrelation distances. The values for autocorrelation distances for shear strength reported in Chapter 2 were determined from measurements using cone penetration devices. Each shear strength measurement is taken at a "point" in the soil, i.e. shear strength is measured over a volume of soil on the order of a few cubic centimeters. The values for the autocorrelation distances calculated in this chapter were determined using inferred shear strengths, not at points, but over the large lateral distance of the segments between contour lines. Recall that the slope angle and shear strength were assumed constant for each segment. Thus, each shear strength used in these computations is inferred over a volume of soil on the order of 10's to 100's of cubic meters.

#### **5.4 Propagation of Errors Associated in Calculating the Scale of Fluctuation**

In the following sections, the effects of propagation of errors in determining the slope profile from the bathymetry charts on the expected value and uncertainty of the scale of fluctuation are investigated. Several potential sources of error are discussed. The propagation of error was determined using a series of Monte Carlo simulations and the results are presented in a following section.



#### 5.4.1 Sources of Error

There are a variety of potential sources of error associated with evaluation of the scale of fluctuation. These sources may come from: (1) the method used to measure the bathymetry information, as discussed in Chapter 2, (2) scaling the bathymetry measurements from the contour plots, and (3) the assumption that the factor of safety for the slope is equal to unity along the entire length of the slope in order to back-calculate values for  $\phi'$ .

Each of these errors would be expected to have an influence on the uncertainty of the value of the scale of fluctuation calculated in the previous section. Of all the potential sources of error discussed, the error associated with scaling the dimensions from bathymetry charts was chosen in part due to the ease in which the propagation of error may be represented and modeled. The error associated with scaling the dimensions from the bathymetry charts to obtain slope geometry for cross-section C-C will be investigated in the following sections.

A scale with 60 divisions per inch was used to measure the horizontal distances between the contour intervals. Interpolation beyond this scale was done to one half of one division i.e. 1/120 inch. The error associated in measuring the data was assumed to be normally distributed and independent between measurements with a mean of zero and a standard deviation of 1/4 of a division,  $N(0, 0.25)$ . The errors were assumed independent between measurements because it was felt that errors in the measurements were random and not systematic. Monte Carlo simulations were used to model the error

in order to understand how the mean and variance for the distribution of the scale of fluctuation is affected. Numerical methods, as opposed to analytical methods, were used to estimate the mean and variance since the actual distribution of the slope geometry is unknown.

#### **5.4.2 Monte Carlo Simulation**

The uncertainty in the results determined from the simulations is related to the number of Monte Carlo simulations performed. If a large number of simulations is performed, there will be a smaller amount of uncertainty in the results compared to results determined using a smaller number of simulations. Thus, with each additional simulation performed the confidence in the results increases.

The number of Monte Carlo simulations performed for this investigation was chosen based on the information that was needed to understand how the propagation of error in the measurements affects the response of the mean and the variance for the scale of fluctuation. In addition, a practical limit to the number of simulations was set since the process used to determine a value (or range in values) for the scale of fluctuation for each simulation was not automated. The number of simulations was chosen to be 80. This number of simulations (80) corresponds to an error of  $\pm 4$  percent in the mean, for a coefficient of variation of 0.2 and error of  $\pm 31$  percent in the variance with 95 percent confidence bounds.

To model the uncertainty in the measurement of horizontal distances between contour intervals, a series of uniformly distributed random variables was transformed

into an associated change in the length for a single measurement. Thus, if the measured horizontal distance between two successive contour intervals was 21 divisions and the normally distributed random error,  $N(0,0.25)$ , associated with that measurement is 0.125 divisions, then the new horizontal distance between the points becomes 21.125 divisions (21+0.125). This procedure was done for cross-section C-C using an independent normally distributed random error for each segment of the slope. These new horizontal distances for each segment of the slope result in new slope angles for each segment and, hence, a new value for the back-calculated effective stress friction angle (assuming infinite slope procedures and  $F = 1.0$ ). New horizontal coordinates and the associated shear strength parameter  $\phi'$  were determined for each simulation and the correlation coefficients were evaluated using VARREDF allowing the scale of fluctuation to be evaluated. The entire process of developing new horizontal coordinates and associated effective stress friction angles, calculating the correlation coefficients, and determining the scale of fluctuation was repeated 80 times.

The process of converting uniformly distributed random variables between the range of 0 and 1 to normally distributed variables with the desired mean  $\mu$  and standard deviation  $\sigma$ ,  $N(\mu, \sigma)$  is given in detail by Ang and Tang (1990). A rough outline of the procedure follows. First, a uniformly distributed random variable between zero and one is generated. Next, the inverse of the cumulative distribution function for the normal distribution is evaluated using the random number. The result is a normally distributed number with a mean of zero and standard deviation of one,  $N(0, 1)$ . Next, this number,

$N(0, 1)$ , is transformed to the desired normally distributed parameter  $N(\mu, \sigma)$  by multiplying the number by the desired standard deviation and adding the desired mean. The result is a series of normally distributed errors  $N(\mu, \sigma)$ . The following example illustrates this process.

Consider a measured segment length of 21 divisions and an assumed normally distributed error with a mean of zero divisions and standard deviation of 0.25 divisions. Furthermore assume a uniformly distributed random number equal to 0.6915 is generated. The inverse cumulative distribution function evaluated at 0.6915 can be determined using a standard normal probability table and is equal to 0.5. This value, 0.5, is converted to the desired distribution by multiplying by 0.25 divisions (the desired standard deviation) and adding zero divisions (the desired mean), i.e.  $0.25 \cdot (0.5) + 0 = 0.125$  divisions. This result is then added to the original measured length, i.e.  $21 + 0.125 = 21.125$  divisions, which reflects the new segment length incorporating the potential error in the original measurement.

#### 5.4.3 Results

For each simulation, the scale of fluctuation was determined by taking the average of the upper and lower bounds for the scale of fluctuation as previously described in Section 5.3.3. Table 5.4 indicates the frequency distribution for the difference between the upper and lower bounds of the scale of fluctuation for each of the 80 simulations. The results indicate that four of the simulations yielded a range for the

Table 5.4  
Frequency distribution for the difference between the maximum and the minimum value  
of the scale of fluctuation for each of the 80 simulations

Difference between upper and lower bounds for the scale of fluctuation	Frequency
$\leq 100$	4
100 - 150	13
150 - 200	22
200 - 250	24
250 - 300	12
$> 350$	5
total	80

scale of fluctuation less than 100 meters and five simulations gave ranges greater than 350 meters. The frequency distribution for the average scale of fluctuation determined for each of the 80 simulations is shown in Figure 5.8. The distribution shown in Figure 5.8 indicates the new distribution for the scale of fluctuation based on the normally distributed error,  $N(0, 0.25)$ , associated with the measurement of the horizontal distances from the bathymetry data. The expected value for the scale of fluctuation of this new distribution is equal to 297 meters with a standard deviation of 36 meters. These new statistics indicate that the propagation of error from measuring the bathymetry lowered the expected value of the scale of fluctuation from 325 to 297 meters and increased the uncertainty in the value of the scale of fluctuation as shown by the range in values for the scale of fluctuation shown in Figure 5.8. The decrease in the value for the scale of fluctuation was expected since the errors in the measurements were assumed to be independent. By adding an independent random error to the measured distances, the values for the correlation coefficients defining the correlation structure will decrease in value, i.e. the scale of fluctuation will decrease. The increase in uncertainty in the value for the standard deviation was expected since the errors modeled in the Monte Carlo simulations were assumed to be independent between measurements.

As stated previously, the error in the mean value of scale of fluctuation was determined to be  $\pm 10$  percent for 80 simulations and assuming a value for the coefficient of variation ( $\delta$ ) of 0.20. A value for the coefficient of variation had to be assumed since

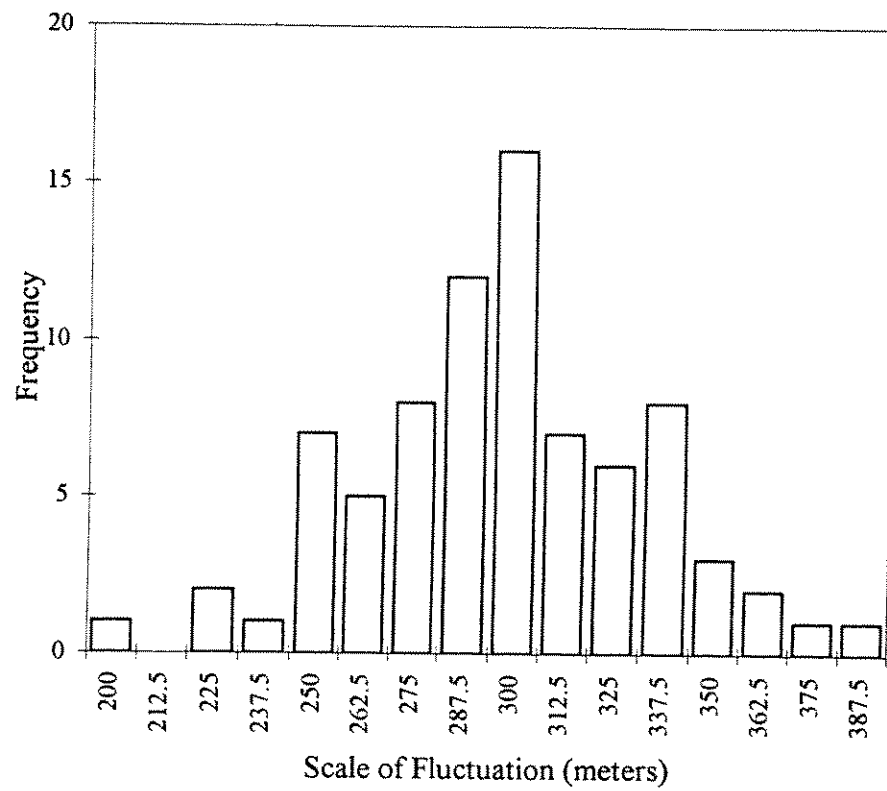


Figure 5.8 Frequency distribution for the scale of fluctuation based on 80 Monte Carlo simulations

the mean and standard deviation of the distribution was not yet known. Based on the outcome of the 80 simulations the coefficient of variation  $\delta$  was equal to 0.12. This value is lower than the value (0.20) used to estimate the error in the mean value of scale of fluctuation. Thus, the error in the mean value of scale of fluctuation using the more accurate value of  $\delta$  equal to 0.12 (instead of 0.20) and 80 simulations becomes  $\pm 3$  percent as opposed to the  $\pm 4$  percent originally calculated. The error in the variance of the scale of fluctuation is not dependent on the coefficient of variation.

## 5.5 Conclusion

The scale of fluctuation ( $\theta$ ) in the lateral direction for the shear strength of soil was calculated for a slope cross-section in Pigmy Basin of the Gulf of Mexico. The shear strength was back-calculated from slope angles assuming the cohesion ( $c'$ ) was zero and the friction angle ( $\phi'$ ) was equal to the slope angle. Thus, the scale of fluctuation which was calculated for the shear strength is the same as the scale of fluctuation for the slope angle.

A value for the scale of fluctuation of 325 meters was determined by fitting an exponential correlation function to the values for correlation coefficients. The correlation coefficients were determined using a computer program (VARREDF) written specifically for this purpose. The program accepts as input the lateral coordinates and corresponding values for the friction angle. Values for the autocorrelation distance of 125 meters and 200 meters were determined using values of



250 and 400 meters for the scale of fluctuation, respectively. The calculated value for the scale of fluctuation and the autocorrelation distances may be large due to the course resolution of the bathymetric data used in the analyses. Higher resolution bathymetric data may lead to lower values calculated for the scale of fluctuation and autocorrelation distances.

The effect from the error in the measurements, used to determine slope geometry from bathymetry charts, on the expected value for the scale of fluctuation was evaluated using Monte Carlo simulations. The results indicate that the error caused a decrease in the expected value of the scale of fluctuation and an increase in the uncertainty of the scale of fluctuation.

The method presented to calculate the scale of fluctuation in this chapter has inherent problems. The method requires that the data be placed in discrete groups or "bins" as opposed to analyzing the data in its original and continuous form. The effect from forcing the data into bins may influence the value calculated for the scale of fluctuation. An additional problem lies in the fact that the confidence in the calculated value for the scale of fluctuation can not be quantified using the method of analyses described in this chapter. A method used to calculate the scale of fluctuation which overcomes these problems has been suggested by Gilbert and McGrath (in press).

## 6. Characterizing Stability along the Length of an Irregular Slope

### 6.1 Introduction

In Chapter 4, slope stability was computed along three cross-sections using "infinite slope" analyses. In this chapter results of slope stability computations using Spencer's procedure of slices and more general-shaped shear surfaces than those of the infinite slope are presented. All of the computations presented in this chapter are for a single cross-section, section C-C.

At the outset of this study it was thought that infinite slope procedures could be used to characterize the stability along the length of the cross-section provided that the soil was cohesionless ( $c' = 0$ ). This was expected because slopes offshore are typically of large lateral extent. For slopes of great lateral extent and cohesionless soil, the critical potential shear surface should be a shallow plane parallel to the face of the slope. This, however, was discovered to not be the case for slopes like the ones examined in Pigmy Basin. Thus, the infinite slope procedure used in Chapter 4 to calculate the variability in stability along the slope profiles may not produce the minimum factor of safety for some points on the slope profiles.

In order to access stability along the length of a slope, a new procedure was developed to characterize the minimum factor of safety along an irregular slope and represent the factor of safety as a function of position. The new procedure and results are presented in this chapter. The procedure used to determine the variation in factor of

safety along a slope is different for soils with no cohesion and soils exhibiting at least some cohesion. The procedures for these two cases ( $c = 0$ ;  $c > 0$ ) are presented in separate sections.

## **6.2 Slope Stability**

Spencer's (1967) limit equilibrium procedure of slices was used to perform all the calculations presented in this chapter. Buoyant unit weights were used to account for submergence. The buoyant unit weight was assumed to be  $4.72 \text{ kN/m}^3$  based on several density measurements taken from samples retrieved from drop cores at approximately four meters below the mud line near the location of cross-section C-C. The density profiles are shown in Figure 6.1.

## **6.3 Cross-Section C-C**

Figure 6.2 shows cross-section C-C in Pigmy basin. The dashed extensions on either end of the slope were added to represent a horizontal ground surface so stability analyses could be performed near the ends of the slope.

## **6.4 Searching Method Restricting Lateral Coordinate of the Center of the Circle**

A special search method that restricts the lateral coordinate of the center of the circular shear surface was used to determine stability along cross-section C-C. The search was conducted by varying the radius of the circular shear surface and varying the vertical location of the center of the circular shear surface for a given lateral coordinate.

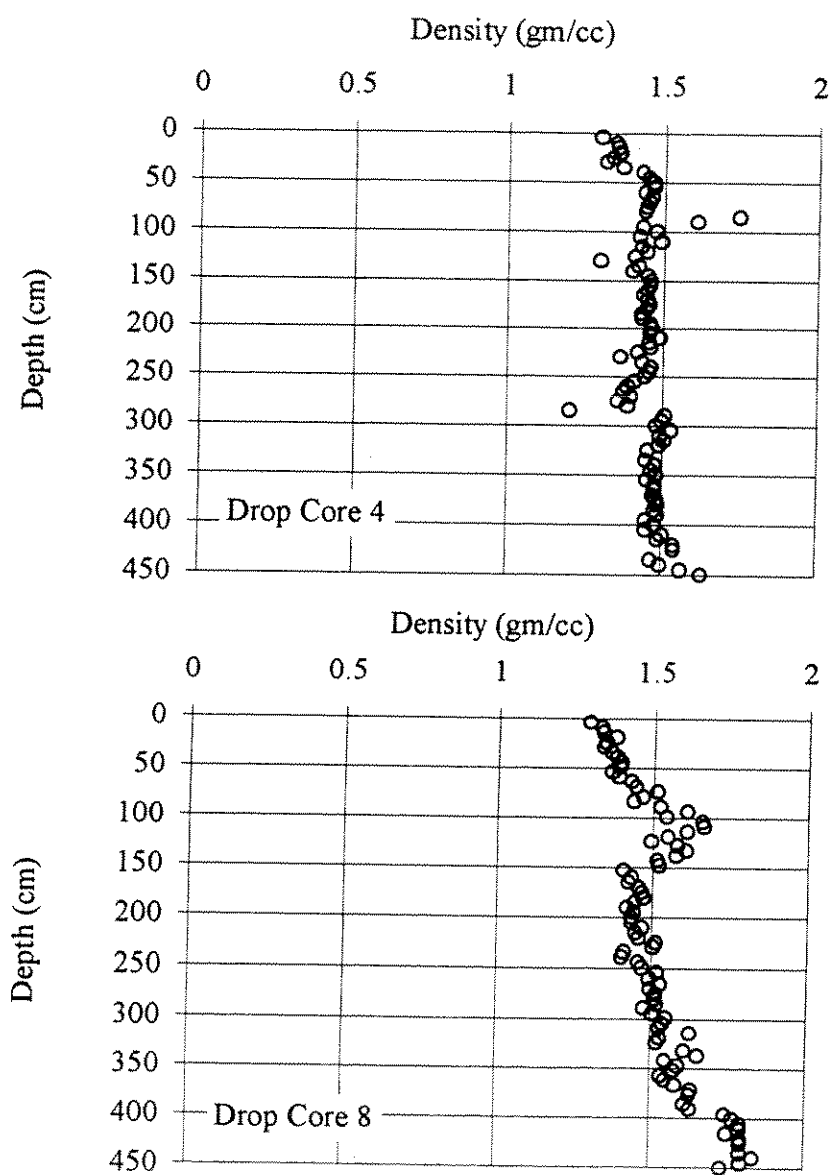


Figure 6.1 Soil densities for drop cores 4 and 8 in Pigmy Basin (after Bryant et al., 1995)

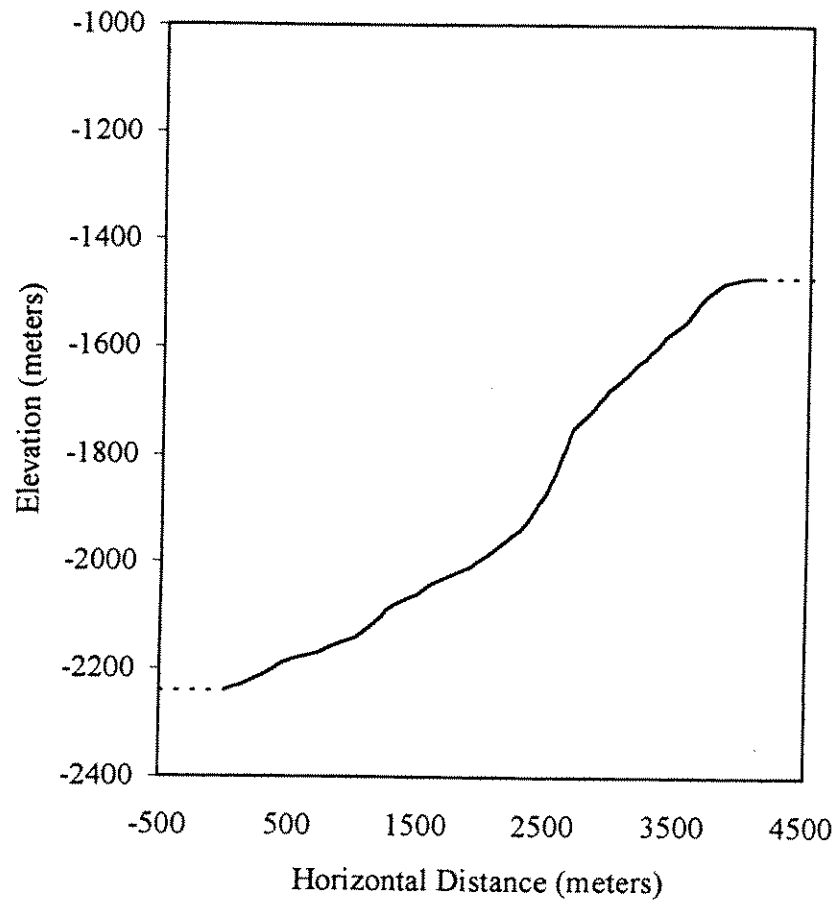


Figure 6.2 Cross-section C-C with horizontal extensions

An example of this search scheme is shown in Figure 6.3. The vertical line represents the lateral coordinate where the center of the circles are located. The points labeled "A", "B", and "C" illustrate three different vertical positions for the centers of circles. An example of two different radii for a given center point is also shown in Figure 6.3 for the center located at point A. Once stability calculations have been performed by varying the radius at point A, the process of varying the radius is repeated at point B, then at point C. The search is then repeated for other lateral positions of the center points. From the results of such calculations, the minimum factor of safety can be determined for each lateral coordinate. A special version of the computer program UTEXAS3 (Wright, 1991), modified to "search" in the manner described, was used for this purpose.

#### **6.4.1 Description of Search Method**

Stability calculations were performed for cross-section C-C using the procedure described above. Centers were spaced at 152.4 meter intervals along the 3810 meters of slope profile. Twenty-six lateral positions for center points were examined (Figure 6.4).

For each lateral position of the center point, the vertical location of the center was varied in prescribed increments between two selected limits. The lower limit for the vertical position of the center was selected to be five meters above the surface of the slope. The upper limit was selected to be approximately 15,000 meters above the surface of the slope, which was well above the maximum vertical location of any of the critical circles found. Initially, the increment for locating center points between these

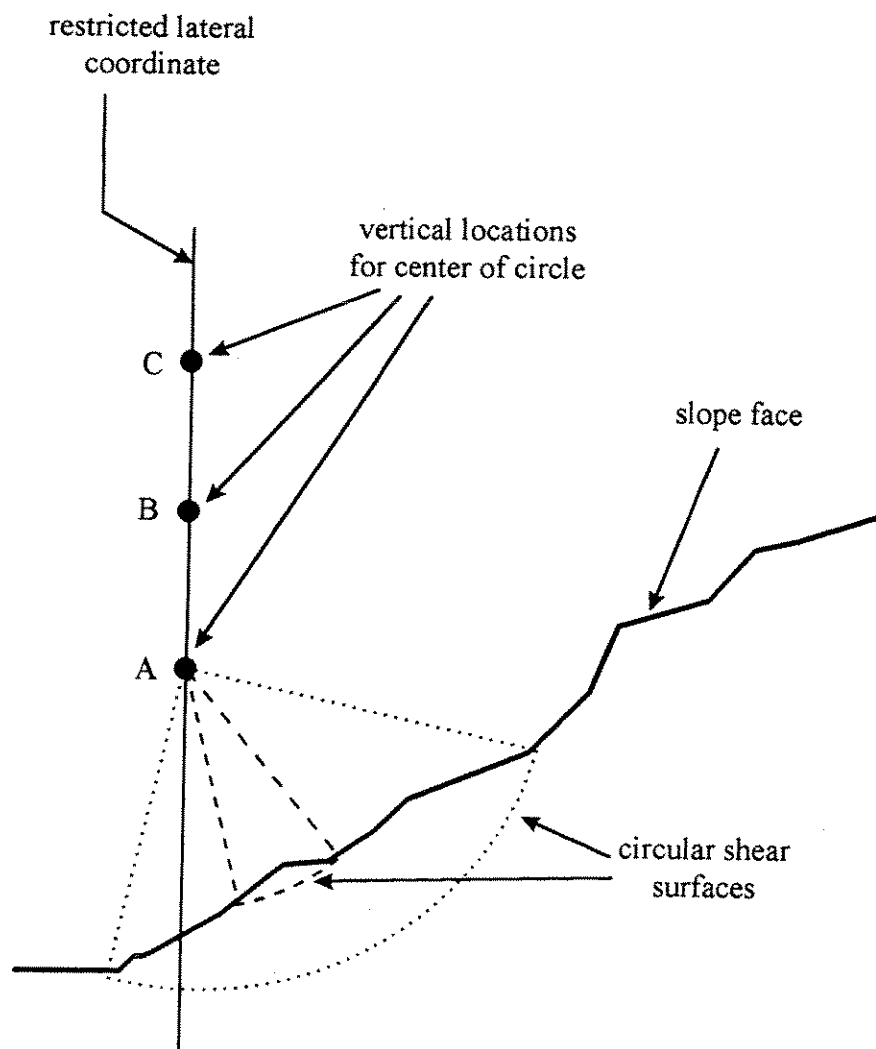


Figure 6.3 Example of search method restricting lateral coordinate of the center of the circle

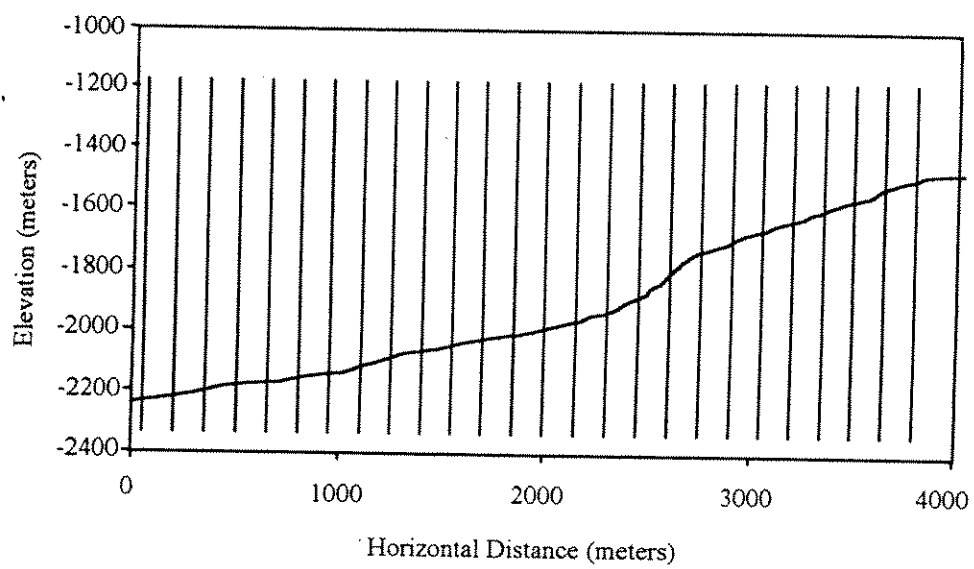


Figure 6.4 Twenty-six vertical lines spaced 152.4 meter apart used for restricting the circular shear surface centers



two limits was set to 500 meters. After examining results from the stability calculations for each particular lateral coordinate, the upper and lower limits were moved closer together to reflect the vertical region where the factor of safety was smallest. The increment was then reduced and the search repeated. A final value of 10 meters was used for the vertical spacing between center points of the circle.

At each vertical location for the center of the circles, the radius of the circles was varied between prescribed limits. The minimum radius for a given center point was equal to the minimum distance between the center point and some point on the face of the slope, i.e. the smallest radius for a circle to intercept the slope. The maximum radius was defined as the distance from the center to a set of line segments parallel to the face of the slope at a prescribed depth below the surface of the slope. The distance below the surface of the slope to the line segments used to determine the maximum radius was initially set to 1000 meters; however, after viewing results from the first few sets of analyses a value of 500 meters was determined to be sufficiently deep. The radius of the circular shear surface was varied between the minimum and maximum values in 20 equal increments. Once the factors of safety were evaluated for the 21 radii, the radii in the vicinity of the lowest factors of safety were successively reduced until the increment between successive radii was less than or equal to 0.3 meters. The process of subdividing the increments of radii around the "local" minimum is shown in Figure 6.5: Factors of safety for five initial radii are shown by the solid squares. The lowest initial factor of safety is 1.90 and occurs for a radius of 140 meters. The open

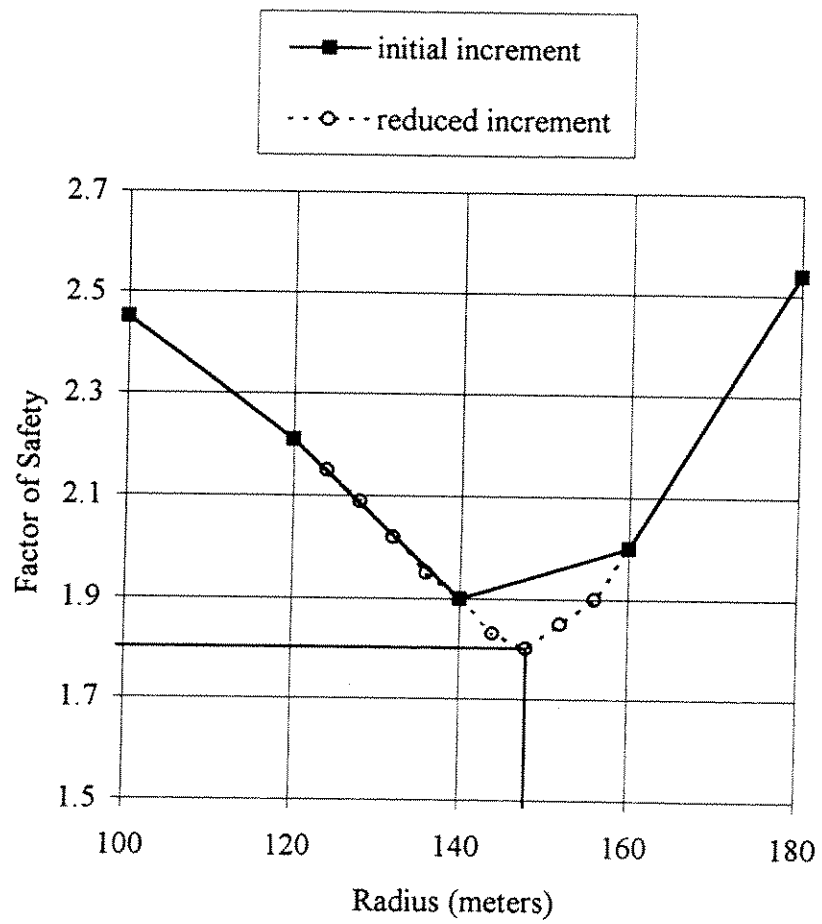


Figure 6.5 Example of subdividing radius around local minimum factor of safety

circles in Figure 6.5 illustrate the factors of safety calculated by subdividing the radii between 120 and 160 meters using increments of four meters. A new minimum factor of safety of 1.80 is then determined at a radius of 148 meters. In the actual analyses the radii in the location of the local minimum were even further subdivided until the increments in radii were no larger than 0.3 meters.

#### **6.4.2 Results for Searching Method Restricting Lateral Coordinate of the Center of the Circle**

The first set of computations for the slope was performed assuming an effective stress friction angle,  $\phi'$  equal to 16 degrees and no cohesion. The computed variation in factor of safety along the slope is shown in Figure 6.6. Also shown in Figure 6.6 are the factors of safety from the infinite slope analyses presented earlier in Chapter 4. As seen in Figure 6.6, the factor of safety along the slope using circular shear surfaces is constant ( $F=0.41$ ) between the toe of the slope and a point approximately 2600 meters up from the toe. This large range over which the factor of safety was constant seemed unrealistic.

Further examination of the results of the analyses summarized in Figure 6.6 revealed that the critical circles with centers located between the toe of the slope and the point 2600 meters from the toe were all essentially the same circle. The critical circles all intersected the irregular slope near a point located approximately 2600 meters from the toe. This effect is illustrated for several typical center point locations in Figure 6.7. Each critical circle shown is located at approximately the same region of the slope

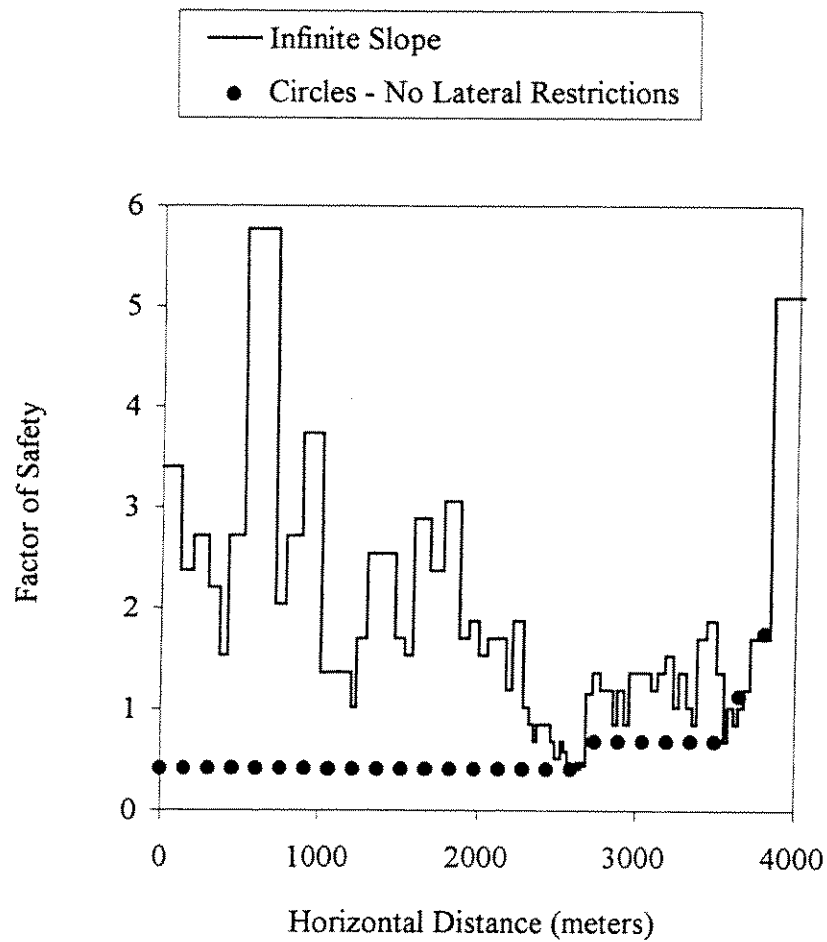


Figure 6.6 Comparison of factors of safety using infinite slope and restricted center for cross-section C-C assuming cohesionless soil

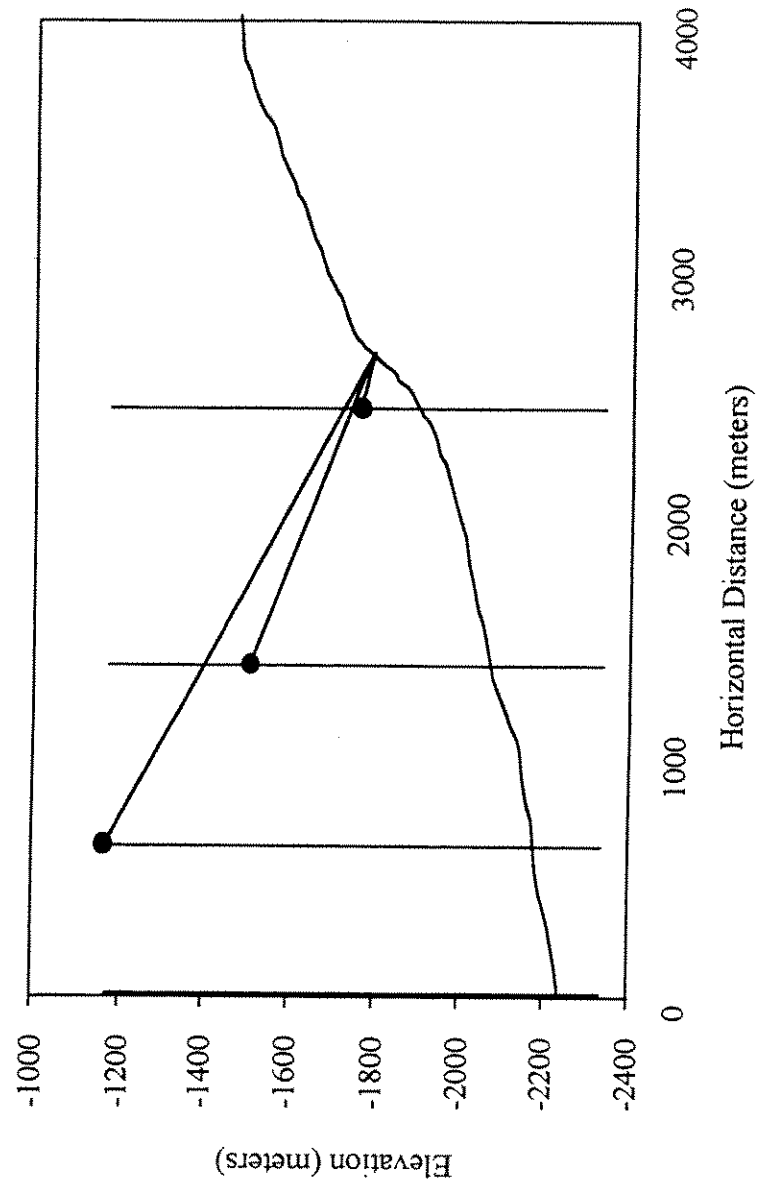


Figure 6.7 Figurative example of result for the variation in the factor of safety for cross-section C-C for the search method using restricted centers

regardless of the location of the center, and all produce essentially the same value for the factor of safety (0.41). All of the circles are relatively shallow and are located at a portion of the slope inclined at approximately 35 degrees. The value of 0.41 for the factor of safety corresponds closely to the value for an infinite slope inclined at 35 degrees, i.e.  $F = \tan\phi' / \tan\beta = \tan 16^\circ / \tan 35^\circ$ .

As the centers of circles move to locations further than 2600 meters from the toe of the slope the factors of safety shown in Figure 6.6 increase. This is because there is no segment of slope beyond 2600 meters from the toe that is as steep as 35 degrees. Also, it is generally not possible geometrically for a circle to lie entirely down-slope from the center. Because of this geometric constraint the search method described in Section 6.4 will usually find the critical shear surfaces at the steepest portion of the slope at or up-slope from the center point.

The analyses presented above reveal that while the center of a critical circle may be fixed in the lateral direction the shear surfaces are not necessarily located at or near the center in the lateral direction. Thus, the search method and scheme for calculating factors of safety does not characterize the variation in stability with position along the length of the slope in a very meaningful way, rather it finds the portion of the slope with the lowest factor of safety at or uphill from the point of interest.

### **6.5 Searching Method with Shear Surface Restricted to Pass Beneath the Center Point**

To better characterize the variation of stability along the length of the slope, an alternative method was developed. The alternative method is identical to the method described previously above except the shear surface was restricted to pass beneath the center point. Any circles which did not meet this criteria were rejected. Examples of conditions which may lead to the rejection and acceptance of a circle are shown in Figure 6.8. Of the two circular shear surfaces shown in Figure 6.8 only the shear surface represented by the solid line is accepted.

Stability analyses were performed on cross-section C-C using the modified search method described above. Except for rejecting circles that did not pass beneath the center point, the search scheme and parameters used were identical to the ones used previously. UTEXAS3 (Wright, 1991) was further revised to automate the modified searching process.

The variation of stability along cross-section C-C was determined using the revised search method. Calculations were performed and results are presented for two different shear strength characterizations: (1) a cohesionless ( $c' = 0$ ) soil, and (2) a soil with both cohesion and friction.

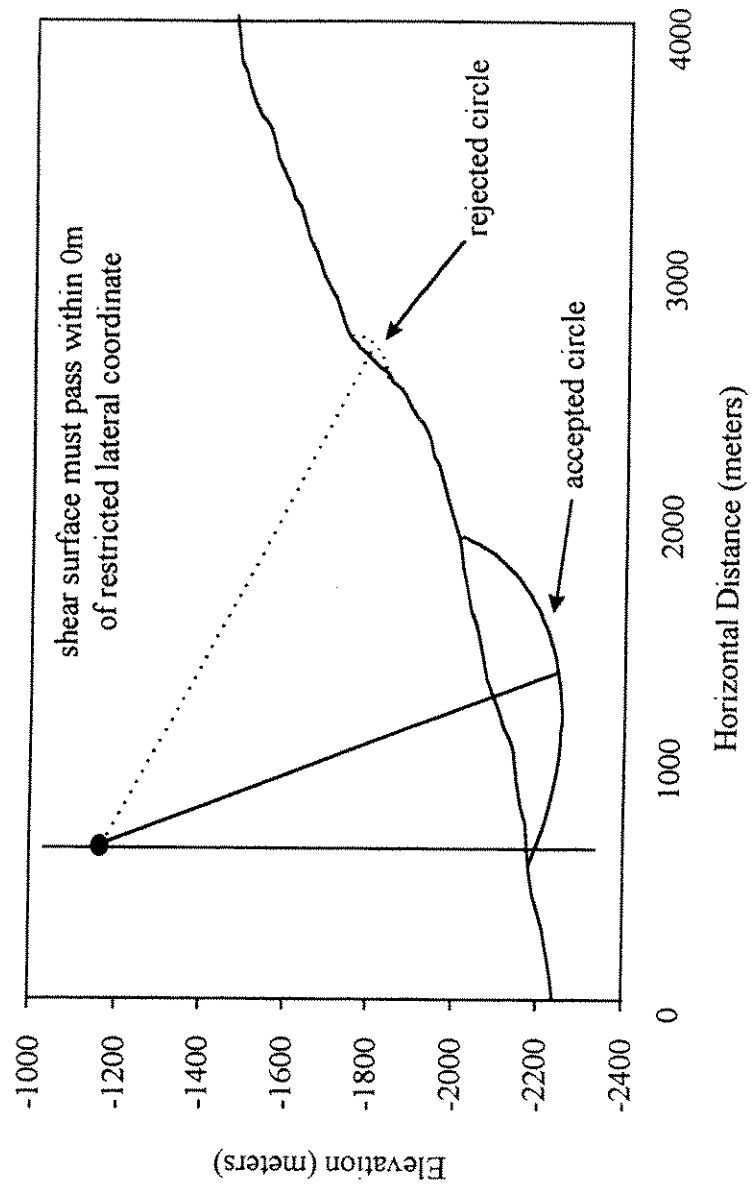


Figure 6.8 Example of accepted and rejected shear surfaces based on criteria restricting location of shear surface relative to lateral coordinate of center



### 6.5.1 Cohesionless Soil

For the cohesionless soil, the value for the effective stress friction angle was assumed to be 16 degrees. Results for the revised search scheme are summarized in Figure 6.9 along with results obtained previously using infinite slope procedures and the earlier search scheme where circles were not required to pass beneath the center point. The variation in the factor of safety along the length of the slope is smoother for the new search scheme where the shear surface is restricted to pass beneath the center point. The factors of safety calculated using circular shear surfaces with the revised search scheme was lower than the factors of safety calculated for an infinite slope, except for three points located at horizontal distances of 1219, 2591, and 3658 meters from the toe of the slope. The stability calculations performed using circular shear surfaces did not produce factors of safety as low as those from the infinite slope analyses due to a geometrical constraint: For a circular shear surface which passes vertically beneath the center point, the minimum angle ( $\theta$ ) subtended by the circle must be twice the slope angle ( $\beta$ ) as shown in Figure 6.10. The minimum possible subtended angle occurs when the shear surface exits just below the center point. As illustrated in Figure 6.11 the depth ( $d$ ) of the circle can be related to the radius ( $R$ ) and the subtended angle ( $\theta$ ) by,

$$d = R - R \cos\left(\frac{\theta}{2}\right) = R \left[ 1 - \cos\left(\frac{\theta}{2}\right) \right] \quad (1)$$

Also, the length ( $l$ ) of the circular shear surface can be related to the radius and the subtended angle by,

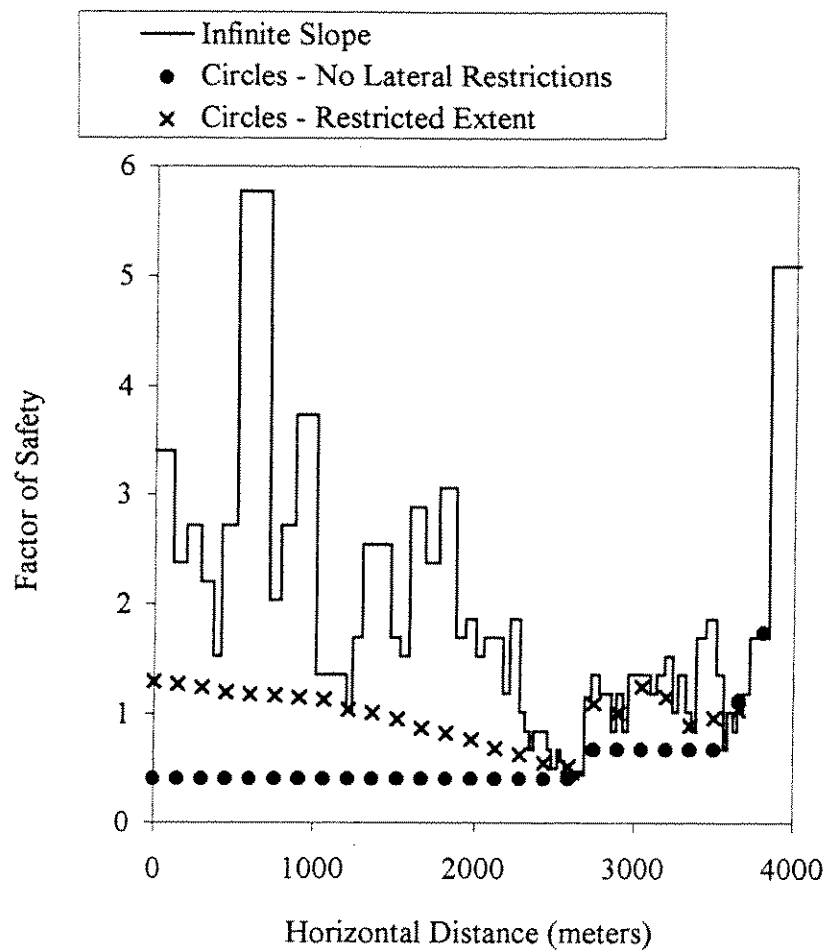


Figure 6.9 Variation in factors of safety with location using location (infinite slope) or center point (circle) using infinite slope, restricted center, and restricted center and restricted shear surface extent for cross-section C-C assuming cohesionless soil

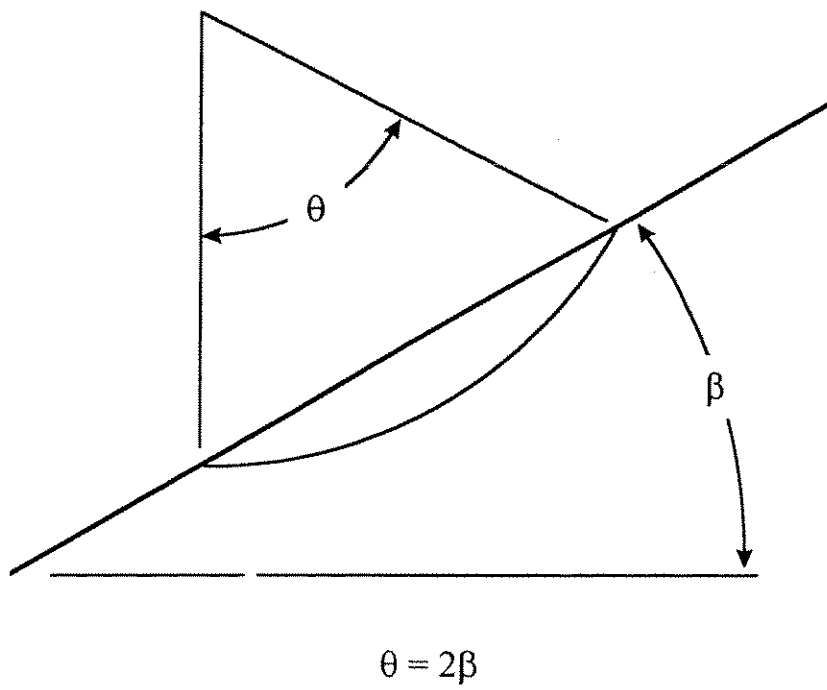


Figure 6.10 Relationship between subtended angle ( $\theta$ ) and the slope angle ( $\beta$ )

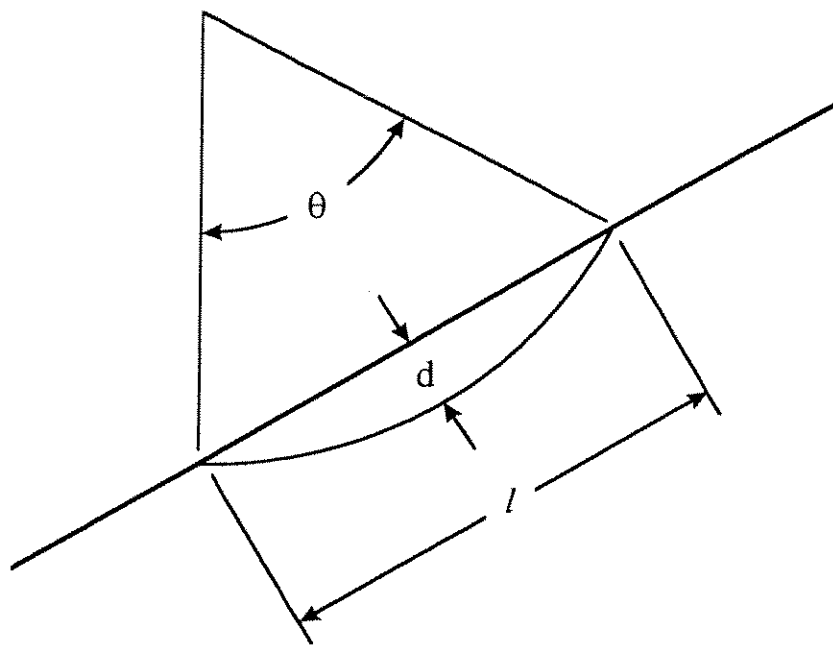


Figure 6.11 Relationship between subtended angle ( $\theta$ ), the slope angle ( $\beta$ ), and the relative slide depth  $d/l$

$$l = 2R \sin\left(\frac{\theta}{2}\right) \quad (2)$$

Thus, the ratio of the depth of the circle to the length of the circle along the slope is,

$$\frac{d}{l} = \frac{1 - \cos\left(\frac{\theta}{2}\right)}{2 \sin\left(\frac{\theta}{2}\right)} \quad (3)$$

or,

$$\frac{d}{l} = \frac{1 - \cos(\beta)}{2 \sin(\beta)} \quad (4)$$

Equation 4 expresses the minimum slide depth to length ratio of a circular shear surface that exits at a point vertically beneath the center point.

For some slopes and, especially steep slopes, it is not possible for circular shear surfaces to exit at the center point and at the same time correspond to very shallow slides. Thus, such circles may not produce the minimum factor of safety, especially for cohesionless soils. An example of this is shown in Figure 6.12 for a 30 degree slope where the minimum factor of safety occurs at point P on the slope. The minimum depth to length ratio for a circle that exits at point P and whose center is above point P is approximately 13 percent for this 30 degree slope. An example of such a circle is shown in Figure 6.12 labeled "A". In contrast, another circle such as the one labeled "B" can exit at point P and have a much shallower depth to length ratio. The length to depth ratio for Circle B is approximately six percent. If the soil in the slope is

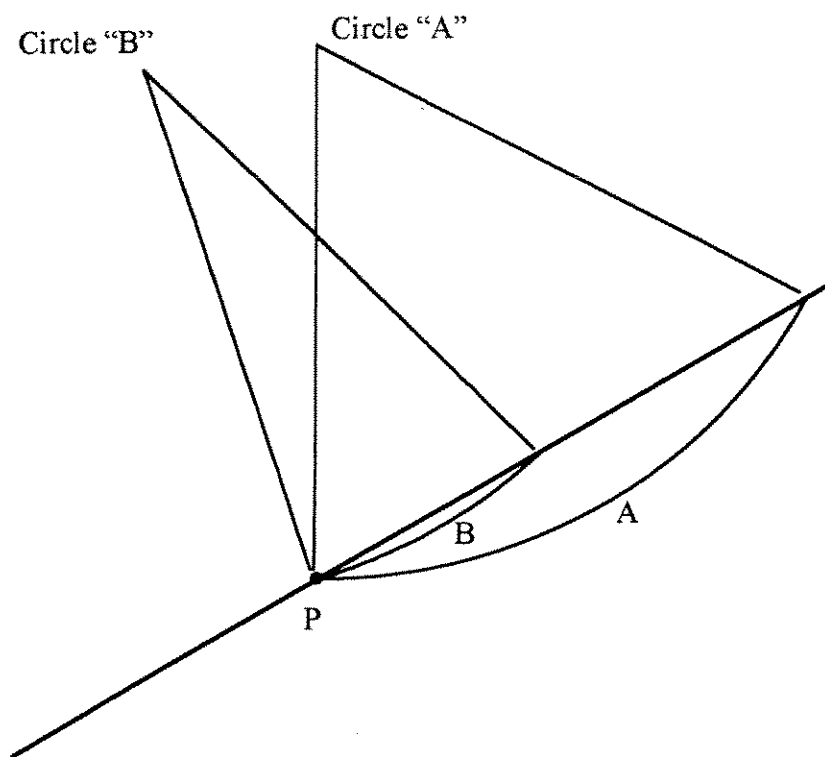


Figure 6.12 Comparison of circle crossing beneath center with circle not passing beneath center

cohesionless, Circle B will produce a lower factor of safety. Figure 6.13 shows how the depth to length ratio effects the factor of safety for slope angles of 15 and 30 degrees and cohesionless soil with effective stress friction angles equal to 15 and 30 degrees, respectively. For an infinite slope analysis these two slopes will have factors of safety equal to unity. The large, solid symbols shown in Figure 6.13 represent the points where the exit point of the circle lies vertically beneath the center point of the circle. Depth to length ratios lying to the left of the points represented by the solid symbols represent conditions where the circles exit up-slope from the center point; depth to length ratios lying to the right of the solid symbols represent conditions where the circle exits down-slope from the center point. From the results presented in Figure 6.13 the factors of safety can be determined, for a slope of cohesionless soil with a slope angle and effective stress friction angle of 30 degrees and a depth to length ratios of 13 percent (Circle A in Figure 6.12) and six percent (Circle B in Figure 6.12) to be 1.15 and 1.03, respectively. These calculations show that restricting the circle to pass beneath the center point increases the depth to length ratio of the circle which increases the calculated factor of safety for a circular shear surface in a cohesionless soil.

To eliminate the problem described, the minimum factor of safety can be taken as the minimum factor of safety from either an infinite slope analysis or from the search with circular shear surfaces restricted to pass vertically beneath the center point. The factors of safety determined in this manner are shown in Figure 6.14.

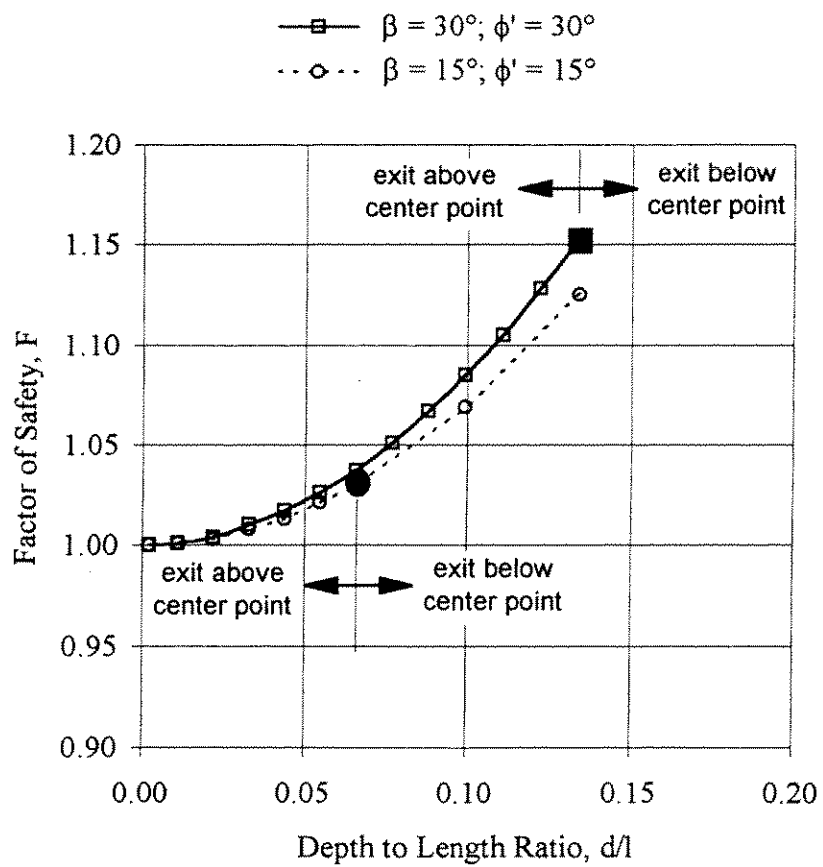


Figure 6.13 Influence of depth to length of circle on the factor of safety for cohesionless soil



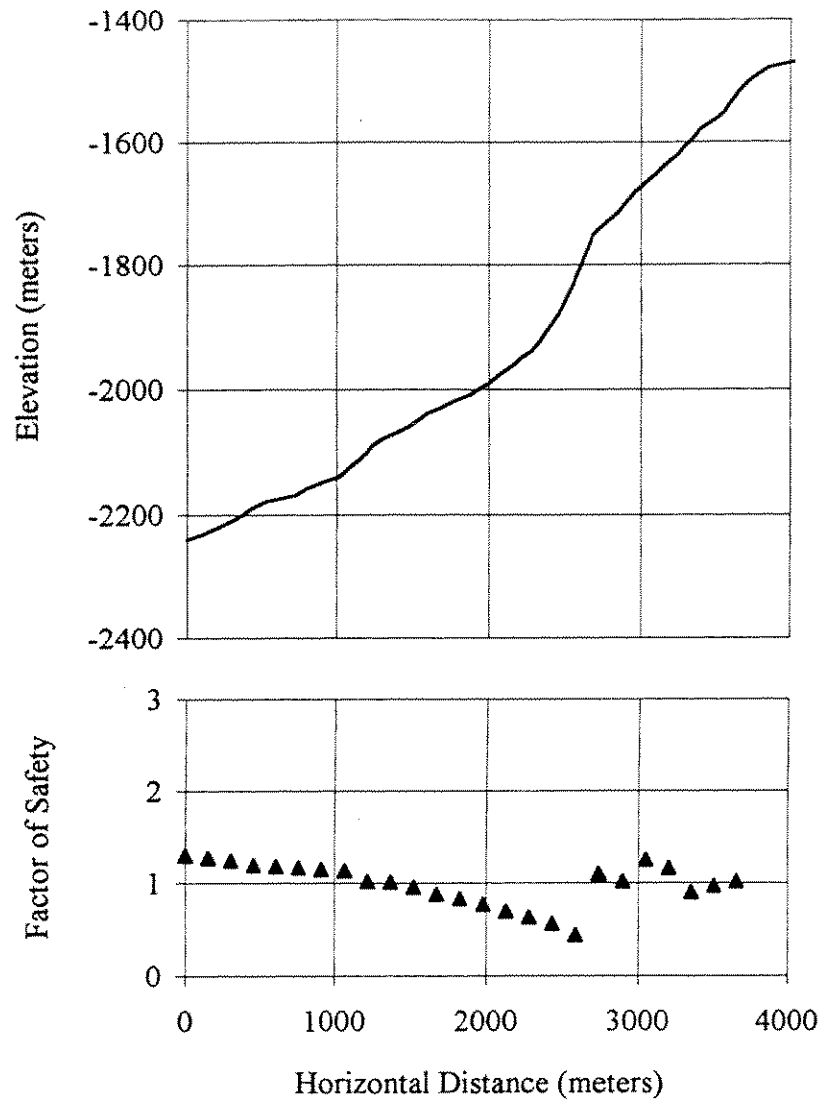


Figure 6.14 Minimum factor of safety for slope using results from infinite slope and the modified search method restricting the lateral extent of the circle

### 6.5.2 Cohesive and Frictional Soil

Additional stability computations were performed for the same slope, represented by cross-section C-C, except the soil was assumed to have both cohesion and friction. A friction angle of 16 degrees was assumed. The cohesion was chosen such that the contribution of the cohesion was neither dominant nor negligible relative to the contribution (large or small) of friction. For large values of cohesion, the fraction of the shear strength attributed to cohesion becomes dominant and the critical circle tends to go deeper into the slope and is of greater lateral extent. In such cases, effects of an irregular slope profile on the factor of safety become much smaller. On the other hand, if the cohesion is small, the friction becomes dominant and the critical circular shear surface tends to become very shallow as already shown for a cohesionless soil in the previous section. Based on these considerations, a value of 14.4 kPa was chosen for cohesion. The cohesion, like the friction angle, was assumed constant both laterally and vertically in the entire slope.

With cohesion included the critical shear surface passes to at least some depth such that "end effects" become important. Thus, infinite slope procedures generally do not apply when cohesion is present unless a much firmer strata exists at a relatively shallow depth compared to the length of the shear surface. Since it was assumed that no firmer strata exists, infinite slope analyses were not performed for the slope containing cohesion.

Circular shear surfaces with the shear surface restricted to pass beneath the center point were used to compute stability along a portion of the length of slope defined by the cross-section C-C. Only about 1500 meters of the slope near the steeper segments was analyzed. The results are shown in Figure 6.15

Figure 6.16 shows the effects of cohesion on the variation in the factor of safety along the slope profile. Figure 6.16 compare the factors of safety shown in Figures 6.14 and 6.15 for no cohesion and a soil with cohesion and friction, respectively. In order to more closely compare the results for the two shear strength characterizations ( $c' = 0$ ;  $c' > 0$ ) the factors of safety were normalized by dividing the values by the respective maximum values calculated along the cross-section (between 1800 and 3200 meters). The results shown in Figure 6.16 indicate that adding cohesion to the soil smoothes and dampens the variation in the factor of safety along this irregular slope.

## 6.6 Conclusion

The variation in stability along the length of a slope was examined using circular shear surfaces and results were compared with results previously determined using infinite slope procedures. The calculations showed that for cohesionless slopes factors of safety were lower using circular shear surfaces than the factors of safety calculated using infinite slope procedures because of the contributions of adjacent, steeper segments of the slope to the stability.

Several schemes were examined for calculating stability as a function of position along the length of the irregular slope. It was found that an appropriate way to

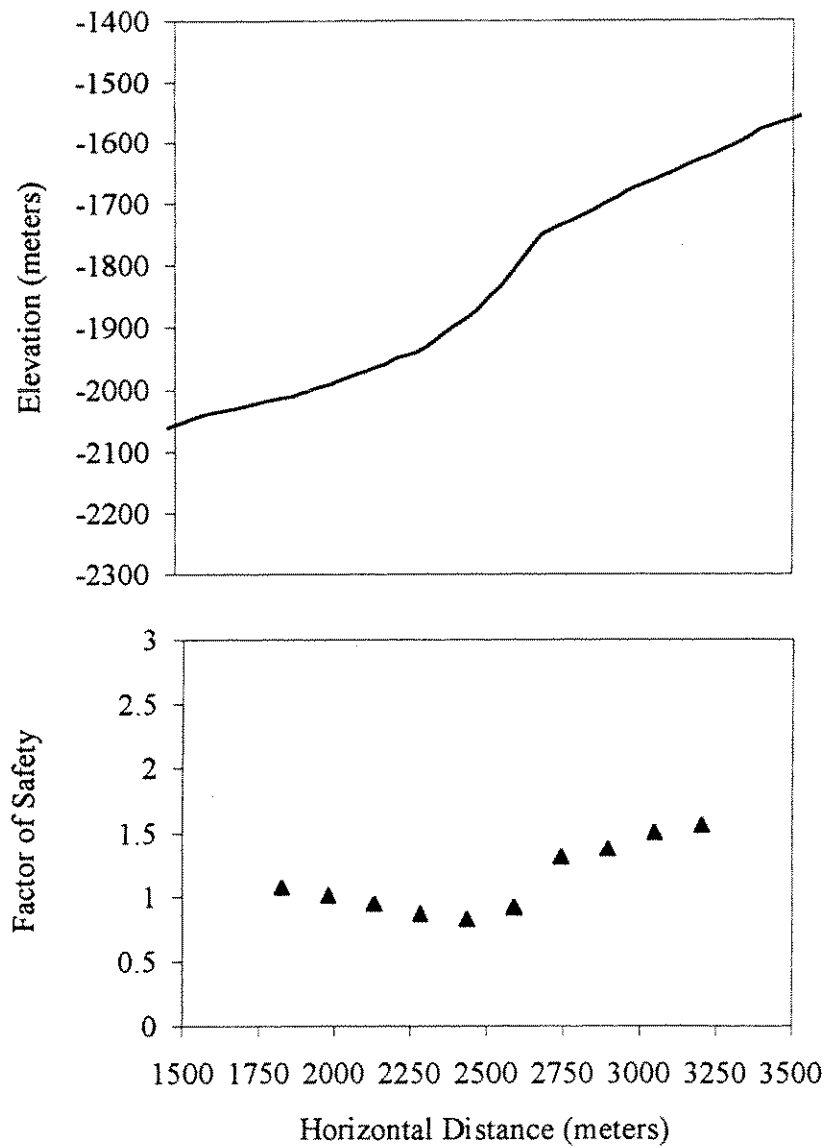


Figure 6.15 Variation in factor of safety with the center point (circle) using the restricted center and restricted shear surface extent along cross-section C-C for a soil containing both friction and cohesion

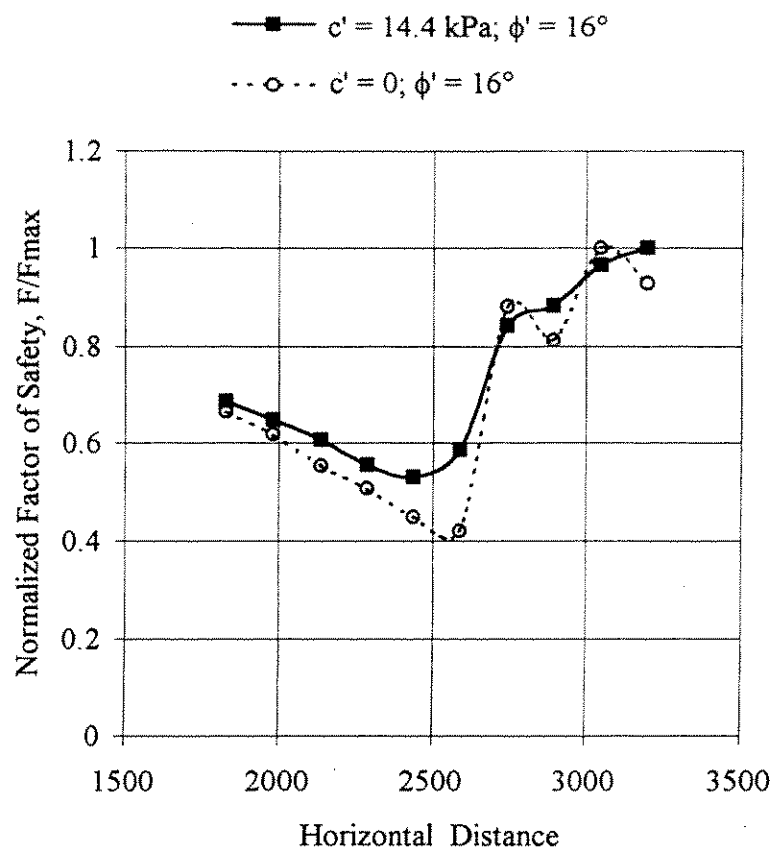


Figure 6.16 Results showing how the addition of cohesion smooths the variation in the factor of safety along an irregular slope

compute the factor of safety at points along the slope was to require that the shear surface pass beneath the center point of the circle and then vary the lateral position of the center. In a few cases infinite slope analyses give lower factors of safety due to limitations caused by requiring the circle to pass vertically beneath the center point. In such cases and at such points along the slope the lower factor of safety from infinite slope analyses is used.

The effect of cohesion was also investigated. It was found that the variation in the factor of safety was smaller if the soil contained both cohesion and friction as compared to a cohesionless soil for the irregular slope analyzed in this chapter.

## **7. Summary, Conclusions, and Recommendations for Future Work**

### **7.1 Summary and Conclusions**

The purpose of this thesis was to investigate slope stability and shear strength in deep water. Work in this thesis was broken up into computational investigations of simple, hypothetical slopes and stratigraphies, and more complex, irregular slopes based on actual bathymetry from offshore surveys.

In Chapter 3, results of parametric studies were presented to quantify and show the effect of variability of shear strength in the vertical direction on slope stability. In particular, the effects on slope stability from the depth, thickness, and shear strength of a thin weak seam of soil were determined. Results showed;

1. variability of shear strength in the vertical direction will effect the location of a potential shear surface,
2. for slopes where shear strength increases with depth and a given seam strength, there exists a depth for which the seam, regardless of its thickness will not affect slope stability, and
3. when seams do exist the difference between the factors of safety calculated using noncircular shear surfaces and circular shear surfaces may be significant.

It was also shown that for soils where strength increased with depth, the thickness of the seam required to "capture" the shear surface (shear surface located in the seam)

increased as the depth to the seam increased. However, for a soil where shear strength is not a function of depth, the thickness of the seam required for the shear surface to be "captured" by the seam decreased as the depth to the seam increased.

In Chapter 4, the variation of stability and shear strength was examined along three slope cross-sections using bathymetry data from Pigmy Basin located in the Gulf of Mexico. Large variations in stability along the cross-sections were found when infinite slope analyses and cohesionless soil were assumed. Similarly, large variations in shear strength along the cross-sections were back-calculated using infinite slope analyses and assuming a constant factor of safety. The variations in stability and shear strength shown in Chapter 4 may represent the maximum variability of stability and shear strength since the computations used to determine this variability were performed assuming the values of the effective stress friction angle and the factor of safety, respectively, were held constant along the slope.

In Chapter 5 the correlation structure of shear strength in the lateral direction was inferred using results obtained in Chapter 4 for the variation of shear strength along the slope. Also, it was shown that the effect from the uncertainty in the measurements used to infer the correlation structure from the bathymetry data on the scale of fluctuation was to decrease the mean value for the scale of fluctuation and increase the uncertainty of the calculated value for the scale of fluctuation. The resolution of the bathymetry data, used to back-calculate shear strength which in turn was used to determine the autocorrelation distance, was on the same order of magnitude as the



values calculated for the autocorrelation distance. Thus, it is possible that an autocorrelation distance lower in value than the value determined in Chapter 5 could be calculated if the resolution of the bathymetry data had been greater.

In Chapter 6 the variation in stability along a cross-section was evaluated using method of slices procedures and circular shear surfaces. Several searching methods were tried for locating critical circles having the minimum factor of safety before a suitable method to compute and represent the minimum factor of safety spatially along a slope was found. It was shown in Chapter 6, that for a cohesionless soil, it is possible to calculate factors of safety using method of slices procedures and circular shear surfaces which are lower than the factors of safety calculated using infinite slope procedures for the same region of an irregular slope. Also, it was shown that the variation in stability along the slope becomes less irregular if the soil has some cohesion.

## **7.2 Recommendations for Future Work**

Based on the work presented in this thesis several recommendations for future work can be made. As described in Chapter 2, there is significant uncertainty in bathymetry data. Bathymetry is an important parameter needed for both forward modeling of slope stability and back-calculating shear strength. It was also shown in Chapter 2 that large variations of shear strength can occur. Shear strength information is required for forward modeling of slope stability.

In order to more fully understand the impact from both the uncertainty in bathymetry data and the variability of shear strength on slope stability, further analyses

must be performed using real data. The resolution of the data must be higher than the resolution of the data used for the analyses presented in this thesis; because, as shown in Chapter 5, the magnitude of the values calculated for the correlation structure of shear strength were on the same order as the uncertainty in the data. Also, it remains uncertain what the impact of higher resolution data will have on the outcome of slope stability analyses. In addition, the effects from using more representative cross-sections which including stratigraphy on back-calculated shear strengths needs to be investigated.

Knowledge of correlation structures for topography and shear strength are additional pieces of information which may be useful for characterizing stability at an offshore site. The development of correlation structures for topography and shear strength will increase the reliability of existing shear strength information and can be used as a tool to help minimize the number of soil samples in deep water needed to characterize a site for slope stability analyses.

## Appendix A

### Back-Calculated Nonlinear Shear Strength "Resistance" Envelope

#### A.1 Introduction

One approach to back-calculating shear strengths is to back-calculate what Casagrande (1950) called a "resistance envelope". Casagrande developed the concept of a resistance envelope to allow engineers to examine various possible shear strength envelopes and determine which envelopes are least safe. Casagrande observed that a problem associated with the limit equilibrium slope stability calculations was that a particular solution was only good for one set of shear strength values ( $c$  and  $\phi$ ). Thus, if an engineer wished to reevaluate a design based on a different set of shear strength parameters the calculations would have to be repeated. Casagrande suggested the resistance envelope as a means of overcoming this problem.

Casagrande presents the resistance envelope in a figure where the dimensionless quantity of shear strength divided by the product of the slope height ( $H$ ) and the unit weight of the soil ( $\gamma$ ) was plotted on the vertical axis and the dimensionless quantity of normal stress divided by the product of the slope height and unit weight of the soil was plotted horizontal axis. The resistance envelope is nonlinear. An example of the figure presented in Casagrande's 1950 paper is shown Figure A.1. Casagrande did not indicate the procedure used to develop the resistance envelope nor present the resistance envelope

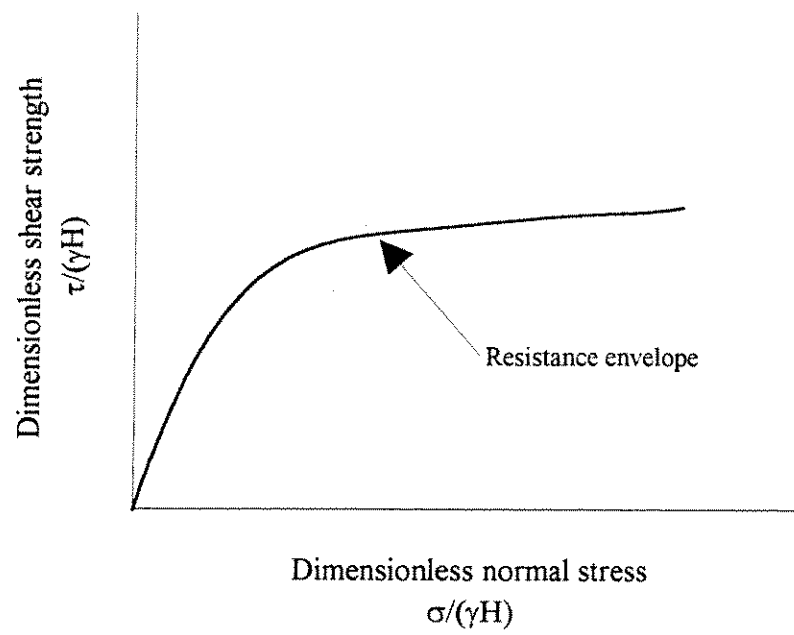


Figure A.1 Representation of resistance envelope suggested by Casagrande (1950)

in a form suitable for use: The curve he presented lacked a scale and numerical values on either axis.

A procedure which can be used to develop a nonlinear shear strength envelope similar to the envelope suggested by Casagrande is presented in this appendix. The resulting resistance envelope is plotted as a dimensionless nonlinear shear strength envelope. Once this envelope is developed, various shear strength envelopes can be compared to the dimensionless envelope. Two examples are presented to illustrate these uses.

## A.2 Variables

The variables used in the computations for the resistance envelope are shown in Figure A.2. Various combinations of, slope height ( $H$ ), buoyant unit weight ( $\gamma'$ ), effective stress cohesion ( $c'$ ), and effective stress friction angle ( $\phi'$ ) were chosen to produce selected values of the dimensionless quantity,  $\lambda_{c\phi}$ , expressed by

$$\lambda_{c\phi} = \frac{\gamma' H \tan \phi'}{c'} \quad (1)$$

Values used for  $\lambda_{c\phi}$ , ranged from zero ( $\phi' = 0$ ) to infinity ( $c' = 0$ ) with 46 intermediary values.

In order to calculate the resistance envelope, pairs of shear strength parameters ( $c'$  and  $\phi'$ ) which produce a factor of safety of unity must be determined. For a given value of  $\lambda_{c\phi}$  and slope angle it can be shown that there is a unique  $c'/\gamma'H$  and  $\tan \phi'$  that will produce a factor of safety equal to one. The following example illustrates this.

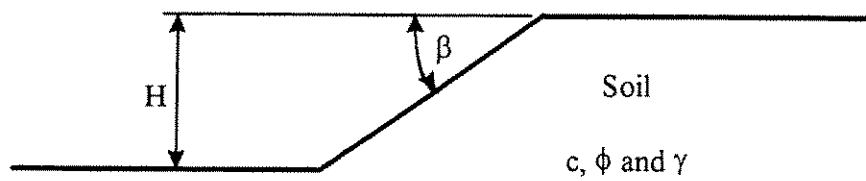


Figure A.2 Slope geometry and variables

Two sets of stability calculations were performed. In the first set of analyses, the values for the slope height, unit weight and cohesion were varied while keeping the values for the dimensionless parameters  $c'/(\gamma'H)$ ,  $\tan\phi'$ , and  $\lambda_{c\phi}$  constant. In the second set of analyses, values for slope height, unit weight, cohesion, and friction angle were varied in such a way that the value for  $\lambda_{c\phi}$  remained constant and the values for  $c'/(\gamma'H)$  and  $\tan\phi'$  varied. Consider a slope with a slope height of 50 m, buoyant unit weight of  $5.0 \text{ kN/m}^3$ , effective stress cohesion of 20.0 kPa, effective stress friction angle of 9.13 degrees, and slope angle of 30 degrees. For these values,  $\lambda_{c\phi}$  is equal to 2.0,  $c'/(\gamma'H)$  is equal to 0.080, and  $\tan\phi'$  is equal to 0.161 and are shown in Table A.1 along with the factor of safety which was determined to be unity. The effect of changing the values for  $c$  and  $\gamma'$  on the factor of safety, while keeping  $c'/(\gamma'H)$  constant, is shown in the second row of Table A.1. The effect of changing the values for  $c$  and  $H$  on the factor of safety, while keeping  $c'/(\gamma'H)$  constant, is shown in the third row. And finally, the effect of changing the values for  $H$  and  $\gamma'$  on the factor of safety, while keeping  $c'/(\gamma'H)$  constant, is shown in the fourth row. In all cases the values for  $c'/(\gamma'H)$  and  $\tan\phi'$  are constant and the value for the factor of safety is determined to be one. The final three rows (fifth, sixth, and seventh rows) shown in Table A.1 show the effects from changing  $\phi'$ ,  $c'$ ,  $\gamma'$ , and  $H$  on the factor of safety while not keeping  $c'/(\gamma'H)$  and  $\tan\phi'$  constant. The fifth set of data (fifth row) show the effect from changing  $\phi'$  and  $c'$  on the factor of safety. The sixth set of data show the effect from changing  $\phi'$  and  $H$  on the factor of safety. The seventh, and final set of data, show the effect from changing  $\phi'$  and  $\gamma'$  on the factor of

Table A.1

Table showing that unique values for the dimensionless quantities  $c'/(\gamma'H)$  and  $\tan \phi'$  are necessary to produce a factor of safety equal to unity

H (m)	$\gamma'$ (kN/m <sup>3</sup> )	$c'$ (kPa)	$\phi'$ (deg)	$c'/(\gamma'H)$	$\tan \phi'$	$\lambda_{cf}$	$F^*$
50.0	5.0	20.0	9.13	0.080	0.161	2.00	1.00
50.0	10.0	40.0	9.13	0.080	0.161	2.00	1.00
100.0	5.0	40.0	9.13	0.080	0.161	2.00	1.00
100.0	2.5	20.0	9.13	0.080	0.161	2.00	1.00
29.9	5.0	20.0	15.00	0.134	0.268	2.00	1.67
50.0	2.5	20.0	18.00	0.163	0.325	2.00	2.03
50.0	5.0	28.9	13.00	0.116	0.231	2.00	1.44

\* slope angle of 30° used for all cases



safety. These final three sets of data indicate that for a constant value for the dimensionless parameter  $\lambda_{c\phi}$ , the variables  $c'$ ,  $h$ ,  $\gamma'$ , and  $\phi'$  must form unique values for  $c'/(\gamma'H)$  and  $\tan \phi'$  in order for a value for the factor of safety equal to one to be calculated.

### **A.3 Stability Analysis**

To determine a resistance envelope a series of slope stability calculations was performed. Various combinations of  $H$ ,  $\gamma'$ ,  $c'$ , and  $\phi'$  were chosen and the factor of safety was calculated. The slope stability program UTEXAS3 (Wright, 1991) was used to calculate the factor of safety for the various values of  $H$ ,  $\gamma$ , and  $c$  and  $\phi$  using a slope angle ( $\beta$ ) equal to 30 degrees. Circular shear surfaces were used for all the analyses. The slopes considered were assumed to be submerged. Thus, buoyant unit weights were used to compensate for the effects of submergence.

### **A.4 Methodology**

A series three steps were used to calculate the resistance envelope. The steps are described below.

#### **A.4.1 Determine Combinations of $c'$ and $\phi'$ Which Produce a Factor of Safety Equal to One**

A series of slope stability calculations was performed for various values of  $\lambda_{c\phi}$ . A slope angle of 30 degrees, slope height of 30.5 m ,and unit weight of 15.7 kN/m<sup>3</sup> were

assumed and kept constant. Various values of  $c'$  and  $\phi'$  were assumed to produce different values of  $\lambda_{c\phi}$ . The 48 combinations of  $c'$  and  $\phi'$  used in the computations are shown in Table A.2. For each set of values, slope stability computations were performed and the factors of safety, shown in Table A.2, were determined. Once a given set of values for  $c'$  and  $\phi'$  was assumed and the factor of safety calculated, values of  $c'$  and  $\phi'$  that produce a factor of safety equal to unity are simply calculated from

$$c'_{F=1} = \frac{c'}{F} \quad (2)$$

$$\phi'_{F=1} = \tan^{-1} \left( \frac{\tan \phi'}{F} \right) \quad (3)$$

where  $F$  is the factor of safety calculated using the assumed shear strength parameters  $c'$  and  $\phi'$ .

#### A.4.2 Determine Minimum Shear Strength Envelope

The Mohr-Coulomb shear strength envelopes required to produce a factor of safety of unity for the various combinations of  $c$  and  $\phi$  (various  $\lambda_{c\phi}$ 's) are plotted in Figure A.3. The envelopes are expressed as shear strength versus normal stress.

For each normal stress in Figure A.3 several shear strengths exist depending on the particular Mohr-Coulomb envelope. To obtain the resistance envelope the minimum shear strength for each normal stress was determined and plotted versus normal stress to obtain the nonlinear envelope shown in Figure A.4. The envelope in Figure A.4 represents the lower bound of all the Mohr-Coulomb envelopes in Figure A.3.

Table A.2  
Combinations of  $c'$  and  $\phi'$  and the corresponding factors of safety used in the analyses

$\lambda_{cr}$	$\phi'$	$c'$	F	$c'_{F=1}$	$\phi'_{F=1}$
Infinite	30	0.0	1.00	0.0	30.0
10000	15	0.3	0.47	0.6	29.7
9000	15	0.3	0.47	0.6	29.7
8000	15	0.3	0.47	0.7	29.7
7000	15	0.4	0.47	0.8	29.6
6000	15	0.4	0.47	0.9	29.6
5000	15	0.5	0.47	1.1	29.6
4000	15	0.7	0.47	1.4	29.5
3000	15	0.9	0.48	1.9	29.4
2000	15	1.3	0.48	2.8	29.2
1000	15	2.7	0.48	5.5	29.0
900	15	3.0	0.48	6.2	29.0
800	15	3.3	0.49	6.9	28.9
700	15	3.8	0.49	7.8	28.8
600	15	4.5	0.49	9.1	28.7
500	15	5.4	0.49	10.9	28.6
400	15	6.7	0.50	13.5	28.4
300	15	8.9	0.50	17.8	28.1
200	15	13.4	0.51	26.2	27.6
100	15	26.8	0.54	49.7	26.4
90	15	29.8	0.55	54.6	26.2
80	15	33.5	0.55	60.7	25.9
70	15	38.3	0.56	68.4	25.6
60	15	44.7	0.57	78.3	25.2
50	15	53.6	0.58	91.8	24.6
40	15	67.0	0.60	110.9	23.9
30	15	89.3	0.64	140.0	22.8
20	15	134.0	0.69	195.0	21.3
10	15	267.9	0.83	324.4	18.0
9	15	297.7	0.85	348.6	17.4
8	15	334.9	0.89	377.2	16.8
7	15	382.8	0.93	411.2	16.1
6	15	446.6	0.99	452.9	15.2
5	15	535.9	1.06	504.6	14.2
4	15	669.9	1.17	573.0	12.9
3	15	893.2	1.34	665.5	11.3
2	15	1339.7	1.67	802.2	9.1
1	15	2679.5	2.60	1031.4	5.9
0.9	15	2977.2	2.80	1064.1	5.5
0.8	15	3349.4	3.04	1100.3	5.0
0.7	15	3827.8	3.36	1140.9	4.6
0.6	15	4465.8	3.77	1186.1	4.1
0.5	15	5359.0	4.33	1237.4	3.5
0.4	15	6698.7	5.17	1296.4	3.0
0.3	15	8931.6	6.53	1367.2	2.3
0.2	15	13397.5	9.24	1449.5	1.7
0.1	15	26794.9	17.19	1558.6	0.9
0	0	1808.3	1.00	1808.3	0.0

$$H = 30.5 \text{ m}, \beta = 30^\circ, \gamma = 15.7 \text{ kN/m}^3$$

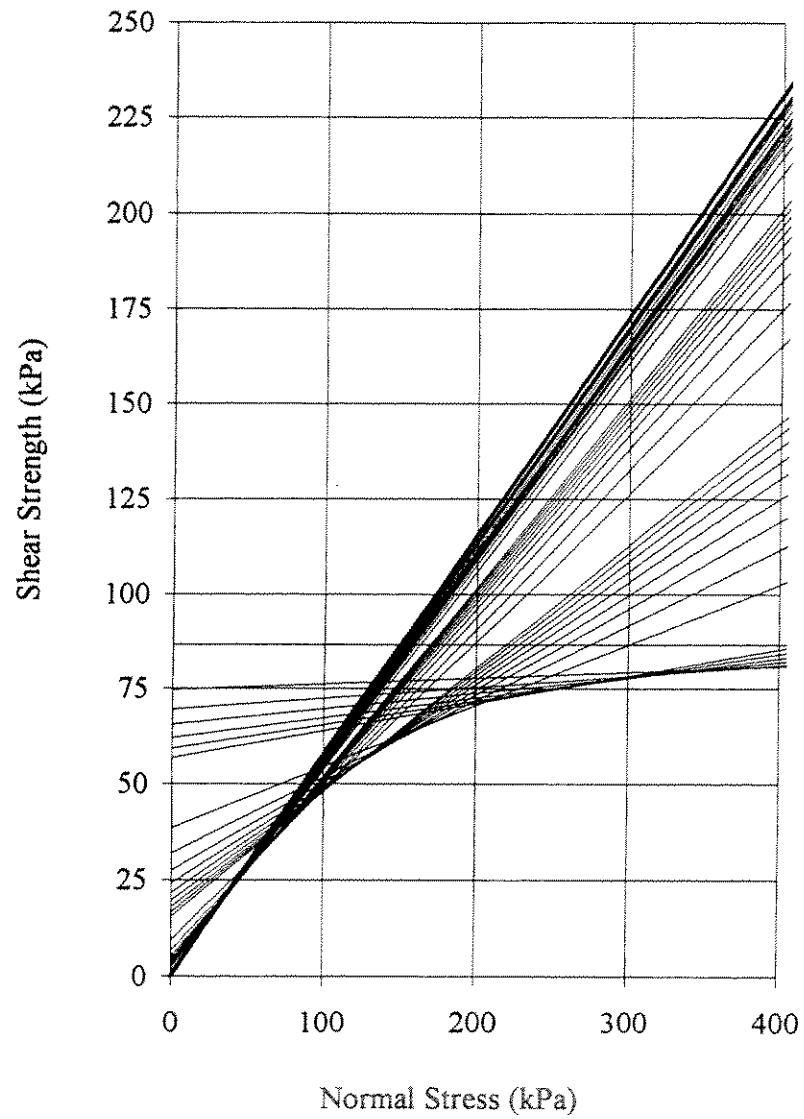


Figure A.3 Linear shear strength envelopes corresponding to  $F = 1.00$  and  $H = 30.5 \text{ m}$  for  $\gamma = 15.7 \text{ kN/m}^3$  and  $\beta = 30$  degrees

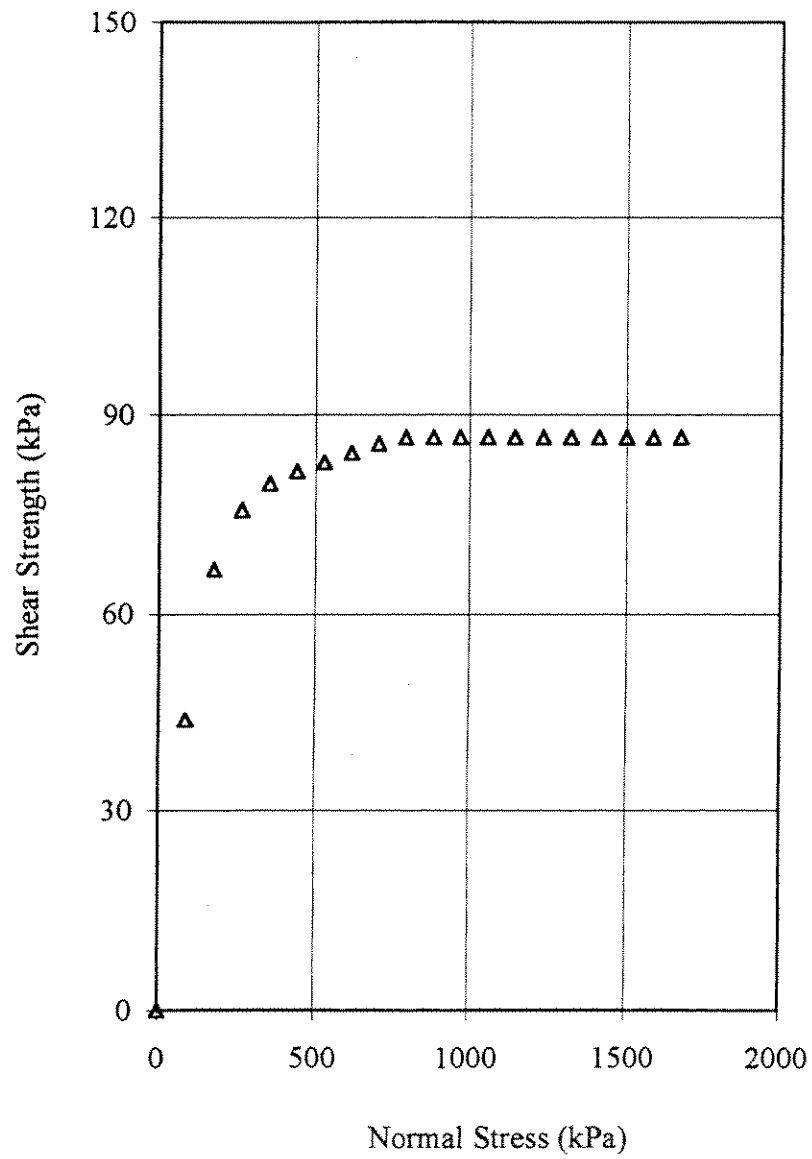


Figure A.4 Minimum shear strength envelope for  $H = 30.5$  m,  $\gamma = 15.7$  kN/m<sup>3</sup> and  $\beta = 30$  degrees

#### A.4.3 Determine Normalized Nonlinear "Resistance Envelope"

The resistance envelope shown in Figure A.4 can be expressed in dimensionless form by dividing the quantities on each axis by the product of the slope height ( $H$ ) and the unit weight of the soil ( $\gamma$ ). The resulting dimensionless resistance envelope is shown in Figure A.5 in terms of dimensionless variables,  $\tau/(\gamma H)$  and  $\sigma/(\gamma H)$ . The curve shown in Figure A.5 is believed to represent what Casagrande considered the "resistance envelope" (shown in Figure A.1).

Any linear Mohr-Coulomb shear strength envelope can be plotted in dimensionless form on Figure A.5. If such an envelope lies completely above the resistance envelope the Mohr-Coulomb envelope will result in a factor of safety in excess of one for the slope (assuming a slope of 30 degrees). Any Mohr-Coulomb shear strength envelope that lies or passes below any portion of the resistance envelope will result in a factor of safety less than one. Mohr-Coulomb envelopes that are tangent to the resistance envelope will result in factors of safety equal to one.

The dimensionless form of the resistance envelope shown in Figure A.5 is convenient because it is independent of both the slope height and the unit weight of the soil and is only dependent upon the slope angle. Thus, the calculations necessary to determine the resistance envelope need only be performed for one value of slope height and one value of unit weight of the soil. Additional calculations were performed to show that the dimensionless resistance envelope is independent of both slope height and unit weight of the soil, as confirmed by results presented in the following section.

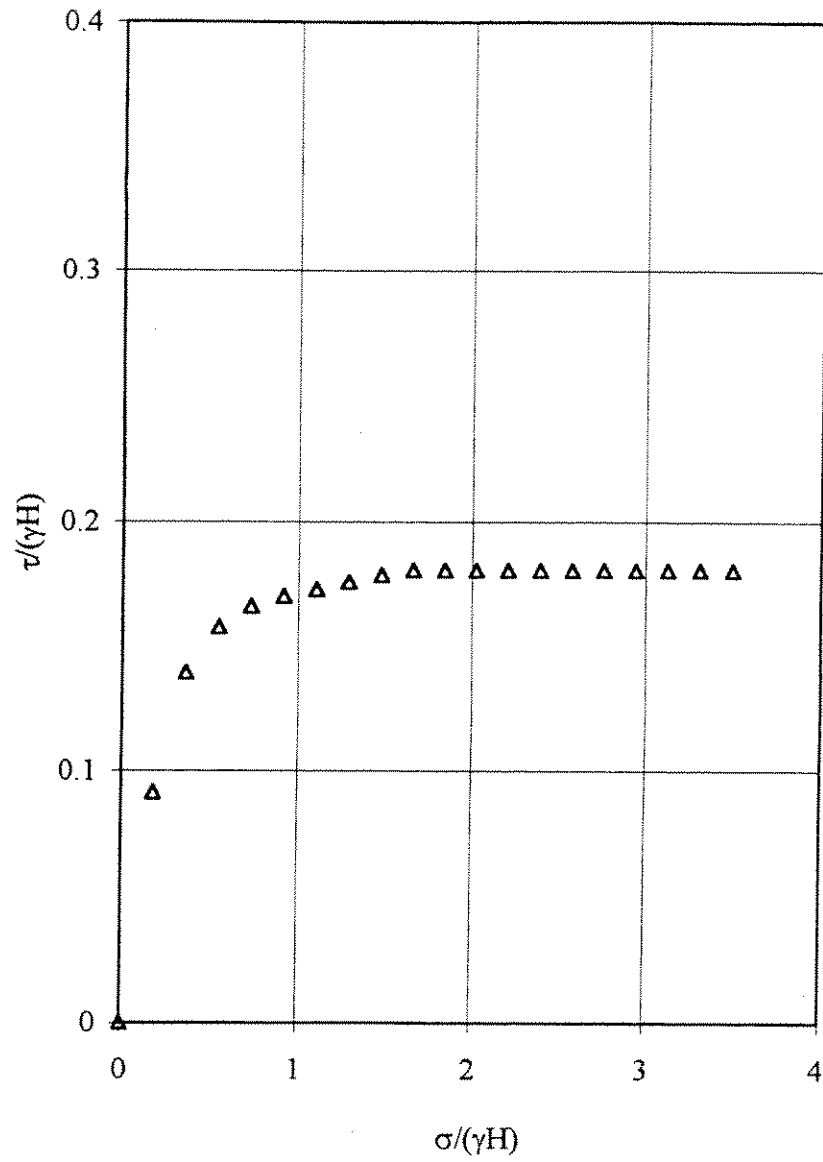


Figure A.5 "Resistance envelope" for  $H = 30.5$  m,  $\gamma = 15.7$  kN/m<sup>3</sup> and  $\beta = 30$  degrees

## **A.5 Verification of Dimensionless Variables**

To illustrate the uniqueness of the dimensionless resistance envelope shown in Figure A.5, additional shear strength computations were performed for a slope angle of 30 degrees using different slope heights and unit weights. Results are presented below.

### **A.5.1 Effect of Slope Height**

Figures A.6 and A.7 show the Mohr-Coulomb shear strength envelopes required to produce factors of safety of unity for 30 degree slopes with heights of 12.2 m and 106.7 m respectively and a unit weight for the soil equal to  $15.7 \text{ kN/m}^3$ . Again, the resistance envelope can be determined by finding the minimum shear strengths associated with a series of normal stresses for each slope height.

The resistance envelopes determined from the data presented in Figures A.6 and A.7 are shown in Figure A.8. Also included in Figure A.8 is the resistance envelope previously determined for the slope height of 30.5 m. The general shapes of the implied resistance envelopes are all similar.

Each of the resistance envelopes in Figure A.8 is replotted in dimensionless form in Figure A.9 by dividing the quantities on each axis by  $\gamma H$ . The resulting resistance envelopes can be seen to be identical, independent of slope height.



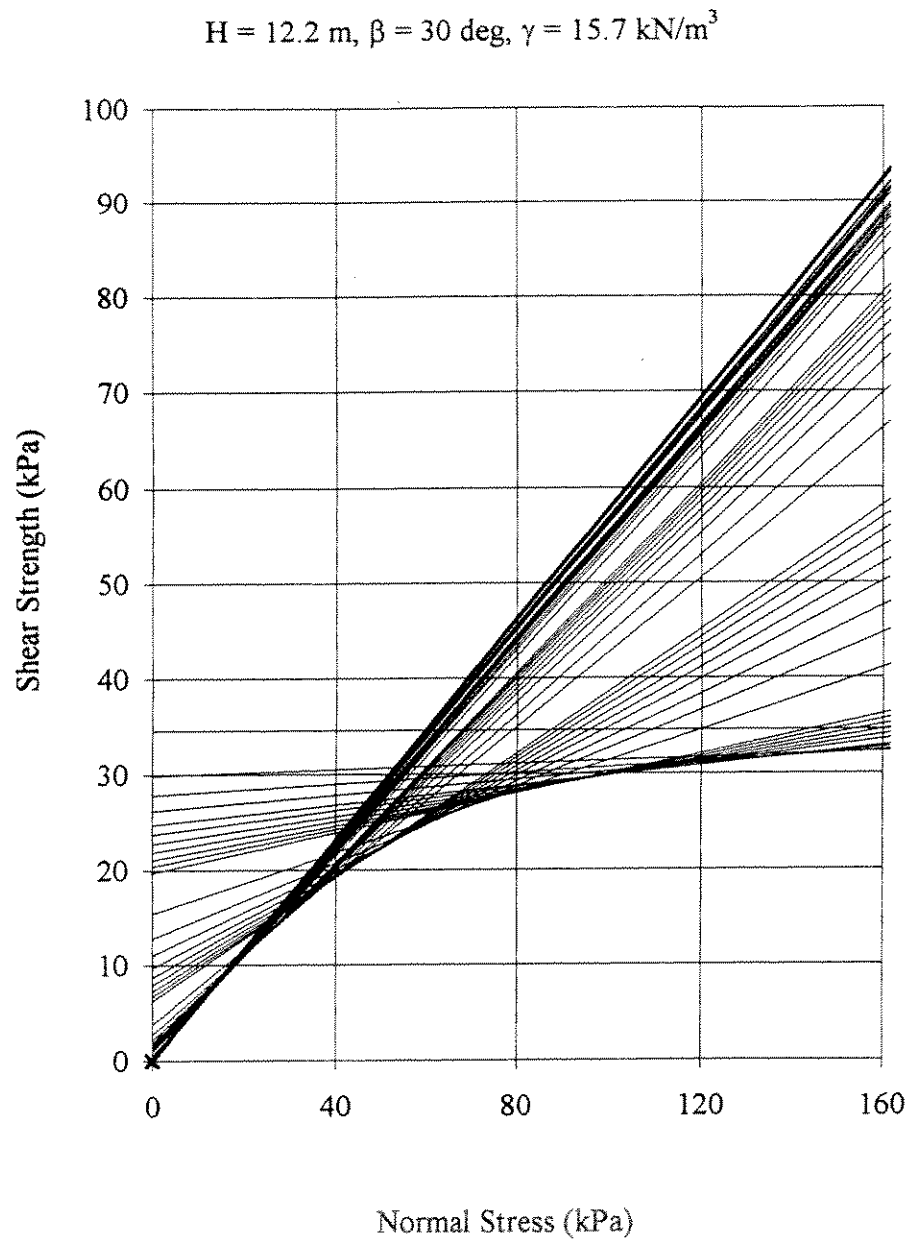


Figure A.6 Linear shear strength envelopes corresponding to  $F = 1.00$  and  $H = 12.2 \text{ m}$   
for  $\gamma = 15.7 \text{ kN/m}^3$  and  $\beta = 30 \text{ degrees}$

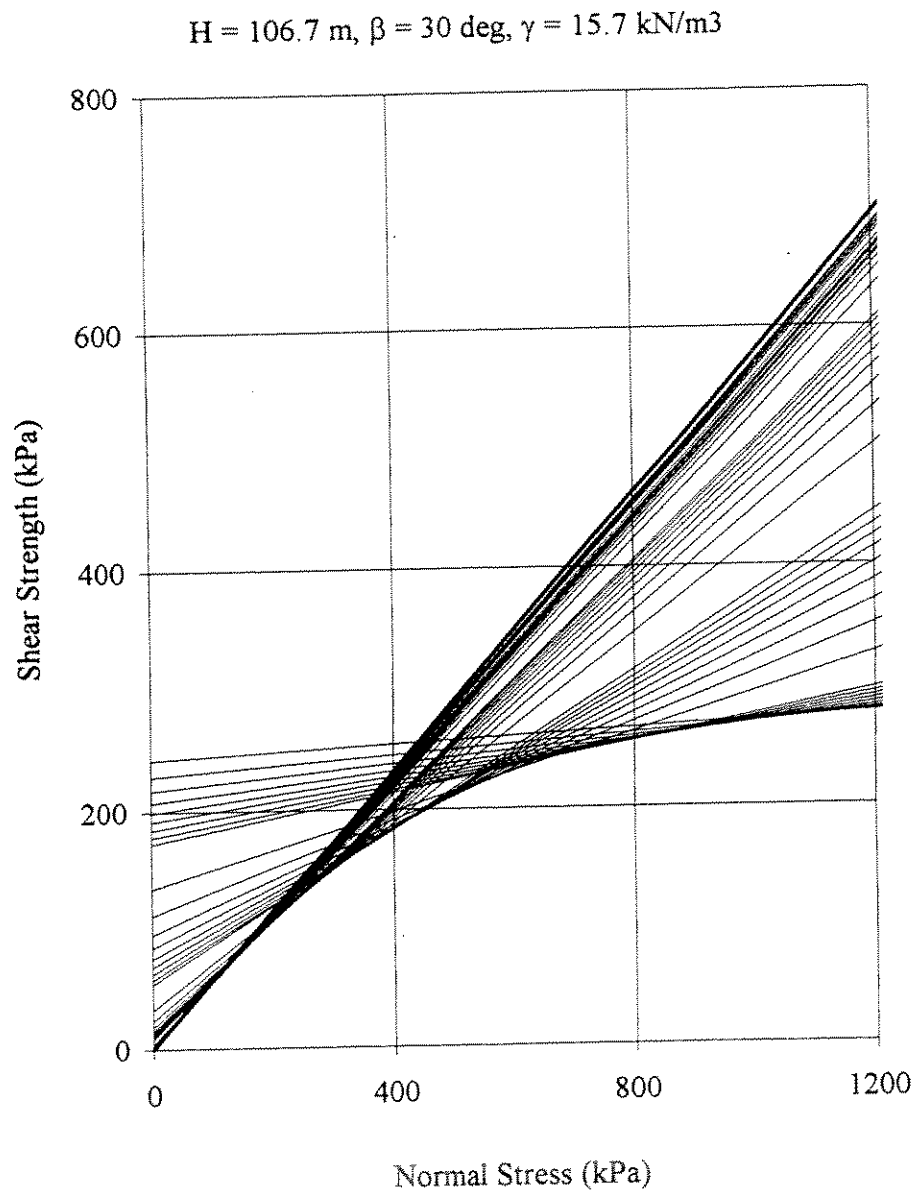


Figure A.7 Linear shear strength envelopes corresponding to  $F = 1.00$  and  $H = 106.7$  m for  $\gamma = 15.7 \text{ kN/m}^3$  and  $\beta = 30$  degrees

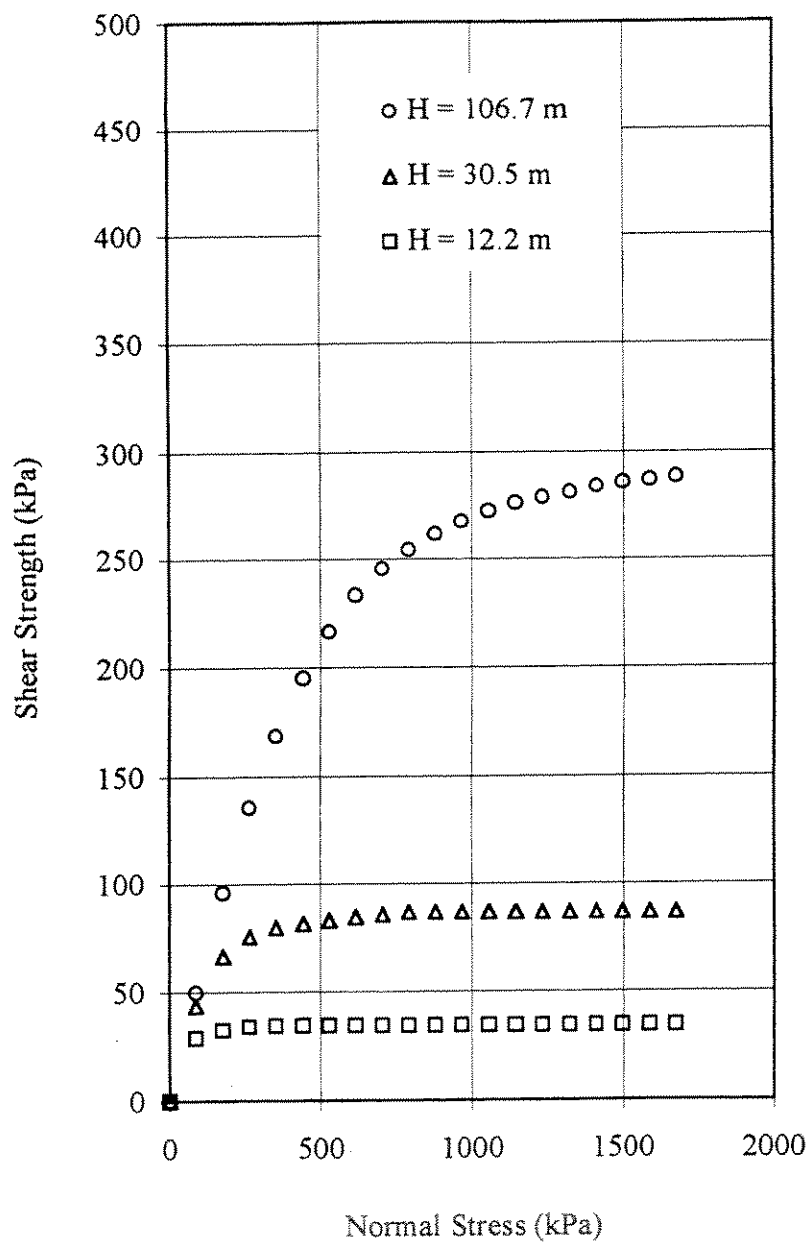


Figure A.8 Minimum shear strength envelopes for each slope height for  $\gamma = 15.7 \text{ kN/m}^3$  and  $\beta = 30 \text{ degrees}$

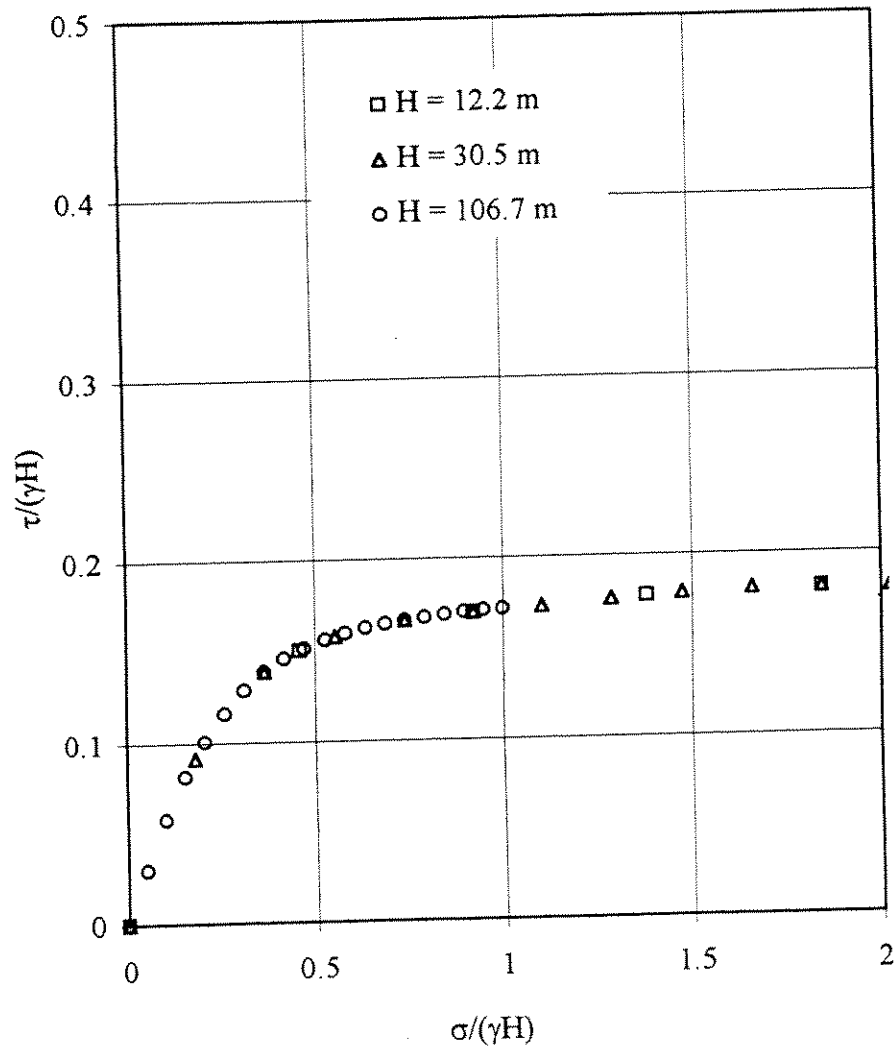


Figure A.9 "Resistance envelope" independent of slope height for  $\gamma = 15.7 \text{ kN/m}^3$  and  $\beta = 30 \text{ degrees}$

### A.5.2 Unit Weight

Additional analyses were performed to investigate the effect of unit weight using a unit weight  $5.5 \text{ kN/m}^3$  compared to the value of  $15.7 \text{ kN/m}^3$  used in the previous analyses. A unit weight of  $5.5 \text{ kN/m}^3$ , is more representative of the values for submerged unit weights one might expect for offshore soils. Analyses were performed for a slope height of 106.7 m and a slope angle of 30 degrees.

Results obtained for these computations were similar to the results obtained in the previous computations. The resistance envelope determined using a unit weight of  $5.5 \text{ kN/m}^3$  is shown in Figure A.10 along with the envelope obtained previously using a unit weight of  $15.2 \text{ kN/m}^3$  and a slope height of 106.7 m. Figure A.11 shows the resistance envelopes plotted in dimensionless form. The envelopes shown in Figure A.11 are identical, indicating that a single dimensionless resistance envelope exists independent of unit weight.

The results presented in Figures A.9 and A.11 confirm that the dimensionless resistance envelope is independent of both the unit weight and the height of the slope. The dimensionless resistance envelope depends only on the slope angle and is presented again in Figure A.12 for a slope angle of 30 degrees.

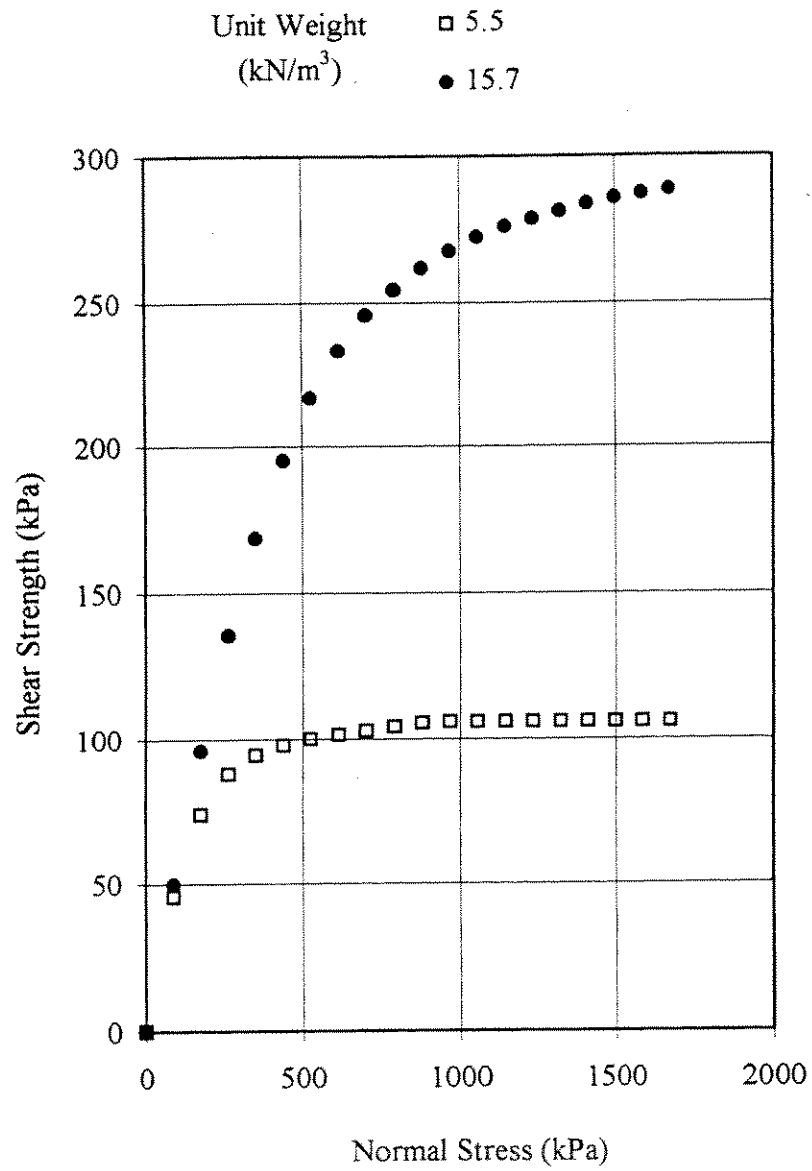


Figure A.10 Minimum shear strength envelopes for each unit weight for  $H = 106.7$  m and  $\beta = 30$  degrees

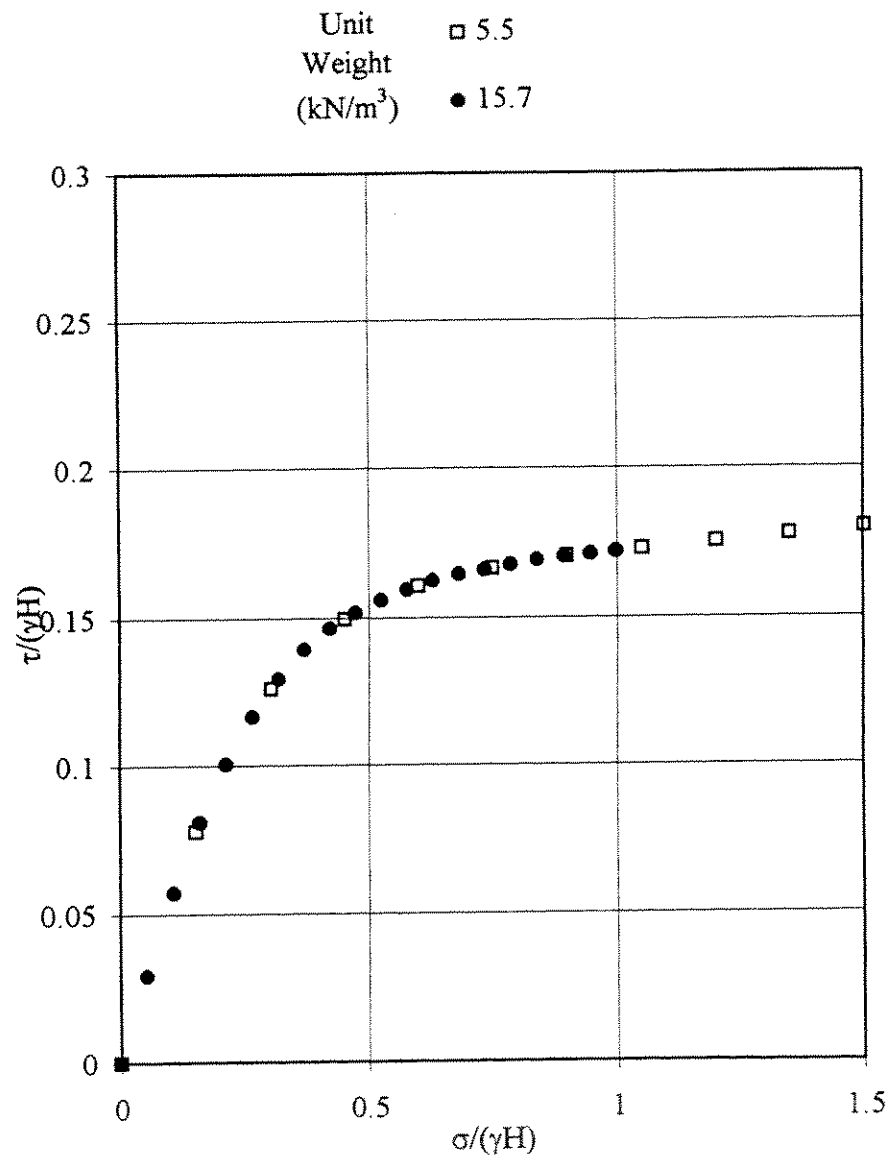


Figure A.11 "Resistance envelope" independent of unit weight for  $H = 106.7$  m and  $\beta = 30$  degrees

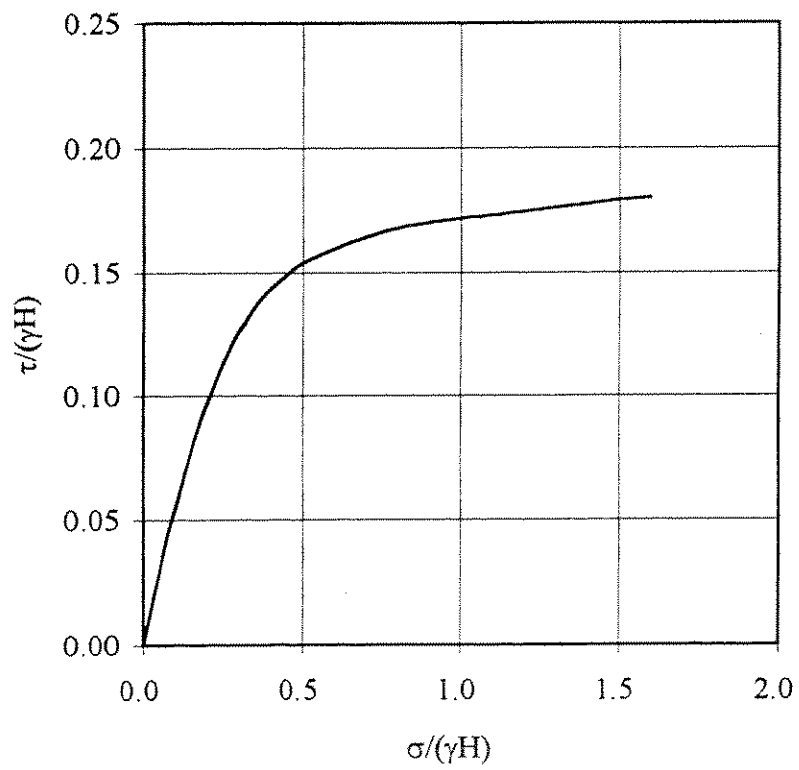


Figure A.12 "Resistance Envelope" for  $\beta = 30$  degrees



## A.6 Illustrative Example Calculations

Resistance envelopes can be used for both accessing stability and back-calculating shear strength parameters. Use of the dimensionless resistance envelope is demonstrated using two examples. The first example is a forward analysis to determine if a slope is stable. The second example is a back analysis to determine the shear strength envelope for a failed slope.

### A.6.1 Forward Analyses

For the forward analysis  $c'$  and  $\phi'$  are assumed to be known and the factor of safety is to be determined. The following values were assumed:  $c' = 75 \text{ kPa}$ ,  $\phi' = 25^\circ$ ,  $\gamma = 17 \text{ kN/m}^3$ ,  $H = 150 \text{ m}$ , and  $\beta = 30^\circ$ . The first step is to calculate and plot a shear strength envelope. The shear strength can be expressed as,

$$\tau = c + \sigma \tan \phi \quad (4)$$

$$\text{or } \frac{\tau}{\gamma H} = \frac{c'}{\gamma H} + \frac{\sigma}{\lambda H} \tan \phi' \quad (5)$$

Thus, the slope of the dimensionless, linear shear strength envelope is  $\tan \phi'$  and the intercept is  $c'/(\gamma H)$ . An envelope with this slope and intercept is plotted on a diagram along with the corresponding dimensionless resistance envelope in Figure A.13. The linear Mohr-Coulomb envelope corresponding to the assumed cohesion and friction angle is represented by the dashed line. Since this envelope does not intersect or lie tangent to the resistance envelope the slope is stable. The factor of safety can be

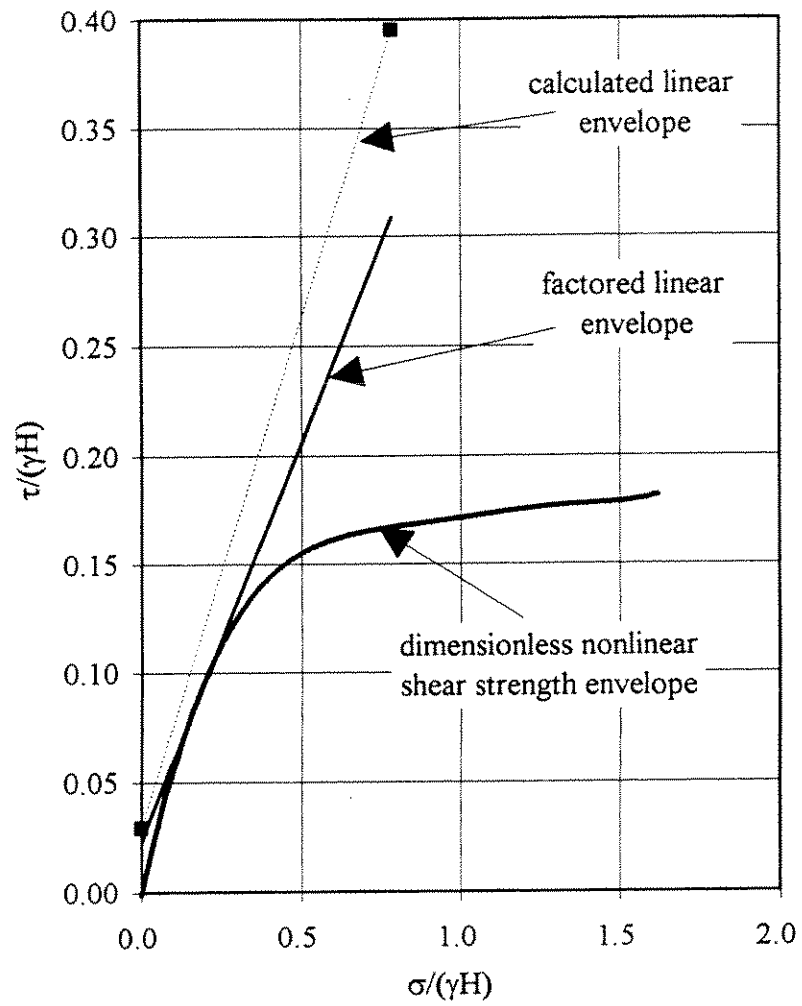


Figure A.13 Resistance envelope and linear envelope for forward analysis example

determined by dividing  $c'/(\gamma H)$  and  $\tan \phi'$  by an assumed value for the factor of safety until the linear, dimensionless Mohr-Coulomb envelope lies tangent to the dimensionless resistance envelope. The value of the factor of safety that places the Mohr-Coulomb envelope tangent to the dimensionless resistance envelope is then the factor of safety for the slope. For this problem a value of 1.3 for the factor of safety places the dimensionless Mohr-Coulomb envelope tangent to the dimensionless resistance envelope and thus the factor of safety for the slope is 1.3.

#### A.6.2 Back Analysis

The second analysis is a back analysis for a slope which is assumed to have failed ( $F = 1.0$ ). In this case it is necessary to assume that either  $c'$  or  $\phi'$  is known. For this example the cohesion was assumed to be known.

The following values were assumed:  $\gamma' = 5 \text{ kN/m}^3$ ,  $H = 70 \text{ m}$ ,  $\beta = 30^\circ$ , and  $c' = 25 \text{ kPa}$ . Thus, the dimensionless intercept for the Mohr-Coulomb envelope  $c'/(\gamma' H)$  is 0.071. Since the slope is assumed to have failed the Mohr-Coulomb envelope must also be tangent to the resistance envelope. A line can, thus, be drawn with an intercept of 0.071 and tangent to the dimensionless resistance envelope as shown by the dashed line in Figure A.14. The resulting envelope has a slope ( $\tan \phi'$ ) of 0.185. Thus, the back-calculated friction angle corresponding to  $c'$  of 25 kPa is 10.5 degrees ( $\tan^{-1} 0.185$ ).

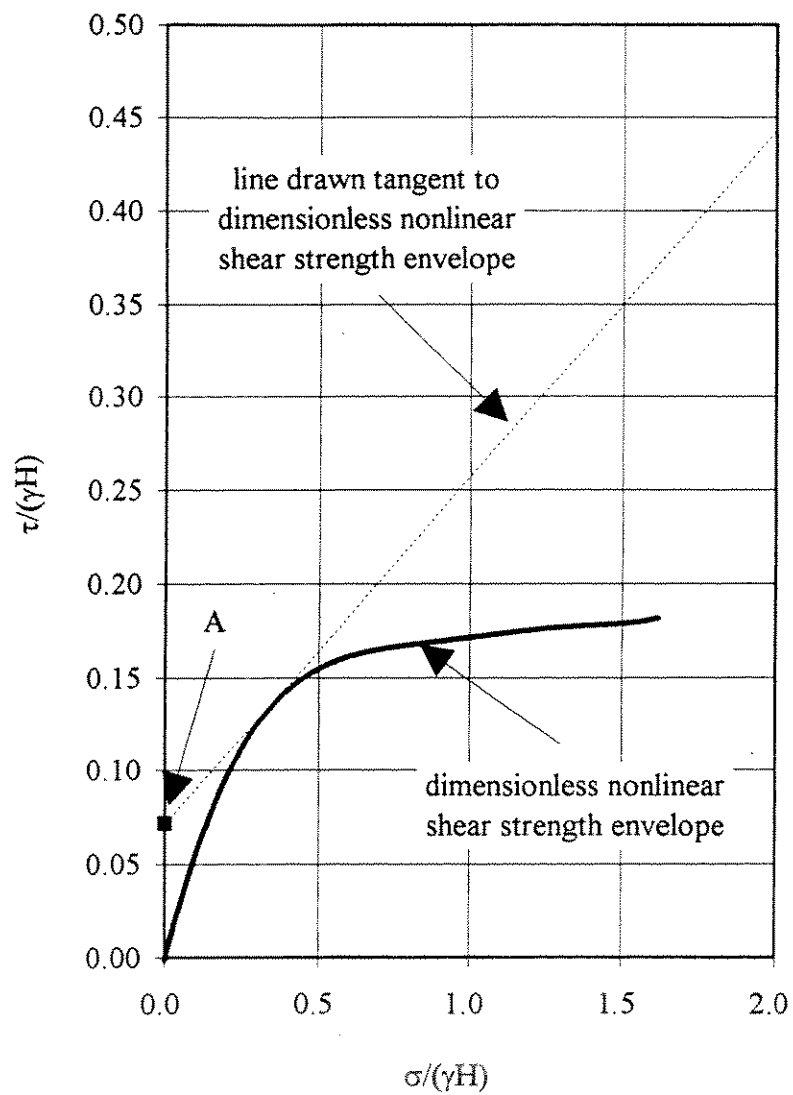


Figure A.14 Resistance envelope and linear envelope for back analysis example

## A.7 Conclusion

A method is presented for determining a dimensionless resistance envelope following the suggestion of Casagrande (1950). The resistance envelope depends only on the slope angle and can be used to either determine if a slope is stable or to back-calculate shear strength. The two examples are presented to illustrate these applications.

## Appendix B

### Source Code for Computer Program VARREDF

```
C          VARREDF
C
      INTEGER M,BINSIZE,NUMPAIRS,K,J,I,NUMBIN
      REAL COUNT(0:500)
      REAL SUMJ(0:500),SUMK(0:500),SUMJK(0:500)
      REAL DELTADIST,SIGMASQ(0:500)
      REAL LATCOORD(500),PHI(500),VARREDF(0:500)
      REAL V(0:500), MEAN(0:500), SUMSQ(0:500)
C
C  OPEN INPUT.DAT FOR INPUT
C
      OPEN(UNIT=1, FILE='INPUT.DAT')
C
C  OPEN OUTPUT.DAT TO WRITE OUTPUT
C
      OPEN (UNIT=2, FILE='OUTPUT.DAT')
C
C  READ BIN SIZE, NUMBER OF DATA PAIRS AND NUMBER OF BINS
C  FROM FILE INPUT.DAT
C
      READ (1,*) BINSIZE
      READ (1,*) NUMBIN
      READ (1,*) NUMPAIRS
C
C  READ DATA PAIRS, LATERAL COORDINATE AND CORRESPONDING
C  SHEAR STRENGTH
C
      DO 10 I=1,NUMPAIRS,1
10      READ(1,*) LATCOORD(I),PHI(I)
C
C  INITIALIZE MATRICES TO ZERO
C
      DO 15 I=0,500,1
          SUMJ(I)=0.
          SUMK(I)=0.
          SUMJK(I)=0.
          COUNT(I)=0.
          V(I)=0.
15      MEAN(I)=0.
C
```

```

C  CALCULATE DISTANCE BETWEEN DATA POINTS
C
      DO 20 J=1,NUMPAIRS-1,1
      DO 20 K=J+1,NUMPAIRS,1
      DELTADIST=(LATCOORD(K)-LATCOORD(J))
C
C  DETERMINE WHICH BIN THE CORRESPONDING DISTANCE JUST
C  CALCULATED BELONGS
C
      DO 25 M=NUMBIN,0,-1
      IF (DELTADIST .GT. M*BINSIZE) THEN
C
C  SUM VALUES FOR TWO PHIS CORRESPONDING TO THE
C  ASSOCIATED BIN
C
      SUMJ(M)=PHI(J)+SUMJ(M)
      SUMK(M)=PHI(K)+SUMK(M)
      SUMJK(M)=PHI(J)*PHI(K)+SUMJK(M)
      COUNT(M)=COUNT(M)+1
      GOTO 20
      ENDIF
25    CONTINUE
20    CONTINUE
C
C  CALCULATE COVARIANCE OF PAIRS OF PHIS IN EACH BIN
C
      DO 30 M=0,NUMBIN,1
C
C  IF NO VALUES ARE IN THE BIN SET MEAN AND VARIANCE
C  TO ZERO
C
      IF (COUNT(M) .EQ. 0) THEN
      V(M)=0.
      MEAN(M)=0.
C
C  IF VALUES ARE PRESENT IN THE BIN CALCULATE MEAN
C  AND COVARIANCE
C
      ELSE
      V(M)=SUMJK(M)/COUNT(M) -
1    SUMJ(M)/COUNT(M)*(SUMK(M)/COUNT(M))
      MEAN(M)=.5*(SUMJ(M)+SUMK(M))/COUNT(M)
      ENDIF
30    CONTINUE
C
C  CALCULATE VARIANCE FOR ALL BINS
C

```

```

DO 40 J=1,NUMPAIRS-1,1
DO 40 K=J+1,NUMPAIRS,1
DELTADIST=LATCOORD(K)-LATCOORD(J)
DO 50 M=NUMBIN,0,-1
IF (DELTADIST .GT. M*BINSIZE) THEN
SUMSQ(M)=(PHI(J)-MEAN(M))**2+(PHI(K)-
MEAN(M))**2+SUMSQ(M)
GOTO 40
ELSE
ENDIF
50 CONTINUE
40 CONTINUE
C
C CALCULATE CORRELATION COEFFICIENT FOR EACH BIN
C
DO 60 M=0,NUMBIN
IF (COUNT(M) .EQ. 0) THEN
VARREDF(M)=0.
ELSE
SIGMASQ(M)=SUMSQ(M)/COUNT(M)/2.
VARREDF(M)=V(M)/SIGMASQ(M)
C
C WRITE OUTPUT TO OUTPUT.DAT
C
WRITE(2,2000)M*BINSIZE,(M+1)*BINSIZE,
1 VARREDF(M),COUNT(M)
ENDIF
60 CONTINUE
C
C CLOSE INPUT AND OUTPUT FILES
C
CLOSE (UNIT=1)
CLOSE (UNIT=2)
C
C FORMAT STATEMENTS
C
2000 FORMAT('BIN ',I4,1X,'TO',1X,I4,3X,'CORR.
COEF.',2X,F6.3
1 ,2X,'COUNT',3X,F6.0)
C
STOP
END

```



## Appendix C

### Users Manual for VARREDF

#### C.1 Input

User input consists of information on the size of the bins, the number of bins, the number of pairs of data points, the lateral coordinates of the data points and the corresponding value for the effective stress friction angle. Units for the size of the bins and the lateral coordinates must be length and consistent (English or S.I.). Units for the effective stress friction angle can be either degrees or radians. The lateral coordinates where the effective stress friction angles are known must be input in ascending order and can start from any initial value greater than, less than or equal to zero. Table C.1 shows the format of the input.

#### C.2 Output

The output is composed of a list of information. For each row the upper and lower bounds for each bin, the calculated correlation coefficient and the number of elements in the bin is listed. This line is repeated for the number of bins (NUMBIN) specified by the user. An example of two lines of output from VARREDF is shown in Table C.2. For the data shown in the first row of Table C.2; the lower and upper bound for the bin is 0 and 30 (units of length), the computed value for the correlation coefficient equal to 0.699 (dimensionless), and the number of pairs of data in the bin equal to 24.

Table C.1  
Data input format for VARREDF

Input Line No.	Data Field No.	Variable	Description
1	1	BINSIZE	Size of bins used to determine the correlation coefficient
2	1	NUMBIN	Number of bins to sort data into. The last bin will be used as a catch all for any and all data that would require a larger bin
3	3	NUMPAIRS	Number of pairs of lateral coordinates and effective stress friction angles to read as input.
4	1	LATCOORD	Lateral coordinate where the effective stress friction angle is known
4	2	PHI	Corresponding effective stress friction angle.

Repeat Line 4 for additional pairs of data to the number of pairs of data (NUMPAIRS).

Table C.2  
Data output format for VARREDF

BIN	0 TO 30	CORR. COEF.	.699	COUNT	24
BIN	30 TO 60	CORR. COEF.	.761	COUNT	63

## References

- Alanzo, E.E. and Krizek, R.J. (1975). "Stochastic Formulation of Soil Properties," Proceeding 2<sup>nd</sup> Conference on Application of Probability and Statistics to Soil and Structural Engineering Vol. II, Aachen, Germany, pp. 9-32.
- Ang, A.H-S. and Tang, W.H. (1990). *Probability Concepts in Engineering Planning and Design, Vol. II*, John Wiley and Sons, New York, 562 p.
- Bea, R.G., Wright, S.G., Sircar, P. and Niedoroda, A.W. (1983). "Wave-Induced Slides in South Pass Block 70, Mississippi Delta," *Journal of Geotechnical Engineering*, ASCE, Vol. 109, No. 4, pp. 619-644.
- Bishop, A.W., Webb, D.L. and Lewin, P.I. (1965). "Undisturbed Samples of London Clay from the Ashford Common Shaft: Strength-Effective Stress Relationships," *Geotechnique*, Vol. 15, No. 1, pp. 1-31.
- Bryant, W.R., Dunlap, W.A., Rutledge, A.K., and Liu, J.Y. (1995). "Continental Slope Innovative Foundations - Geological Oceanography Support," World Wide Web <http://www-sgiliu.tamu.edu:443/OTRC/contents.shtml>.
- Bryant, W., Wetzel, A., and Sweet, W. (1983). "Geotechnical Properties of Intraslope Basin Sediments, Gulf of Mexico, Deep Sea Drilling Project Leg 96, Site 619," *Initial Reports of the Deep Sea Drilling Project*, Vol. 96, September-November, pp. 819-824.
- Byrne, R.J., Kendall, J. and Brown, S. (1992). "Cause and Mechanism of Failure, Kettleman Hills Landfill B-19, Unit IA," *Proceedings ASCE Specialty Conference on Stability and Performance of Slopes and Embankments - II*, Vol. 1, Berkeley, California, June 29-July 1, pp. 1188-1215.
- Casagrande, A. (1950). "Notes on the Design of Earth Dams," *Journal of the Boston Society of Civil Engineers*, Vol. 37, No. 4, pp. 231-255.
- Chiasson, P., Lafleur, J., Soulié, M., and Law, K.T. (1995). "Characterizing Spatial Variability of a Clay by Geostatistics," *Canadian Geotechnical Journal*, Vol. 32, No. 1, pp. 1-54.
- Davis, E.E., Currie, R.G., Sawyer, B.S. and Kosalos J.G. (1986). "The Use of Swath Bathymetric and Acoustic Image Mapping Tools in Marine Geoscience," *Sonar Technology for Science and Commerce*, Vol. 20 No. 4, pp. 17-27.

- Doyle, E.H. (1994) "Geotechnical Considerations for Foundation Design of the Auger and Mars TLP's," Seventh international Conference on the Behavior of Offshore Structures, Massachusetts Institute of Technology, July 12-15.
- Duncan, J.M., Byrne, P., Wong, K.S., and Mabry, P. (1978). "Strength, Stress-Strain and Bulk Modulus Parameters for Finite Element Analyses of Stresses and Movements in Soil Masses," *Rep. No. UCB/GT78-02*, University of California, Berkeley, California.
- Duncan, M.J. and Stark, T.D. (1992). "Soil Strength from Back Analyses of Slope Failures," Proceedings ASCE Specialty Conference on Stability and Performance of Slopes and Embankments - II, Vol. 1, Berkeley, California, June 29-July 1, pp. 890-904.
- Duncan, M.J. and Wright, S.G. (1980). "The Accuracy of Equilibrium Methods of Slope Stability Analysis," *Engineering Geology*, Amsterdam, The Netherlands, Vol. 16, No. 1/2, July, pp. 88-100.
- Fredlund, D.G. and Krahn, J. (1977). "Comparison of Slope Stability Methods of Analyses," *Canadian Geotechnical Journal*, Vol. 14, No. 3, pp. 429-439.
- Gilbert, R.B. and McGrath, T.C. (in press) "Design of Site Investigation Programs for Geotechnical Engineering," in *Uncertainty Modeling and Analysis in Civil Engineering*, edited by Bilal Ayyub, CRC Press Inc., Boca Raton, FL.
- Gilbert, R.B., Wright, S.G., and Liedtke, E.A. (1996). "Uncertainty in Back Analysis of Slopes," Proceedings of Uncertainty '96, Uncertainty in the Geologic Environment, Vol. 1, Madison, WI, July 31-August 3.
- Hoeg, K. (1986). "Geotechnical Issues in Offshore Engineering," *Marine Geotechnology and Nearshore/Offshore Structures*, ASTM STP 923, R. C. Chaney and H. Y. Fang, Eds., American Society for Testing and Materials, Philadelphia, pp. 7-50.
- Hoag, K. and Tang, W. (1976). "Probabilistic Considerations in the Foundation Engineering of Offshore Structures," Proceedings 2<sup>nd</sup> ICOSSAR, Aachen, Germany, 29 p.
- Janbu, N. (1954). "Stability Analysis of Slopes with Dimensionless Parameters," *Soil Mechanics Series No. 46*, Harvard University, January, 81 p.
- Keavenly, J., Nadim, F., and Lacasse, S. (1989). "Auto Correlation Functions for Offshore Geotechnical Data," Proceedings 5<sup>th</sup> ICOSSAR, San Francisco, USA, pp. 263-270.

- Lacasse, S. and de Lanballerie, J.Y. (1995). "Statistical Treatment of CPT Data," Proceedings CPT'95. Linköping, Sweden.
- Lacasse, S. and Nadim, F. (1996). "Uncertainties in Characterizing Soil Properties," Geotechnical Special Publication No. 58, Uncertainty in the Geologic Environment: From Theory to Practice, Madison, Wisconsin, July 31-August 3, pp. 49-75.
- de Moustier, C. and Kleinrock, M.C. (1986). "Bathymetric Artifacts in Sea Beam Data: How to Recognize Them and What Causes Them," Journal of Geophysical Research, Vol. 91, No. B3, pp. 3407-3424.
- NOAA (1992). *Atlas of NOAA's multibeam sounding data in the Gulf of Mexico Exclusive Economic Zone, Vol. 1*. NOAA/NOS/Coast and Geodetic Survey, Rockville, MD, 69 p.
- Richards, A.F. and Zuidberg, H.M. (1986). "Sampling and In-Situ Geotechnical Investigations Offshore," Marine Geotechnology and Nearshore/Offshore Structures, ASTM STP 923, R. C. Chaney and H. Y. Fang, Eds., American Society for Testing and Materials, Philadelphia, pp. 51-73.
- Seed, R. B., Mitchell, J. K. and Seed, H. B. (1990). "Kettleman Hills Waste Landfill Slope Failure II: Stability Analyses," Journal of Geotechnical Engineering ASCE, Vol. 116, No. 4, pp. 669-690.
- Spencer, E. (1967). "A Method of Analysis of the Stability of Embankments Assuming Parallel Inter-Slice Forces," Geotechnique, UK, Vol. 17, No. 1, pp. 11-26.
- Stark, T.D. and Eid, H.T. (1994). "Drained Residual Strength of Cohesive Soils," Journal of Geotechnical Engineering, ASCE, Vol. 120, No. 5, pp. 856-871.
- Stark, T.D. and Poepfel, A.R. (1994). "Landfill Liner Interface Strengths from Torsional Ring Shear Tests," Journal of Geotechnical Engineering ASCE, Vol. 120, No. 3, pp. 597-615.
- Tang, W. (1979). "Probabilistic Evaluation of Penetration Resistance," Journal of Geotechnical Engineering, ASCE Vol. 105, No. 10, pp. 1173-1191.
- Tyce, R.C. (1986). "Deep Seafloor Mapping Systems - A Review," Sonar Technology for Science and Commerce, Vol. 20 No. 4, pp. 4-16.

Vanmarcke, E. (1977). "Probabilistic Modeling of Soil Profiles," *Journal of Geotechnical Engineering*, ASCE, Vol. 103, No. 11, pp. 1227-1246.

Vanmarcke, E. (1983). *Random Fields*, MIT Press, Cambridge, Mass, USA., 382 p.

Wright, S.G. (1991). "UTEXAS3 A Computer Program for Slope Stability Calculations," The University of Texas at Austin, September, 158 p.

## Vita

Eric Arthur Liedtke was born in Santa Monica, California on October 10, 1965, the son of Constance Elaine Liedtke. He graduated from Arapahoe High School, Littleton, Colorado in 1984. Eric enrolled in Arapahoe Community College, Littleton Colorado during the 1989-1990 academic school year before entering Colorado State University in Fort Collins, Colorado in the Fall of 1990. He received the degree of Bachelor of Science in Civil Engineering in May 1993. Before entering The Graduate School at the University of Texas at Austin in January 1995, he served as a Peace Corps Volunteer teaching math and science at the high school level in Sierra Leone, West Africa.

### Publication:

Gilbert, R.B., Wright, S.G., and Liedtke, E., "Uncertainty in Back Analysis of Slopes," Geotechnical Special Publication No. 58, Uncertainty in the Geologic Environment, Madison, Wisconsin, July 31 - August 3, 1996, pp. 494-517.

### Permanent Address:

1707 Woodwind Lane  
Austin, Texas 78758

This thesis was typed by the author